MINISTÉRIO DA EDUCAÇÃO
UNIVERSIDADE FEDERAL DO RIO GRANDE DO SUL
PROGRAMA DE PÓS-GRADUAÇÃO EM ENGENHARIA MECÂNICA

COAL-FIRED FURNACE MODELING ORIENTED TO OPERATIONAL DECISION SUPPORT

por

Conrado Ermel

Dissertação para obtenção do Título de
Mestre em Engenharia

Porto Alegre, Março de 2019

COAL-FIRED FURNACE MODELING ORIENTED TO OPERATIONAL DECISION SUPPORT

por

Conrado Ermel
Engenheiro Mecânico

Dissertação submetida ao Corpo Docente do Programa de Pós-Graduação em Engenharia Mecânica, PROMEC, da Escola de Engenharia da Universidade Federal do Rio Grande do Sul, como parte dos requisitos necessários para a obtenção do Título de

Mestre em Engenharia

Área de Concentração: Fenômenos de Transporte

Orientador: Prof. Dr. Paulo Smith Schneider

Aprovada por:

Prof. Dr. Edson Bazzo ..... POSMEC / UFSC

Prof. Dr. Fernando Marcelo Pereira ..... PROMEC / UFRGS

Prof. Dr. Felipe Roman Centeno .....PROMEC / UFRGS

Prof. Dr. Fernando Marcelo Pereira
Coordenador do PROMEC

Porto Alegre, 25 de Março de 2019

ACKNOWLEDGMENTS

I would like to thank my family for the love, support, and encouragement. My wife Ana Paula, for her love, and partnership.

My sincere thanks to Paulo Smith Schneider, my thesis advisor, for his guidance, support, and friendship, certainly an example to be followed. I am also thankful to my colleagues and friends from UFRGS who shared with me this intense study period, especially the ones who help me to develop this work.

I like to acknowledge EDP - Energia de Portugal, for the financial support that made possible the development of SMART-PECÉM R&D project. In the name of Guilherme de Oliveira, I would like to thanks to the entire EDP technical team, that highly contributed to the development of this work.

Finally, I am very thankful for the financial support of the Coordenação de Aperfeiçoamento de Pessoal de Nível Superior (CAPES).

RESUMO

Esta dissertação enfoca o desenvolvimento de um modelo de suporte a decisão de operação de uma fornalha de carvão pulverizado, explorando as bases teóricas de dois métodos de solução. O modelo de combustão do carvão utiliza uma descrição da combustão que não considera características dimensionais da fornalha, baseando-se no balanço de átomos, e estimando assim importantes parâmetros de processo como o poder calorífico do carvão, ar necessário à combustão, vazão e temperatura do gás de combustão assim com a concentração dos principais poluentes. O modelo de combustão trata a zona gasosa da fornalha como um reator perfeitamente misturado, sendo sensível à composição química do carvão, assim como à parâmetros de processo como a vazão e temperatura de entrada do ar e combustível. Resultados considerando a fornalha como um único reator, quando comparados à dados reais de operação, apresentaram desvios relativos de 18.46% para a temperatura do gás de combustão e -1.32% para o HHV e 1.82% para o LHV do carvão. Quanto à emissão de poluentes o modelo apresentou desvios relativos de 4.82% para o SO_2, 14.72% para CO_2, -89.61% para o NO e 53.85% para o O_2. A segunda abordagem foi realizada dividindo-se o domínio da fornalha em múltiplas zonas de gás. A radiação foi abordada pelo Método Zonal de Hottel, o qual subdivide o domínio da fornalha em um conjunto de zonas isotérmicas (de superfície e gasosas) e utiliza-se de áreas de troca diretas, determinadas através das correlações polinomiais de Tucker. As áreas de troca totais foram calculadas para contabilizar as múltiplas reflecções dentro da fornalha, enquanto balanços de energia em cada zona foram resolvidos iterativamente. A validação do modelo foi obtida simulando a caldeira de referência estudada por Ström, 1980, onde apesar de ter sido adotado um coeficiente de absorção médio constante ($K = 0.5$), desvios relativos máximos de 7.6% foram encontrados em relação ao trabalho original. O desvio relativo médio dos resultados em comparação aos dados apresentados por Ström foi de apenas 1.7%. A avaliação de um caso real foi proposta, combinando-se as duas abordagens apresentadas, formando um modelo aplicado a fornalha da caldeira de PECÉM, instalada no estado do Ceará-BR. Um esquema de duas zonas foi proposto, incluindo o modelo de combustão desenvolvido. O resultado do modelo para a temperatura dos gases de combustão apresentou um desvio relativo de apenas 13.12% em relação aos dados obtidos de PECÉM. Em relação a capacidade de predição de poluentes do modelo, diferenças

maiores foram observadas. A predição da concentração de dióxido de enxofre apresentou um desvio relativo aos dados reais de 4.04%, enquanto para o CO_2 e O_2 as diferenças foram de 19.46% e 23.53%, respectivamente. Predições de NO aparecem como um interessante resultado, uma vez que apesar da discretização limitada proposta no modelo, relativa concordância foi observada (desvios relativos de -75.75%). O presente modelo provou ser uma abordagem adequada para a descrição da operação de uma fornalha a carvão pulverizado, combinando processamento rápido com uma implementação simplificada. O modelo apresentou bons resultados para a predição da temperatura do gás de combustão e poder calorífico do carvão. A emissão de poluentes, por outro lado, exige maior detalhamento em sua descrição através de equações de taxa de reação, buscando melhorar a precisão do modelo. Não obstante, o modelo foi capaz de sugerir cenários de operação da fornalha em função de diferentes composições de carvão e dos parâmetros de processo, atingindo os requisitos de um modelo básico de suporte à decisão operacional.

Palavras-chave: Método Zonal; Modelagem de Fornalha; Suporte à Decisão de Operação; Combustão de Carvão; Radiação.

ABSTRACT

This master thesis focuses on the development of a coal-fired furnace operational decision support model, exploring the theoretical basis of two solution methods. The so-called combustion model is a zero-dimensional approach for coal combustion, based in atomic balance, which estimates important process parameters such as coal Higher Heating Value (HHV), Lower Heating Value (LHV), air flow rate and flue gas temperatures, followed by the concentration of main chemical species in furnace outlet. Combustion model approaches the gas zones as perfect stirred reactors, sensitive to the coal chemical composition and the input process parameters such as inlet flow rates and temperatures. Results were generate considering the entire furnace domain as one reactor, where 18.46% relative deviation was found to the measured flue gas temperature, while HHV and LHV deviates only -1.32% and 1.82%, respectively. Model results for pollutant emission displayed relative deviations of 4.82% for SO_2, 14.72% for CO_2, -89.61% for NO and 53.85% for O_2. The second solution approach consisted of subdividing furnace domain into multiple gas zones. Radiation was approached by means of Hottel's Zonal Method (ZM), which considered isotherm zones (surfaces or gas volumes) to calculate direct exchange areas with the help of Tucker's polynomial correlations. Total exchange areas were calculated to account for radiation multiple reflections inside the furnace, while the energy balance equation system was solved iteratively. Model validation was performed by simulating the benchmark furnace studied by Ström, 1980, with a maximum 7.6% relative deviation to real data, despite the assumption of a constant media absorption coefficient ($K = 0.5$). Assessment of a real case was performed by combining both approaches, to model the boiler furnace of PECÉM power plant, installed in Ceará-BR. A two gas-zone scheme was proposed, embedding the developed combustion model to describe PECÉM furnace operation. Model flue gas temperature result was 13.12% distant from the measured value. Prediction on sulfur dioxide concentration displayed 4.04% relative deviation to measured data, while CO_2 and O_2 were 19.46% and 23.53% distant from PECÉM records, respectively. Prediction of NO emission appears as an interesting result since even with a coarse discretization of the domain, relative concordance with real data was observed (-75.75% deviation). The presented model proved to be an interesting approach to describe the behavior of a coal-fired furnace, combining fast processing with a simplified implementation.

Flue gas temperature and coal high heating value were close to measured data. Pollutant emission, however, requires a more detailed treatment, with reaction rate equations, to improve result accuracy. Notwithstanding, the model was able to suggest operation scenarios as a function of different coal compositions and process parameters, meeting the requirements of a basic operation decision support model.

Keywords: Zonal Method; Boiler Furnace Model; Operation Decision Support; Coal Combustion; Radiation.

INDEX

LIST OF FIGURES

LIST OF TABLES

LIST OF INITIALS AND ABBREVIATIONS

AI	Artificial Intelligence
ANN	Artificial Neural Networks
CFD	Computational Fluid Dynamics
C-eff	Computational Effort
DEA	Direct Exchange Area
DFA	Direct Flux Area
DOE	Design Of Experiments
DOM	Discrete Ordinates Method
DTRM	Discrete Transfer Radiation Method
EA	Excess Air Condition
ECO	Economizer
EDP	Energy of Portugal Company
EES	Engineering Equation Solver
FGD	Flue Gas Desulfurization System
FV	Finite Volume
FVM	Finite Volume Method
GA	Genetic Algorithms
GG	Gray Gas
HHV	Higher Heating Value
IFRF	International Flame Research Foundation
IPM	Imaginary Plane Method
IU	International Units System
LBL	Line-by-Line Radiation Solution
LHV	Lower Heating Value
OFA	Over Fire Air
OFAT	One-Factor-at-a-Time
PSR	Perfect Stirred Reactor
Res.Time	Particle residence time, s
RH	Re-Heater
RNM	Reactor Network Model

RSM	Response Surface Methodology
RTE	Radiative Transfer Equation
SH	Super-Heater
SP	Sample
SSG	Surperheated Steam Generator
St	Stoichiometric Condition
TEA	Total Exchange Area
WSGG	Weighted Sum of Gray Gases
ZM	Zonal Method

LIST OF SYMBOLS

Latin Symbols

A	Area, m^2
Abs	DoE factor: gas absorption coefficient, m^{-1}
A_c	Cross-sectional area, m^2
$a_{g,n}$	WSGG weighting coefficient for the n gas
$b_{n,k}$	WSGG coefficient for the n gas and band k
B	Reference length of squared and cubic zones, m
c	Light speed, m/s
C	Carbon (element)
C_{HCN}	Hydrogen cyanide concentration, $kmol/m^3$
C_O	Oxygen radical concentration, $kmol/m^3$
CH_2	Methylene
C_{O_2}	Oxygen molar concentration, $kmol/m^3$
C_{N_2}	Nitrogen concentration, $kmol/m^3$
CO_2	Carbon dioxide
C_p	Specific heat at constant pressure, J/kgK
dA	Infinitesimal area, m^2
dr	Infinitesimal path length, m
dV	Infinitesimal volume, m^3
D_h	Hydraulic diameter, m
E	Emissive power, W/m^2
$Emiss$	DoE factor: emissivity
F	View factor
$\mathbb{F}$	Constant factor for radiant exchange in enclosures
$Flow$	DoE factor: flow rate
$\overline{g_i s_j}$	Direct exchange area from gas-zone i to surface-zone j, m^2
$\overline{g_i g_j}$	Direct Exchange area from gas-zone i to gas-zone j, m^2
G_{ref}	Reflected radiation flux, W/m^2
h	Specific enthalpy, J/kg
H	Enthalpy, J

H	Hydrogen (element)
HCN	Hydrogen cyanide
i_c	Chemical enthalpy, J/kg
i_s	Sensible enthalpy, J/kg
I	Radiation intensity, W/(m^2.sr)
J	Radiosity, W/m^2
${}_iJ_j$	Total leaving flux from j, when $E_i = 1$, W/m^2
K	Gas absorption coefficient, m^{-1}
$\overline{K}$	Gas absorption coefficient, m^{-1}
k_f	Fluid thermal conductivity, W/(m K)
$\dot{m}$	Mass flow rate, kg/s
n	Mole number
N	Nitrogen (element)
NO	Nitric oxide
NO_X	Nitrogen oxides
N_2	Nitrogen (gas)
$\overline{Nu}_x$	Nusselt number
O	Oxygen (element)
p	Partial pressure of a given species, Pa
P_r	Prandtl number
q	Radiative heat flux, W/m^2
Q	Heat transfer, W
$Q_{c,i}$	Energy per unit time released in combustion processes, W
Q_{comb}	Energy per unit time released in combustion processes, W
$Q_{e,i}$	Energy per unit time transferred by convection and enthalpy flux, W
Q_{u,g_i}	Energy per unit time (unsteady-state process), W
${}_i\left[\dot{Q}_{net,j}\right]$	Net radiative flux in surface i when $E_i = 1$, W
r	Path length between surfaces, m
R_{AF}	Air-Fuel ratio
Re	Reynolds number
Re_c	Critical Reynolds number
r_i	Tube inner radius, mm

r_o	Tube outer radius, mm
S	Path between zones
$\overline{s_i s_j}$	Direct exchange area from surface-zone i to surface-zone j, m^2
$\overrightarrow{S_i S_j}$	Direct flux area from surface-zone i to surface-zone j, m^2
SO_X	Sulfur oxides
SO_2	Sulfur dioxide
t	Time, s
$\overline{U}$	Overall heat transfer coefficient, $W/(m^2K)$
V	Volume, m^3
X	Mole fraction
Y	Mass fraction

Greek Symbols

α	Absorptivity
α	Significance level
β	Extinction or attenuation coefficient, m^{-1}
δ_{ij}	Kronecker delta function
ϵ	Emissivity
ρ	Reflectivity
ρ_0	Fluid specific mass, kg/m^3
σ	Stefan-Boltzmann constant, $W/(m^2K^4)$
σ_s	Scattering coefficient, m^{-1}
θ	Relative angle
τ	Optical thickness or opacity
λ	Excess air coefficient
λ	Wavelength, m

Subscripts

af	Adiabatic flame
alt	Alternative
amb	Ambient temperature
b	Blackbody

$Comb$	Combustion
$Conv$	Convection
db	Dry basis
$duct$	Relative to a duct flow
fg	Flue gas
g	Gas zone
H	Enthalpy, J
i	The i^{th} zone
j	The j^{th} zone
k	The k^{th} zone
n	The n^{th} gas
net	Net exchanged energy
o	Outgoing
P	Duct perimeter, m
$prod$	Reaction products
r	Radiation
R	A Refractory wall
s	Surface zone
S	Refractory wall
u	Velocity, m/s
uns	Unsteady-state
x	Generic variable
x	Characteristic length, m
w	Furnace wall

1 INTRODUCTION

There is no doubt that clean and renewable energies are the long term future for energy production. Technological advances allow for higher efficiency and capacity and bring those kind of energies closer to become the main option to fulfill the world constant growing energy demand [Gielen et al., 2019]. In an extremely competitive world, however, it is hard to imagine that governments and societies will instantaneously stop the use of conventional fossil fuels, as if they were more concerned with the environment then with economic issues. A far more realistic effort lies in updating the existing facilities, in order to enhance efficiency and reduce pollutant emissions. That statement is based on data from the world fuel supply forecast until 2040, presented in Figure 1.1. Although

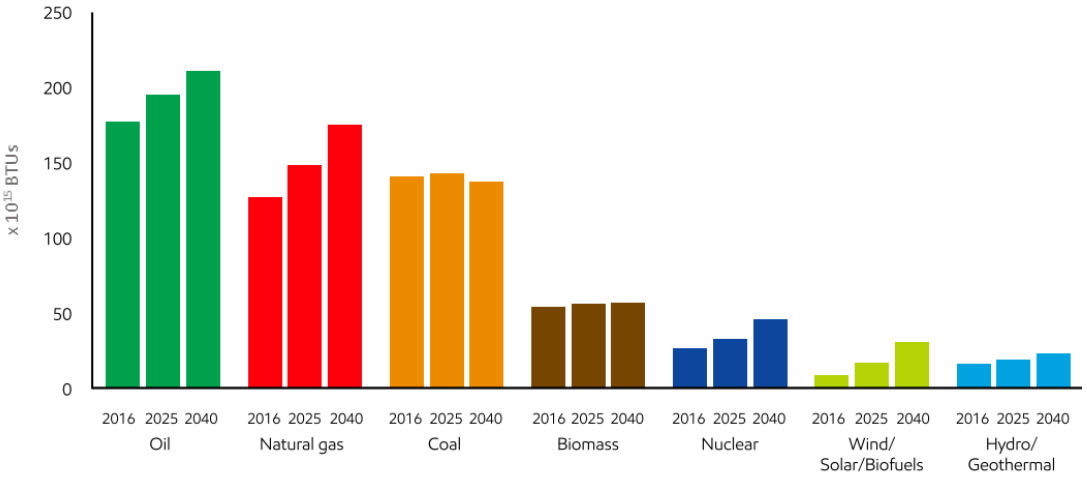

Figure 1.1 – Projection of the global demand by Fuel for 2040 (in quadrillion BTUs) [ExxonMobil, 2018]

renewable energies are in continuous ascendant trend, fossil fuel will remain at the basis of the energy matrix. Projections for 2040 show that coal will be the third most important fuel source, twice ahead from Biomass and other clean energies. In China, the world biggest energy consumer, near 59% of the electricity was produced by coal-fired power plants in 2016, and projections for 2040 suggest that coal power plants will still represent about 33% of the Chinese energy matrix [International Energy Agency, 2017]. Even in countries where the environment is a subject of great concern, such as Germany, the use of coal is far from being extinguished. Hübel et al., 2017 suggested that coal will still represent 25% of the German energy matrix in 2030.

The path to change the global energy landscape and increase the share of renewable sources is not straightforward. As noticed by BP, 2018, in 2017 the decreasing tendency in the use of fossil fuels was reversed. Even if this is a temporary shift, these fluctuations and instabilities in the worldwide environmental-politics endorse the need to invest in approaches that look for advances in the existing process of oil, gas, and coal industry. Gielen et al., 2019 affirm that mitigating environmental impacts involve both renewable energies fostering and improvement of existing processes. This was also verified in the systematic review on Support-Decision-Tool for Energy Efficient Production Planning performed by Biel and Glock, 2016, which highlights the need for researchers to connect, in a realistic manner, the greenhouse gas emission to energy production and consumption.

Power plants are nowadays subjected to strong environmental restriction policies and one possible option to mitigate emissions is to search for alternative suppliers, with coals with different composition and characteristics from the one prescribed by the original plant design. This off-specification operation is not an isolated movement, as it has been followed by several power plants all around the world [Xia et al., 2014]. Different coal composition introduces new challenges to the plant operation, efficiency and safety. Several of those effects can be anticipated by prediction models.

Simulation of coal-fired power plants by means of detailed models is already well established. A wide variety of Computational Fluid Dynamics CFD softwares for power plant simulation are mentioned by Alobaidd et al., 2016, categorized by manufacturer, fuel type and operation regime. Coal combustion demand high computational effort to simulate reactive flow conditions with refined domain meshes [Silva et al., 2010; Madejski, 2018]. Despite the high accuracy of the results, simulation demands powerful machines and are time consuming [Constenla et al., 2013]. The CFD preliminary model proposed by Cho et al., 2018 took two weeks to simulate few seconds of transient operation of a coal boiler, developed in Star-CCM+. CFD has been successfully employed to answer punctual questions [Chen et al., 2017; Echi et al., 2019; Ma et al., 2019], but they were not meant for on line prediction which requires fast response.

With a complete opposite approach, big data models depend on large amounts of records from a given process in order to "learn" with it. Under the great area called Artificial Intelligence (AI), there are branches such as Artificial Neural Networks (ANN), Genetic Algorithms (GA), Fuzzy Logic, and a variety of hybrid models. Based on mathe-

matical rules, the algorithms can identify the process trend and predict its behavior when fed with completely new data. AI has been applied to several industrial segments. As did by Zhou et al., 2004 who proposed a coal-fired power plant model, oriented to air pollutant emission control using the integration of several prediction tools such as inference, fuzzy logic, and Gaussian methods. The model, however, does not considered the involved physical phenomena. The absence of physical modeling may result in inaccurate answers, which led to combine empirical models with analytical process descriptions, such as developed by Rusinowski, 2010. As the authors reported, despite the ANN capabilities, reliable predictions still depend on the physical process description, and better results can be achieved by building combined solutions.

Analytical models, based on mathematical and physical laws, were applied to industrial furnaces since the last century when computational resources were limited. Back there, simplified modeling approaches were assumed to solve problems within a given accuracy. Although the research community can nowaday benefit from the aid of modern and more powerful equipment and solving techniques, such as CFD and IA, simplified analytical models are still helpful specially in the field of control-oriented applications and decision support tools. Simplified-analytical models can balance response accuracy with computational effort and running time. As an example, Oko and Wang, 2014 proposed a model based on physical equations to describe the operation of a 500 MWe coal-fired subcritical power plant, aiming to develop a fast response prediction tool. Authors claimed that their results with the gPROMS commercial platform displayed relative errors below 5% when compared with plant measurements. Concerning computational performance, Cho et al., 2018 reduced the response time of a preliminary 3D CFD model of a swirling flow incinerator from 2 weeks to 800 seconds by means of an analytical model, keeping the required consistency.

Among several modeling approaches, simplified numerical models are an interesting choice for thermal power station boilers. In such applications, thermal radiation is the dominant heat transfer mechanism, reason why several authors had proposed different methods to describe it, according to the application and required accuracy [McAdams and Hottel, 1954; Bazzo, 1992; Ebrahimi et al., 2013]. The zonal method, perhaps one of the most known methods to describe radiative exchange in furnaces, was first proposed by Hottel [McAdams and Hottel, 1954; Hottel and Cohen, 1958] and consists on assigning a

set of surface and gas zones to typify the domain. The method reliability was attested by Johnson and Beer, 1973, who compared the zonal method with experimental from a small-scale furnace, with good agreement for tests with oil and natural gas (10% deviations for heat fluxes). Cañadas et al., 1990 applied the zonal method to a 550 MW pulverized coal furnace, reporting average differences for unburned carbon content of 16% between the model to experimental data. The imaginary plane method IPM was proposed by Ström, 1980 as a variation of the Zonal Method. It imposes that the radiative exchange is restricted to each gas zone, and transfer between adjacent zones is accounted by energy balances, instead of considering the coupling with all surface and gas zones in the enclosure. Although more simplified and less accurate than the zonal method, IPM, overcomes the processing limitation reported in the 1980s by Charette et al., 1989. Zonal method continues to be used to solve radiative exchanges in industrial furnaces, as reported by Díez et al., 2005, who proposed an on-line simulation application for a pulverized coal boiler, due to the fast and accurate response provided by the method.

The method proposed by Hottel perfectly fits simple geometries such as square and cubes, but it can be quite difficult to implement for different volume aspects. Zhang et al., 2014 solved a heat transfer problem on an iron reheating furnace by means of a recast of the zonal method, in which Direct Exchange Areas DEA, and the Total Exchange Areas TEA were calculated by an alternative procedure. That Implementation showed the method flexibility to solve current problems with deviation below 4% in gas temperature, with low computational effort. Zhao et al., 2017 also made use of the zonal method to estimate NO_X formation in a coal-fired utility boiler, on a control-oriented engineering application. Authors solved the radiant heat transfer inside the furnace with the IPM, less accurate then the zonal method, but enough to calculate NO_X concentration as an post-processed procedure.

In addition to the radiation heat transfer modeling, the simplified analytical models must embed a combustion process description. Coal combustion is a complex subject as several phenomena occur simultaneously, where many reactions compete for the species concentration. In a deeper description, it must be considered that volatile components with faster reactions must burn faster than the solid carbon in coal particle, and models with one or two layers must be employed [Coelho and Costa, 2007]. Lockwood et al., 1980 depicted a complete coal combustion process to be adopted in coal-fired furnaces.

However, detailed procedures may not be required depending on the modeling objective, and simpler approaches can be adopted, such as the stoichiometric combustion employed by Asl et al., 2018 for natural gas, or the steady-state energy and species balances under adiabatic combustion condition reported by Hübel et al., 2017 to simulate coal-fired furnaces.

1.1 Bibliometrics

In order to contextualize the zonal method in the academic publishing landscape, a bibliometric study was carried out. Bibliometric methods focus on the objectivity and rigor of scientific literature evaluation, in order to develop a research work frame free of subjective bias. By following a well-defined procedure, research results cover the available literature in a transparent way, highlighting the most influential works, producing then reviews with higher quality [Zupic, 2015]. Bibliometric analysis is used for two different objectives. Performance analysis, where the work impact of specific authors or research groups must be evaluated, and in science mapping, which is a concise procedure that guides researchers into a transparent and not biased literature review. The last one is the objective of the bibliometric analysis developed in this work. Zupic, 2015 presents the five main methods: citation analysis, co-citation, bibliographical coupling, co-author and co-word analysis. In the present work, only three of them were employed, namely citation, co-citation and co-word analysis. The citation analysis measures the direct impact of a work based on the number of citations, without considering the networks and interrelations among researcher groups [Üsdiken and Pasadeos, 1995]. Co-citation analysis indicates the interrelation between authors, and how similar their works are [McCain, 1990]. Different from the other methods, the co-word analysis relates the actual works content and the context where it appears. It is possible then to understand how a given subject is employed and its relation to other subjects [Callon et al., 1983]. Bibliographical coupling and co-author analysis were not explored because results would tend to be very much alike to the ones already presented.

The present bibliometric analysis was developed by searching a set of keywords in SCOPUS database, selected from a set of relevant terms found in the research theme. From usual keywords used in simliar researcher, the adopted keywords were "Zon* Method" AND radia*. Only the roots of the expressions Zonal Method and Radiation were used,

to obtain more comprehensive results. In order to refine results, the searched terms were filtered to fit the following sub-areas: "ENGI", "PHYS", "CENG", "ENER", "MATH", "COMP". The search returned 555 articles of which 144 were included in the analysis after titles review. The selected works were assessed in VOSviewer software version 1.6.9, [van Eck and Waltman, 2010].

Citation analysis was set in Vosviewer to display at least 1 document and 1 citation per author, centered on the most important networks, excluding authors with less expressive results, who appeared isolated from the main network. Figure 1.2 presents the main authors, where the circle sizes represent the number of citations, connected by lines, with a colored pallet to indicate citation year. As expected, the Zone method creator,

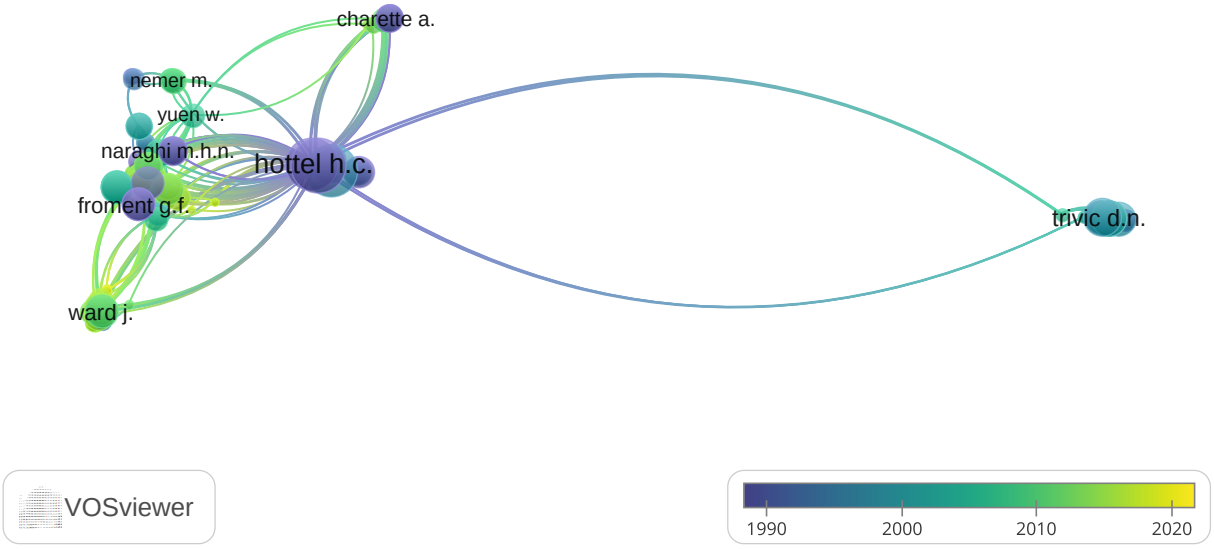

Figure 1.2 – Citation network map obtained by a bibliometric analysis. Search carried out with Scopus database and processed by Vosviewer. Color map indicates the publication year, circle sizes represent the number of citations.

Hottel, was the most cited author with 305 citations, followed by Cohen with 258 citations, although not clear in the citation network map. Viskanta was also a prominent author in this research reaching 253 citations. In recent years, authors such as Ward in 2009 and Broughton in 2013 appeared as relevant authors in the zonal method field.

The co-citation map is presented in Figure 1.3, where authors with 5 citations or more were considered. Only the most important network clusters were analyzed, identified by color, which synthesized similar subjects. Circle size represents the number of citations. Well known names in the radiation field were found in the search. Hottel, in the red

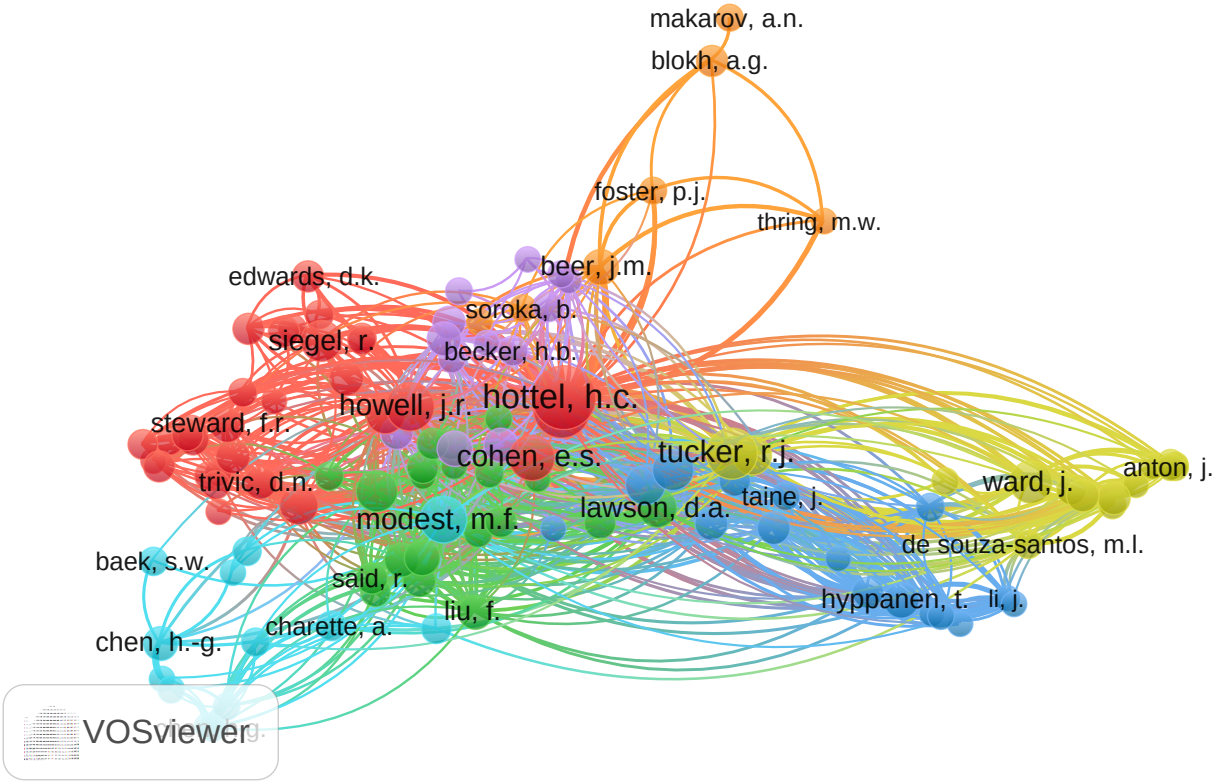

Figure 1.3 – Co-citation network map obtained by a bibliometric analysis. Search carried out with Scopus database and processed by Vosviewer. Color represents a cluster, circle sizes represent the number of citations.

cluster, is the most cited author, related to many authors such as Sarofim, Cohen, Howell, Patankar and many others. Tucker, in the yellow cluster, introduced important algebraic correlations for the direct exchange areas. Modest is the most relevant author in the light blue cluster.

The Co-Word method closes the bibliometric analysis, by clustering keywords with more than 2 occurrences. Figure 1.4 shows the keyword and expressions mentioned in the works listed in the database search. The number of occurrences is linked to the circle sizes. Heat transfer appeared at the map center together with other comprehensive keywords. The word occurrence map depicts the terms that have been used in the past years, and the terms that are in recent works. Although the Zonal or Zone method was first proposed in the 1950s and widely explored until 2000, while computational processing capacity was an issue, the average publication period of this keyword is 2006, which indicates that the zonal method is still a relevant subject, present in current researches. The average publication year of works related to the Direct exchange areas was 2015, confirming that

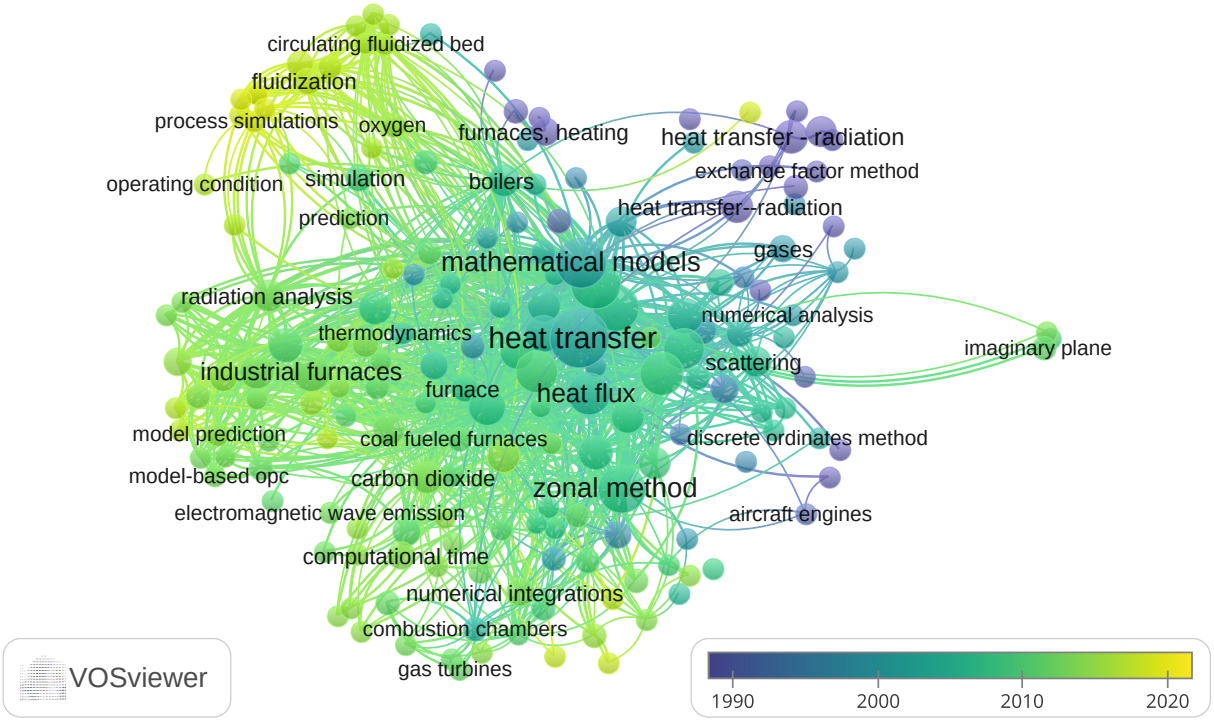

Figure 1.4 – Keyword and expressions map obtained by a bibliometric analysis. Search carried out with Scopus database and processed by Vosviewer. Color indicates the publication year and the the circle sizes are the number of occurrences.

its final user, the zonal method, is in constant improvement. Moreover, one of the most mentioned term since 2016 in works related to the zonal method was "process simulation", which suggests the employment of the method to industrial plant simulation models. The current use of Aspen Plus software related to the zonal method was also observed.

Bibliometric analysis served to point out the most important works in the studied field. It also suggested that zonal method has been recently used in the modeling of combustion process of industrial furnaces.

1.2 Objectives

The present work aims to explore and propose coal-fired furnace models to be employed in computational simulation. The models are meant to be applied in the boiler furnace of the 360 MW power plant of PECÉM. The proposed model has the main objective to orient boiler operation and support operational decision, therefore, fast response and relative accuracy are demanded.

The specific objectives are the following:

- Propose a simplified coal combustion model to be incorporated in a zonal method procedure, capable of predicting some pollutant concentration, with a balance compromise between accuracy and computational processing time.
- Develop a zonal method procedure capable of predicting relevant output such as flue gas temperature and heat fluxes.
- Understand how the zonal method responds to selected input parameters such as the absorption coefficient of the participating media, wall emissivity, and domain discretization.

1.3 Thesis Outline

The present work can be classified as an analytical, applied and quantitative research. It can also be labeled as an exploratory and decision-oriented research [Kothari, 2004]. The research was developed by adopting the simulation method [Banks, 1998]. The work is structured in three independent chapters. Chapter 1 provides the context of coal-fired power plants in the world energy landscape. The role of simplified-analytical models in the power plant modeling scenario is also presented. Zonal method applications and model currency is unveiled by the review of the literature and bibliometric analysis.

Chapter 2 explores the basis of radiation physical and mathematical treatment in the zonal method. Comparison between the most relevant radiation models is presented. The implemented procedure is validated by its application in an example furnace from the book of Hottel and Sarofim, 1967. Since the complete solution of the book example is left to the reader, the present work brings its solution for a gray gas condition.

A simplified combustion model is proposed in chapter 3. Avoiding time-expensive calculation routines, a stoichiometric calculation with element balance is developed, while the boiler furnace is assumed to be a perfect stirred reactor - PSR. A post-processed NO_X model is employed to predict the formation of this pollutant. Model results are compared with measured data from PECÉM power plant. Extrapolation of the power plant operation is accomplished by testing different coal compositions, simulating the power plant off-specification operation.

The last chapter proposes the employment of a zonal method computational code to the real 360 MW coal-fired power plant of PECÉM. Two different zoning schemes

and geometries are proposed: 2 and 5 chambers. Real operational data from PECÉM boiler were used to feed the models. The zonal method results are evaluated by means of sensitivity analysis and a response surface method - RSM. In addition, a comprehensive comparison with real data from PECÉM's power plant is carried out.

2 FURNACE MODEL - RADIATION: ZONAL METHOD

2.1 Introduction

Coal-fired steam generators are complex equipment not only because of their dimensions but due to the interaction of simultaneous several transport phenomena. The combustion process is the driving motor that takes place at the equipment furnace, where fluid flow with chemical reactions is coupled to other mechanisms. Radiant transfer was identified by several authors [McAdams and Hottel, 1954; Bazzo, 1992; Ebrahimi et al., 2013] to be the most relevant heat transfer phenomenon to be considered. Following this assumption, different levels of modeling approach were proposed by Hottel and Sarofim, 1967, Modest, 1993, Siegel and Howell, 2002.

The Zonal Method was proposed in the first place by Hottel [Hottel and Cohen, 1958] to solve complex radiative heat transfer exchange in furnaces with participant media, combining resolution to cost-benefit relation, as it displays a relative simplicity in its implementation, allied to low computational effort.

In this chapter a comprehensive review of the theoretical basis of Hottel's Zonal Method - ZM is presented in order to compile and explore its most important aspects. The theory of radiative heat transfer in enclosures is resumed, and an overview of the most relevant solution methods for the radiative transfer equation is provided. Concerning the Zonal Method itself, calculation procedure of the Direct Exchange Areas - DEA, the Total Exchange Areas - TEA, and the energy balances are discussed. The calculation procedure of the Zonal Method is depicted both for Gray Gas - GG model, and the Weighted Sum of Gray Gases - WSGG model. Finally, a computational code is developed to solve a conceptual furnace presented in the book of Hottel and Sarofim, 1967, comparing the differences between DEA values from Hottel's original graphics solution, and values from polynomial correlations [Tucker, 1986]. As Hottel and Sarofim, 1967 does not present the complete solution for the furnace example, the present work generated complete results, employing the Zonal Method, considering a gray gas model with constant absorption coefficient.

2.2 Radiant Exchange Between Surfaces

The radiant exchange between surfaces depends on the surface geometry and orientation, its radiative properties and temperature. Concerning the first two aspects, Figure 2.1 presents the geometric relation for two infinitesimal and diffuse surfaces of area dA_i and dA_j submitted to radiant exchange. Siegel and Howell, 2002 define the view factor

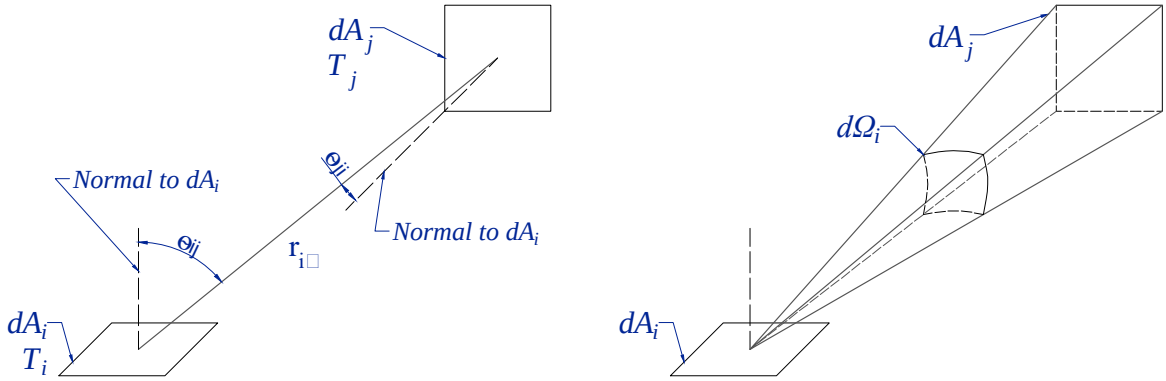

(a) Geometrical relation between surfaces (b) Solid angle definition

Figure 2.1 – Usual nomenclature for the geometrical relations between surfaces submitted to radiative heat exchange. [Hottel and Sarofim, 1967].

F_{i-j} (also known as configuration factor or shape modulus) as the fraction of the radiation leaving surface dA_i that is intercepted by surface dA_j, or in mathematical notation:

$$F_{i-j} = \frac{\int_{A_i}\int_{A_j} \pi I_i \left(\frac{\cos(\theta_{ij})\cos(\theta_{ji})}{\pi r_{ij}^2}\right) dA_j dA_i}{\pi I_i A_i} = \frac{1}{A_i}\int_{A_i}\int_{A_j} \frac{\cos(\theta_{ij})\cos(\theta_{ji})}{\pi r_{ij}^2} dA_j dA_i, \quad (2.1)$$

where θ_{ij} and θ_{ji} are the angles formed between the path r_{ij} and the normal line of each surface. The radiation intensity I_i in, W/m^2, is given by

$$I_i = \frac{dQ_i}{\cos\theta\, d\Omega\, dA}. \quad (2.2)$$

According to Siegel and Howell, 2002, the product of the area with the view factor displays a reciprocity relation of

$$A_i F_{i-j} = A_j F_{j-i}. \quad (2.3)$$

The reciprocity in Equation 2.3 simplifies the calculation routines, as the directional view factor needs to be calculated only once, as demonstrated in the view factor matrix,

Equation 2.4.

$$\begin{bmatrix} F_{ii} & F_{ij} & \cdots & F_{iN} \\ F_{ji} & F_{jj} & \cdots & F_{jN} \\ \vdots & \vdots & & \vdots \\ F_{Ni} & F_{Nj} & \cdots & F_{NN} \end{bmatrix} \tag{2.4}$$

Another important relation is the summation rule. It follows from the conservation requirement that all the radiation leaving the surface A_i must be intercepted by the enclosure surfaces so that $\sum_{j=i}^{N} F_{ij} = 1$. There are several techniques to determine view factors, and common geometric configurations are available in the literature [Siegel and Howell, 2002; Modest, 1993; Incropera et al., 2007].

2.2.1 Radiative Heat Exchange in Enclosures

Considering a transparent medium separating surfaces i and j, the radiative heat transfer hate, in watt, is calculated by the product of the area A_i, radiosity J_i, and the view factor F_{ij}.

$$Q_{i \to j} = (A_i J_i) F_{ij} \tag{2.5}$$

Radiosity is defined as the summing of the radiation emitted by a surface, plus the radiation reflected by the same surface [Siegel and Howell, 2002]. Assuming that both surfaces are black, the radiosity J_i is simplified to the blackbody emissive power $E_{bi} = \sigma T_i^4$, therefore, the net radiative exchange between them, $Q_{b,ij} = Q_{b,i \to j} - Q_{b,j \to i}$ can be written as:

$$Q_{b,ij} = A_i F_{ij} \sigma (T_i^4 - T_j^4) \tag{2.6}$$

and the net radiant heat rate exchanged between surface i and all other surfaces inside the enclosure $Q_{b,i}$ becomes

$$Q_b, i = \sum_{j=1}^{N} A_i F_{ij} \sigma (T_i^4 - T_j^4). \tag{2.7}$$

The net radiant flux for each surface of a black enclosure can be then calculated if surface temperatures are known, and the linear system can be solved by matrix inversion or numeric methods, such as Gauss-Seidel. This model can be sufficient to deliver a first evaluation of actual furnaces with walls covered by soot layers [Modest, 1993].

Radiative heat exchange in enclosures with transparent media and non-black sur-

faces can be modeled by assuming properties of gray surfaces, with constant absorption and reflection values for a given wavelength range, λ. Radiation leaving a gray surface may come from both self-emission or reflection, at the same time as the incident radiation upon an opaque surface can be partially absorbed or reflected. Heat exchange calculations may be significantly simplified by assuming all gray surfaces to be opaque, diffuse and isothermal, with uniform radiosity and irradiation. Under these conditions, emissivity can be considered to be equal to absorptivity, $\epsilon = \alpha$, [Siegel and Howell, 2002]. Thereby, the net radiation exchange at a gray surface Q_i, in watt, is given by the difference between its radiosity J_i and irradiation, G_i.

$$Q_i = A_i(J_i - G_i) \tag{2.8}$$

By adopting the definition of radiosity $J_i \equiv E_{b,i} + \rho_i G_i$, the net radiation exchange can be expressed Equation 2.9.

$$Q_i = A_i(b, i - \alpha_i G_i) \tag{2.9}$$

The combination of Equations 2.8 and 2.9 leads to:

$$Q_i = \frac{E_{bi} - J_i}{(1 - \epsilon_i)/\epsilon_i A_i}. \tag{2.10}$$

Radiation heat transfer in gray enclosures can solve a set of engineering problems. A solution strategy consists on identifying the surfaces temperature or radiative heat flux to write the correspondent radiosity equations to solve $q_{o,j}$, where subscript o represents the outgoing flux [Modest, 1993; Siegel and Howell, 2002]. Equation 2.11 is applied for surfaces with known temperature:

$$q_{o,j} = \epsilon_j E_{b,j} + (1 - \epsilon_j) \sum_{k=1}^{N} F_{j-k} q_{o,k}, \tag{2.11}$$

and Equation 2.12 is used for surfaces with known radiative heat flux.

$$q_{o,j} = q_{r,j} + \sum_{k=1}^{N} F_{j-k} q_{o,k}. \tag{2.12}$$

The subscript k stands for all other surfaces inside the enclosure, aside from j. The term $q_{r,j}$ is the known radiative heat flux, and the summation term accounts for the reflected radiation from the other surfaces. These equations form a linear system of N equations and N unknowns. Once the radiosity is calculated for each surface, the unknown thermal

condition of each surface can be determined. Equation 2.13 can be used to find the unknown heat flux, while Equation 2.14 allows calculating the surface temperature.

$$q_{r,j} = q_{o,j} - \sum_{k=1}^{N} F_{j-k} q_{o,k} \tag{2.13}$$

$$E_{b,j} = \frac{1}{\epsilon_j} q_{o,j} - \frac{(1-\epsilon_j)}{\epsilon_j} \sum_{k=1}^{N} F_{j-k} q_{o,k} \tag{2.14}$$

2.2.2 Participating Medium

Radiant heat transfer in an enclosure with non-participating or transparent medium is a valid simplification for non-polar gases such as O_2 or N_2 since radiation is neither emitted nor absorbed by them. However, many engineering applications involve polar gases such as CO_2, H_2O (vapor), NH_3, and hydrocarbon gases, which emit and absorb over a wide temperature range [McAdams and Hottel, 1954; Incropera et al., 2007; Ebrahimi et al., 2013]. Radiation interaction with this participating media is detailed hereafter.

Considering a radiation ray leaving a given surface along a path S, it is expected that radiative properties of the medium affect it. As radiation passes through a volume element of length dS, its spectral intensity I_λ is reduced by absorption or scattering [Siegel and Howell, 2002], whose attenuation is expressed by

$$dI_\lambda(S, \Omega) = -\beta_\lambda(S) I_\lambda(S, \Omega) dS, \tag{2.15}$$

where Ω is the solid angle. The proportionality constant β_λ is known as the extinction or attenuation coefficient of the medium and comprises both absorption coefficient K_λ and scattering $\sigma_{s,\lambda}$ coefficient

$$\beta_\lambda = K_\lambda + \sigma_{s,\lambda}. \tag{2.16}$$

Performing the integral of the spectral intensity attenuation along path S leads to

$$I_\lambda(S) = I_\lambda(0) \exp\left[-\int_0^S \beta_\lambda(S^*) dS^*\right], \tag{2.17}$$

known as Bouguer's, Beer's or Lambert-Bouguer law. Scattering although present in combustion processes, specially in coal combustion, rises the problem complexity and

consequently, the solution time. If scattering is neglected, Equation 2.15 becomes

$$I_\lambda(S) = I_\lambda(0)\exp(-K_\lambda S). \tag{2.18}$$

The absorption coefficient K_λ depends on the gas temperature, pressure, and composition along the path, and it indicates the medium capacity to absorb radiation. From Equation 2.17 the optical thickness or opacity τ_λ along a path length can be defined as a dimensionless quantity by

$$\tau_\lambda = \int_0^S \beta_\lambda(S^*)dS^* \tag{2.19}$$

which for a medium with uniform properties becomes Equation 2.20.

$$\tau_\lambda(S) = \beta_\lambda S \tag{2.20}$$

For $\tau_\lambda(S) \ll 1$, the medium is called optically thin, while for $\tau_\lambda(S) \gg 1$ the medium is considered optically thick [Siegel and Howell, 2002]. For optically thin medium, a series of simpler equations can be used for solve the radiation flux, whereas for optically thick medium, the radiation exchange is treated like a diffusion process with reasonable results. Since most of the engineering problems are situated in intermediary thickness condition, alternative methods are demanded.

2.3 Radiative Transfer Equation

By considering a small volume element dV with all the cited properties such as absorption, scattering, extinction coefficients among others, it is possible to conceive the conservation equation of radiative energy along a small path increment dS as

Change in Radiative Energy $=$
$+$ Gain due to Emission $-$ Loss due to Absorption
- Loss due to out-scattering $+$ Gain due to in-scattering

The mathematical representation of the *Radiative Heat Transfer Equation* - RTE can be stated, in differential form, as:

$$\begin{aligned}&\frac{\partial I_\lambda(S,\Omega,t)}{c\partial t} + \frac{\partial I_\lambda(S,\Omega,t)}{\partial S} = K_\lambda I_{\lambda b}(S,t) - K_\lambda I_\lambda(S,\Omega,t)\\ &- \sigma_{s,\lambda} I_\lambda(S,\Omega,t) - \frac{1}{4\pi}\int_{\Omega_i=4\pi} \sigma_{s,\lambda} I_\lambda(S,\Omega_i,t)\Phi_\lambda(\Omega_i,\Omega)d\Omega_i\end{aligned} \tag{2.21}$$

where the first term on the left side of Equation 2.21 is only important for ultrafast phenomena. In most of the applications, such as furnaces, it is neglected [Siegel and Howell, 2002]. The first term on the right side of the equation represents the intensity gain due to emission, followed by the loss due to absorption (second term). Scattering effects are addressed by terms three and four.

Many authors have proposed different solutions methods for the radiation transfer equation in the past century. Some of these methods are displayed in Figure 2.2 organized by the problem type (participating or non-participating media) and also classified according to the mathematical approach of the equation (integral or differential form). Various solution methods are cited, however, only a few selected ones are discussed following. Some methods, although presented in Figure 2.2, are not the focus of the present work.

The left branch of Figure 2.2 focus on enclosures with non-participating media. In this situation, radiation heat transfer becomes exclusively a function of geometrical arrangement and surface properties. If the walls of the enclosure are assumed to be black, the radiation can be solved by means of Equations 2.5, 2.6 and 2.7. For gray surfaces enclosure, the radiosity is solved by Equations 2.8 to 2.10. The radiation network solution approach is based on the electric circuit analogy, where the radiosity between two surfaces is the driving potential $(J_i - J_j)$ equivalent to a voltage potential. Resistance is the view factor term $(A_i F_{ij})^{-1}$, and the rate of radiation transfer Q_i is equivalent to the electric current flow. This method is a simplification of the direct approach [Incropera et al., 2007].

There is a category of solution that deals with the differential form of the RTE, which encompass several methods. One of them is the spherical harmonics method, also known as $P_n - Approximation$. It was first proposed by Jeans, 1917, and although it attempts to simplify the radiation heat transfer equation, it requires complex calculations to be performed. The $P_n - Approximation$ describes the radiation transfer by means of several partial differential equations, leading to a system of *N-1* equations and N unknowns. The solution is closed by approximating the local radiation intensity by a series of spherical harmonics [Siegel and Howell, 2002]. The method generates good results in optically thick medium, although it tends to overestimate radiant flux from punctual source/sinks, a common configuration in combustion processes [Modest, 1993].

In the solution category that treats the integral form of the RTE, there is a type of

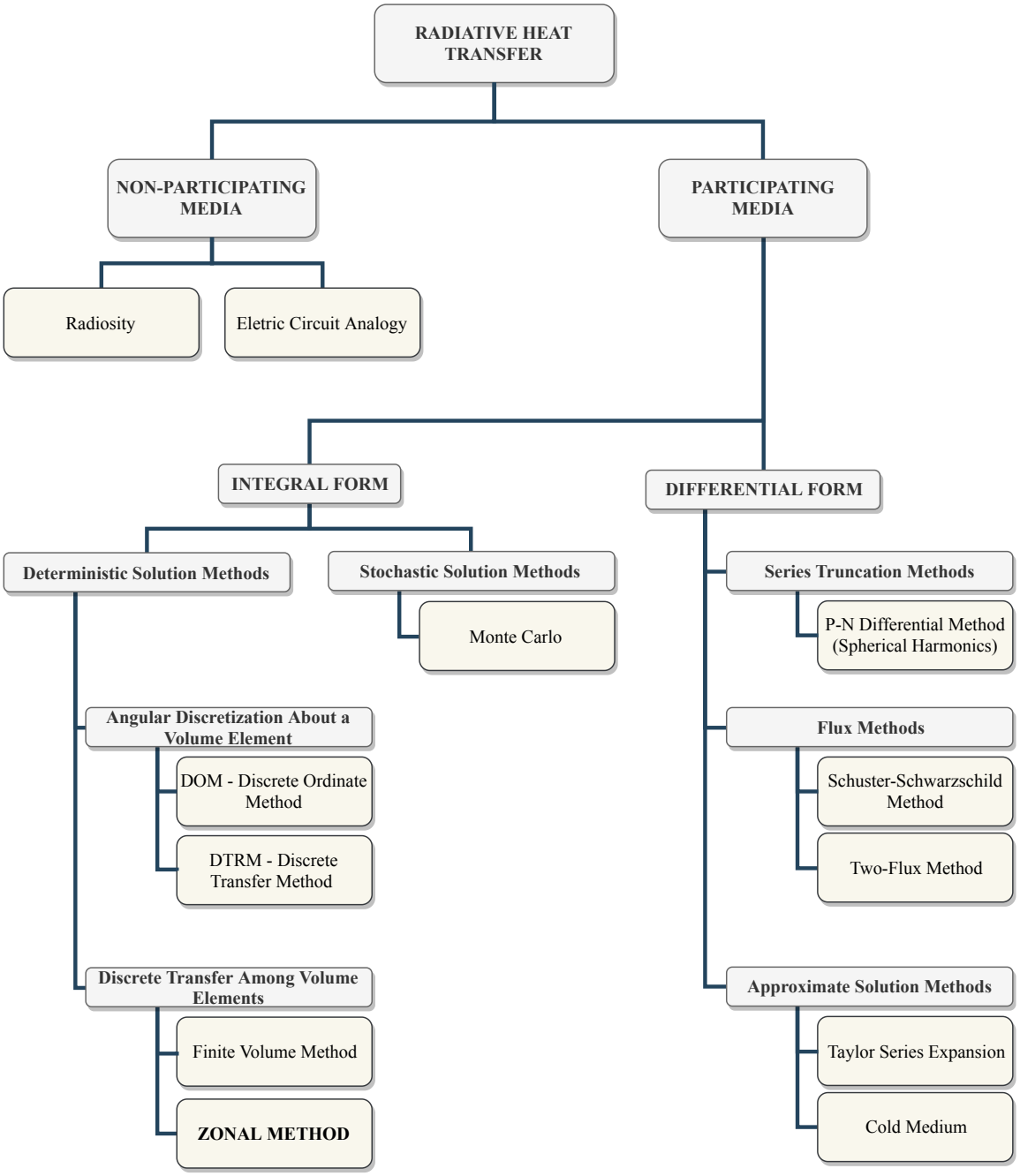

Figure 2.2 – Solution methods for the radiative heat transfer equation [adapted from Siegel and Howell, 2002].

solution based in the angular discretization of volume elements. The *Discrete Ordinates Method* (S_N) - DOM is within that category. It was proposed by Chandrasekhar, 1960 and relies on the subdivision of the total solid angle at a given point into smaller solid angles with uniform intensity. Hence, for each direction, the equation of radiant energy transfer is applied, generating differential equations. Latter Fiveland, 1984 implemented the DOM in

coal-fired furnaces, proposing an iterative solution strategy. Recently the discrete ordinate method has been implemented in Computational Fluid Dynamics - CFD codes to solve radiation in combustion processes with soot [Centeno, 2014] and in industrial furnaces [Mahmoodi et al., 2017].

The Discrete Transfer Radiation Method - DTRM, in turn, is considered a ray-tracing model and was originally proposed by Lockwood and Shah, 1981. It was conceived as a hybrid model since it presents features from previous solution methods. The DTRM is similar to the DOM since the solid angles of a given point in the domain are divided into discrete beams, with smaller solid angles. This hybrid method also holds similarity with the Monte Carlo solution, as both methods trace the intensity line from one surface to another, and with Hottel's Zone Method [Modest, 1993; Carvalho and Farias, 1998]. The method was designed to run fast solutions for CFD codes, especially when dealing with real industrial furnaces. As the method depends on the knowledge of surface radiosities, and consequently the temperature or heat flux of the enclosure walls, it requires a first guess for these parameters to ensure the convergence of the iterative solution. Additionally, the DTRM is suitable for complex geometries, and is flexible concerning computational effort, since the number of discrete rays can be easily changed [Siegel and Howell, 2002]. An important issue when coupling this method to general CFD codes is that DTRM is not a conservative formulation, in contrast to finite volume philosophy, usually employed by CFD codes [Carvalho and Farias, 1998].

The Finite Volume Method FV or FVM, is based on the discrete transfer of radiation among volumes. Despite dealing with radiative heat transfer, this method keeps the same idea of finite volumes applied to fluid mechanics and energy transport. The integral form of the RTE is solved for the incoming and outgoing radiative intensity in each volume, and their summation in all directions gives the energy balance for every volume, allowing local and global analysis of energy conservation [Siegel and Howell, 2002]. The FVM applied to radiation solution was first proposed by Raithby and Chui, 1990, as an effort to develop a radiation method aligned with the solution strategy already adopted to fluid flow and convective heat transfer problems. However, the method holds several issues in its implementation, such as false scattering and ray effects, and the most important, the method cannot guarantee the conservation of radiative energy [Modest, 1993].

A widely known RTE solution approach is the Monte Carlo method. This stochastic model, also classified as a ray-tracing model, is applied in several different research areas and makes use of probability to determine radiant heat transfer. The Monte Carlo method considers that the radiant energy is transmitted in bundles. As radiation is the unknown system, photons are chosen as those bundles, although special attention must be paid to spectral relation of the photons [Modest, 1993]. In the work of Howell and Perlmutter, 1964, the solution procedure starts with the emission of bundles which has a stochastic direction distribution. Insofar as the bundle travels inside the enclosure, it may be absorbed by the gas, according to a random gas-absorption-coefficient function. The bundle emission, absorption, and reflection are recorded until a well-determined number of runs are simulated, generating statistically meaningful average results. Due to a large number of simulations required, the Monte Carlo is a time-expensive method, that demands high processing effort, which precludes its use in fast response models and several engineering applications [Carvalho and Farias, 1998]. Nonetheless, the high accuracy presented by the method allied to its capacity to deal with complex geometries took it to a reference level, since many current works use the Monte Carlo method as a benchmark.

The solution of the RTE in its integral form can be found also in the Zonal Method - ZM, certainly one of the most known among the solution methods. In the ZM the domain is divided into surface-zones and gas-zones, both isothermal and homogeneous. Exchange factors are determined and energy conservation equations are solved for each zone, resulting in a closed system capable of solving the radiation inside an enclosure filled with a participating medium. The Zonal Method has been widely used in engineering applications, especially in industrial furnaces, probably due to its implementation simplicity in comparison to other methods. Radiation heat transfer in industrial furnaces is the problem originally studied by ZM developers Hottel and Cohen, 1958.

In order to summarize the discussed RTE- solution methods, an overview with the main characteristics of each is presented in Table 2.1. There is not a unique method for solving all radiation problems since each one displays advantages and disadvantages depending on the physical situation [Carvalho and Farias, 1998; da Silva, 2005; Centeno, 2014]. The Zonal Method is a viable option to solve industrial furnace problems whenever computational-solution-time matters. Thus the method is detailed in the following sections.

Table 2.1 – RTE Solutions overview [Jeans, 1917; Hottel and Cohen, 1958; Chandrasekhar, 1960; Howell and Perlmutter, 1964; Lockwood and Shah, 1981; Fiveland, 1984; Raithby and Chui, 1990; Modest, 1993; Carvalho and Farias, 1998; Siegel and Howell, 2002; Centeno, 2014; Mahmoodi et al., 2017].

Method	Advantages	Disadvantages
Monte Carlo	High accuracy Suitable for complex geometries	High C-eff[1]
Zonal Method	Implementation simplicity Low C-eff[1] Suitable for furnaces	Simple geometries only Isothermal zones assumption
P-N Differential	Optically thick medium	Bad for combustion process
DOM	Current CFD works	Complexity
DTRM	Fast calculation Flexible C-eff[1]	Not conservative Complexity
Finite Volume	Conventional FV (fluid flow) Flexible C-eff[1]	False scattering Conservation problems

[1] C-eff = Computational Effort / Solution time;

2.4 Zonal Method

Among the several existing methods to solve the radiative heat transfer, the zonal method, also known as the zone method or Hottel's Zonal Method, is one of the most used. It is suitable for numerous applications, although extensively used in engineering design of furnaces. It was originally proposed by Hottel and Cohen, 1958 as a solution to the radiative heat transfer in an industrial furnace. The Zonal Method was meant to solve 3D problems, so performs a spatial approximation, where the domain is subdivided into isothermal-homogeneous zones, i.e. surface zones or gas volumes. Somehow, the method is analogous to the enclosure theory, yet extended to a participating medium condition. Geometrical relations similar to view factors are derived between the zones, taking into consideration the absorption/emission effects of the participating media. Its simplicity and feasibility are the main reasons for its large-scale use.

Although the Zonal Method has gained notoriety due to the work presented by

Hottel and Cohen, 1958, its first drafts were presented by Hottel in McAdams and Hottel, 1954, but explored in more details later on by Hottel and Sarofim, 1967, one of the most important references in the field of radiation heat transfer. As shown in Figure 2.3, the

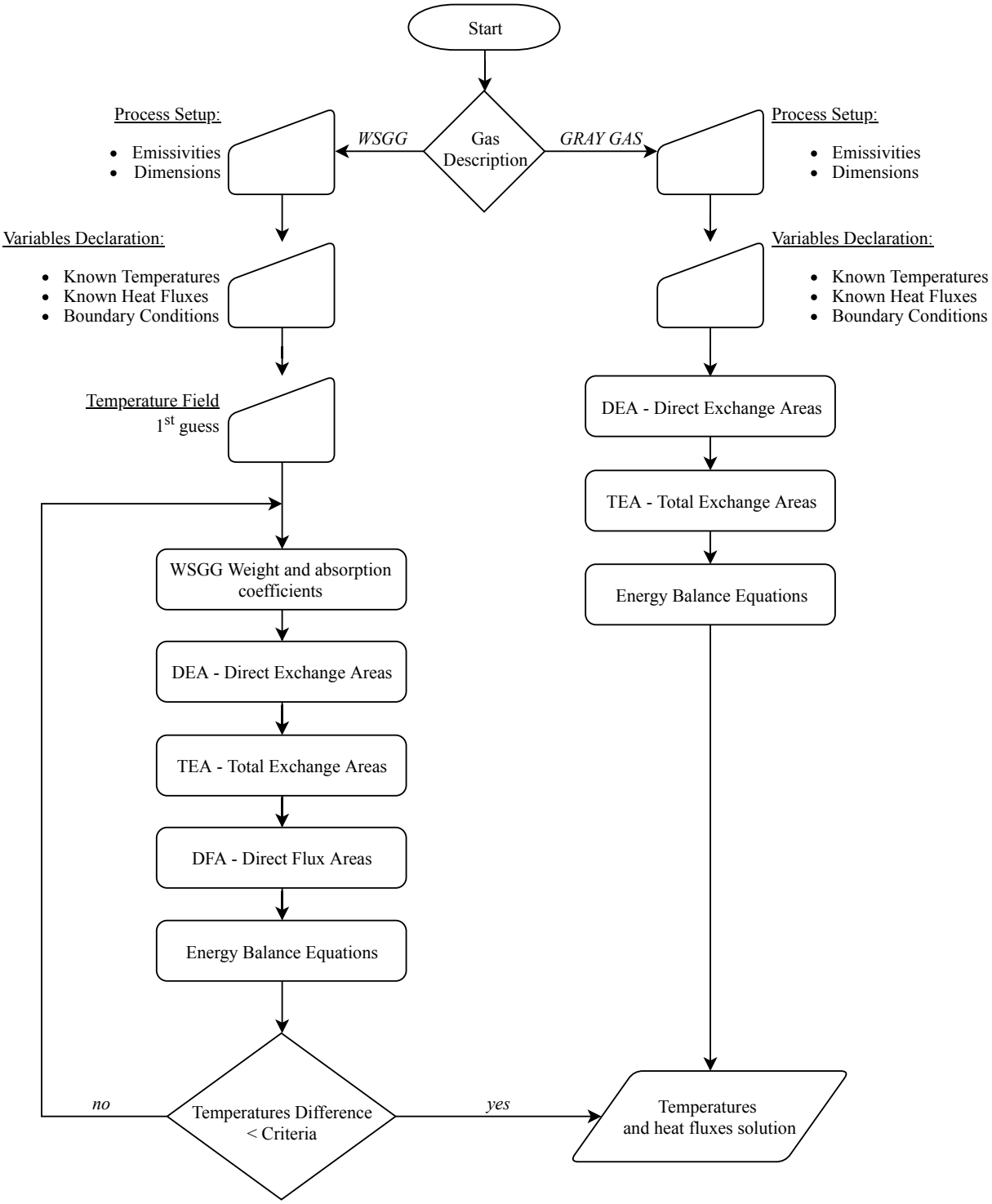

Figure 2.3 – Zonal method general solution procedure.

solution procedure begins with the characterization of the participating medium, i.e. the

adopted gas absorption model. At this point, the Gray Gas model can be assumed, or a band model such as Weighted Sum of Gray Gases, can also be adopted. The WSGG model is explained in more details in the following sections. For each gas model, a different procedure is developed.

In the WSGG model, after determining the problem configuration and the known variables the weighting factors and absorption coefficients must be calculated from the temperature field, hence a first guess is required. Next, the direct exchange areas has to be calculated. This relation accounts only for the direct radiative exchange between two zones not considering the radiation reflections present inside the enclosure. After that, a routine is performed in order to calculate the TEA - *Total Exchange Areas* which considers the view factor between two zones, the effect of the medium in the radiation, and also the multiple reflections inside the enclosure. The DFA - *Direct Flux Area* are calculated in order to weight the different absorption coefficients. Finally, energy balance equations for all zones, surfaces, and gas-volumes, assemble a system with N-equations and N-unknowns, comprising the radiative heat transfer mechanism, convection, heat losses, energy sources/sinks, and enthalpy flux. The unknown temperatures and heat fluxes are determined when the energy balances are solved.

The Zonal Method turns to be easier to solve with the GG assumption, compared to WSGG which demands an interactive procedure, since the calculated gas temperature must be compared to the initial guess. Steps such as the calculation of the DEA, TEA, and Energy Balance, are the same for both approaches. As a relevant difference, the absorption coefficient is considered to be constant in the GG model, avoiding it to calculate DFA. The energy balance embeds all energy introduced in the system, such as the energy released in a combustion process.

2.4.1 Gas Model

The Zonal Method requires the knowledge of the medium radiative properties to calculate the direct exchange areas. Several gas absorption models can be used, as long as the absorption coefficient is determined. The most basic model is the GG assumption, that assumes the gas absorptivity to be both temperature and wavelength independent. In this case, a mean absorption coefficient K is also considered to be constant (independent of temperature and wavelength). This is a strong simplification hypothesis since the

absorption coefficient displays a strong dependence on gas temperature and wavelength [Siegel and Howell, 2002]. Nevertheless, the gray gas model is still adopted in several works, due to its simplicity and reduced solving time, especially in industrial problems. Comparisons of the GG method with more accurate solutions were performed by Liua et al., 1998 and Crnomarković et al., 2016, indicating GG as a reasonable first approach for industrial problems.

One remarkable alternative to taking the temperature and wavelength dependence of the absorption coefficient into account was first proposed by Hottel [McAdams and Hottel, 1954] and developed in [Hottel and Sarofim, 1967], known as the WSGG. The gas emissivity ϵ_i of a given i^{th} gas volume zone is described as a composition of n-gray gases with a given absorption coefficient K_n, constant in the respective band.

$$\epsilon_i = \sum_{0}^{n} \left[a_{g,n}(T_g)\right] \left(1 - e^{-K_n p L}\right) \tag{2.22}$$

In Equation 2.22, the subscript g refers to a gas zone. The exponential term comes from Equation 2.18 where K was replaced by the absorption coefficient weighted by the gas partial pressure $K = K_n p$, and the path distance is denoted by L. The sum of the weighting coefficient of each gray gas must equal one, $\sum_i a_{g,i} = 1$. Smith et al., 1982 proposed that these coefficients $a_{g,i}$ could be determined by the polynomial expression

$$a_{g,n} = \sum_{k=1}^{k} b_{n,k} T^{k-1} \tag{2.23}$$

where n is the gas number, and $k - 1$ is the polynomial order. The authors generated values of emissivity and absorptivity from the exponential wide-band model, for a set of gas mixtures of water vapor and carbon dioxide, determining the coefficients. Recently, Dorigon et al., 2013 determined coefficients for the WSGG model, by performing a Line-by-Line integration (LBL), from the spectral lines of the HITEMP 2010 database [Rothman et al., 2010]. These recent coefficients could improve calculation accuracy.

WSGG proves itself as a powerful method, and has been widely explored by several authors in the recent years, specially for industrial furnace applications. Centeno et al., 2016 explored the WSGG model capacity to predict the radiation field in applications of gas with soot. The model presented normalized errors less than 1.2% when compared to an LBL solution, indicating its suitability to be used to model flue gases from coal combustion process.

2.4.2 Direct Exchange Areas

The concept of *Direct Exchange Area* - DEA, arises from the relation between the radiation emitted by a given surface A_i, and the fraction of it, reaching another surface A_j. According to Cui et al., 2010 and Siegel and Howell, 2002 the physical meaning of direct exchange areas is the value of direct radiation heat flow divided by the emissive power of a zone. If a transparent media is between two surfaces and A_i is considered to be black, the radiation that leaves it and is intercepted by A_j, would be described by

$$Q_{i\to j} = A_i F_{ij} E_i, \tag{2.24}$$

where the view factor F_{ij} is dependent only on the enclosure geometry and is determined by Equation 2.1. Equation 2.24 has the unit of watt. In turn, the product $A_i F_{ij}$ is called Direct Exchange Area, having the dimension of an area. The reciprocity corollary earlier stated for the view factor [Siegel and Howell, 2002] is also valid for the DEA, so that $A_i F_{ij} = A_j F_{ji}$.

The procedure to determine the Direct Radiation Exchange Area is described in McAdams and Hottel, 1954, Hottel and Cohen, 1958 and Hottel and Sarofim, 1967. In Figure 2.1b the radiant energy, in watt, coming from dA_i in the solid angle $d\Omega_i$ and arriving in dA_j is

$$dQ_{i\to j} \;=\; I_i \; dA_i \; d\Omega_i \; \cos\theta_{ij}, \tag{2.25}$$

as $d\Omega_i$ intercepts area dA_j, the apparent area seen by dA_i is $dA_j \;\cos\theta_{ji}$ and the solid angle becomes

$$d\Omega_i = \frac{dA_j \cos\theta_{ji}}{r_{ij}^2}. \tag{2.26}$$

In Figure 2.4a, when uniform temperature is considered in dA_i, the radiative heat rate leaving it in to dA_j can be stated as Equation 2.27.

$$Q_{i\to j} = E_i \; \overline{s_i s_j} = I_i \int_{A_j}\int_{A_i} \frac{(dA_i \cos\theta_{ij})(dA_j \cos\theta_{ji})}{r_{ij}^2} \tag{2.27}$$

By expressing I_i as E_i/π, the relation for the Direct Exchange Area for two surfaces separated by a transparent medium becomes

$$\overline{s_i s_j} = \int_{A_j}\int_{A_i} \frac{(dA_i \cos\theta_{ij})(dA_j \cos\theta_{ji})}{\pi r_{ij}^2} \tag{2.28}$$

Equation 2.28 express the same relation presented by Equation 2.1.

At this point, no radiation absorption by the gas is being considered. If a participating medium is to be considered between two surfaces, which is the interest for furnace applications, the ordinary view factor F, from Equation 2.1, must become a product of the geometric relation with the gas transmittance τ. It is important to notice that this assumption takes into consideration that both terms are not strictly separable after their integration over a finite area.

The derivation of the direct exchange areas is following presented, based in the book of Hottel and Sarofim, 1967, who divided it into three different types *Surface-Surface*, *Gas-Surface* and *Gas-Gas*. The three types of DEA are displayed in Figure 2.4.

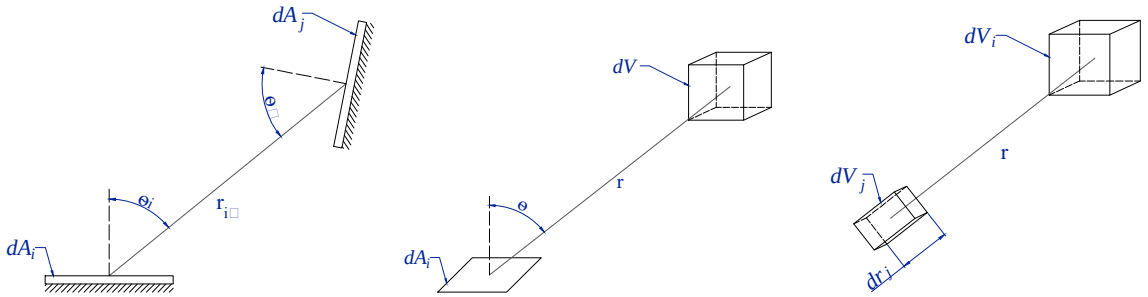

(a) Surface-Surface (b) Surface-Gas (c) Gas-Gas

Figure 2.4 – Direct exchange areas between the three types of shapes [Hottel and Sarofim, 1967].

a) *Surface-Surface Exchange*

The most basic DEA is the Surface-zone to Surface-zone, Figure 2.4a. Differently from Equation 2.28, at this point it is necessary to include a new term in the derivation to make allowance for the effect of the gas transmittance which, as presented in Equation 2.18, is given by $\tau(r) = \exp^{-\int_0^r K dr}$. Here the global attenuation coefficient β was replaced by the absorption coefficient K, since scattering is neglected. Hereafter the subscript λ is also abandoned, once is considered that the quantities are integrated over the whole spectrum. Therefore the radiative heat rate for a gray gas, in watt, is given by

$$dQ_{s_i \rightharpoonup s_j} = \underbrace{\frac{E_i}{\pi} dA_i \cos\theta_i}_{(1)} \quad \underbrace{\frac{dA_j \cos\theta_j}{r^2}}_{(2)} \quad \underbrace{\tau(r)}_{(3)} \tag{2.29}$$

where the term (1) is the emission in direction θ_i, per unit of solid angle, term (2) represents the solid angle subtended by dA_j at dA_i and term (3) is the fraction of radiation transmitted, given by

$$\tau(r) = exp^{-\int_0^r K dr} = \frac{I}{I_0}. \tag{2.30}$$

Considering the two way radiative heat exchange (net heat exchange), the Direct Exchange Area for two given surfaces, separated by a participating medium with absorption coefficient K, is expressed by

$$\overline{s_i s_j} = \frac{Q_{s_i \rightleftharpoons s_j}}{E_i - E_j} = \int_{A_i}\int_{A_j} \tau(r)\frac{\cos\theta_i \cos\theta_j}{\pi r^2} dA_j dA_i. \tag{2.31}$$

The second term of Equation 2.31 brings the net radiant heat rate, $Q_{s_i \rightleftharpoons s_j}$ instead of the one-directional $Q_{s_i \rightharpoonup s_j}$ as a consequence of the law of reciprocity applied to the DEA.

b) *Gas-Surface Exchange*

The second relation is the exchange between a surface dA and a gas-volume dV, shown in Figure 2.4b. For this configuration the radiant heat rate, also given in watt, is described by

$$dQ_{s_j \rightharpoonup g_i} = \underbrace{4\ K\ dV\ E}_{(1)} \quad \underbrace{\frac{dA\cos\theta}{4\pi r^2}}_{(2)} \quad \underbrace{\tau(r)}_{(3)} \tag{2.32}$$

in which the first term (1) is the radiant emission of a gas-volume in 4π steradians [Siegel and Howell, 2002]. The term (2) is the fraction directed towards dA, while the third term is the same presented in Equation 2.30. As derived for Equation 2.31, the Surface-Gas Direct Exchange Area can be determined by

$$\overline{g_i s_j} = \frac{Q_{g_i \rightleftharpoons s_j}}{E_i - E_j} = \int_{V_i}\int_{A_j} = \frac{\tau(r) K_i \cos\theta_j}{\pi r^2} dA_j dV_i \tag{2.33}$$

c) *Gas-Gas Exchange*

The last Direct Radiation Exchange Area is related to the exchange between two gas volumes, as presented in Figure 2.4c. First its necessary to assume that two differential gas volumes are rectangular-parallelepiped shaped, and dV_j is oriented in a way that four of its edges are parallel to r and its face dA_j is perpendicular to r. Hence, from the radiation originally emitted by dV_i, i.e. the term (1) from Equation 2.32, only the fraction $(dA_j/4\pi r^2)\tau(r)$ crosses dA_j into dV_j. The absorbed fraction is given by $K_j\ dr_j$ [Hottel

and Sarofim, 1967]. Therefore, the radiative heat rate $Q_{g_i \to g_j}$ from dV_i to dV_j can be expressed in the unit of watt by

$$dQ_{g_i \to g_j} = \frac{K_i \, dV_i \, K_j \, dV_j \, \tau(r)}{\pi r^2} E_i \tag{2.34}$$

where different absorption for each volume can be computed. The above analysis generates an important limitation in the DEA calculation, especially in tabulated results, since complex gas volume shapes need to be subdivided into rectangular-parallelepipeds. Equation 2.34 when rearranged, is the gas-gas Direct Exchange Area relation presented in Equation 2.35.

$$\overline{g_i g_j} = \frac{Q_{g_i \rightleftharpoons g_j}}{E_i - E_j} = \int_{V_i} \int_{V_j} \frac{\tau(r) \, K_i}{\pi r^2} dV_j dV_i \tag{2.35}$$

The DEA calculating is complex and demands an important share of the computational solution time, which motivated the development of ready-to-use solutions [Hottel and Cohen, 1958; Noble, 1975; Scholand and Schenkel, 1986; Tucker, 1986] with correlations and tables for common geometric configurations. Tucker, 1986 proposed a set of correlations for some of these geometric arrangements, i.e. squares (surface zones) and cubes (gas-volume zones), curve-fitted in algebraic equations (I), specially designed to be used in geometries that allow being divided into smaller squares and cubes, which is the case for conventional furnaces. The characteristic dimension B corresponds to the squares and cubes side. Although Tucker's correlations are easy to employ, they are critically limited exactly by the geometry discretization, which in some cases is unfeasible. The complexity of the solution and its high time demand motivated several researchers to study different approaches to solve the DEA. As an effort to simplify the DEA calculation and make it faster, Tian and Chiu, 2003, for instance, proposed a technique focused on reducing the integration scheme, based on the work of Herman, 1959. Although results shown a solution-time reduction by a factor of six, and a decrease of one in the integrals order, the procedure still implies in a complex and time-costly calculation routine.

Some authors such as Zhou and Qiu, 2015 have proposed solutions of the DEA by means of Monte Carlo technique, which produces better accuracy than other traditional methods (Hottel's graphics solution), though demands higher computational effort and consequently, higher solution time. The solution of the DEA with Monte Carlo is potentially interesting to solve complex geometries problems, and to create benchmark solutions.

2.4.3 Total Exchange Areas

Up to this point, the calculation of the direct exchange areas only considered the radiant exchange between two zones. A further step must be taken to consider radiation coming from other zones and reflections inside the enclosure. Furnace internal surfaces cannot be modeled as black bodies but can be considered as diffuse, following Lambert's cosine law. The procedure developed to represent these conditions is demonstrated in the following.

By performing a radiation balance on a surface zone i, it is found that the radiant energy leaving the surface $A_i J_i$ is

$$A_i \; J_i = A_i \; (\epsilon_i E_i + G_{ref}) \tag{2.36}$$

or introducing the concept of the DEA for the reflected radiation G_{ref}.

$$A_i \; J_i = A_i \epsilon_i E_i + \rho_i \left(\sum_i \overline{s_j s_i} J_j + \sum_j \overline{g_j s_i} E_j \right) \tag{2.37}$$

The last term in Equation 2.37 describes the amount of radiation reflected by the surface i, i.e. the contributions of the incident radiation originated from all other surfaces in the enclosure plus the incident radiation coming from the gas-volumes, times the respective reflectivity ρ_i. This expression was declared by Hottel and Sarofim, 1967 in a different manner to help its implementation in computational codes, as follows:

$$\sum_j \left(\overline{s_j s_i} - \delta_{ij} \frac{A_i}{\rho_i} \right) J_j \; = \; - \; \frac{A_i \epsilon_i E_i}{\rho_i} \; - \; \sum_j \overline{g_j s_i} E_i \tag{2.38}$$

with δ_{ij}, the Kronecker delta function, that assumes 0 whenever $i = j$ and 1 when $i \neq j$). When applied to the set of zone surfaces, the expression becomes a matrix system

$$\begin{bmatrix} \overline{s_i s_i} - \frac{A_i}{\rho_i} & \overline{s_i s_j} & \cdots & \overline{s_i s_n} \\ \overline{s_i s_j} & \overline{s_j s_j} - \frac{A_j}{\rho_j} & \cdots & \overline{s_j s_n} \\ \vdots & \vdots & & \vdots \\ \overline{s_i s_n} & \overline{s_j s_n} & \cdots & \overline{s_n s_n} - \frac{A_n}{\rho_n} \end{bmatrix} \cdot \begin{bmatrix} J_i \\ J_{i+i} \\ \vdots \\ J_n \end{bmatrix} = \begin{bmatrix} \frac{A_i \epsilon_i}{\rho_i} E_i & -\overline{s_i g_i} E_i & \cdots & -\overline{s_i g_m} E_m \\ \frac{A_j \epsilon_j}{\rho_j} E_j & -\overline{s_j g_i} E_i & \cdots & -\overline{s_j g_m} E_m \\ \vdots & \vdots & & \vdots \\ \frac{A_n \epsilon_n}{\rho_n} E_n & -\overline{s_n g_i} E_i & \cdots & -\overline{s_n g_m} E_m \end{bmatrix} \tag{2.39}$$

where each line of the system is the very same Equation 2.38. It is considered that the system is composed of (n) Surface-Zones and (m) Gas-Zones. The effects of the participating media are considered in the recalculated DEA, and the gas term $\overline{s_{(x)} g_{(x)}} E_{(x)}$. An

important assumption is made here, as variations on J and E are neglected. According to Hottel and Sarofim, 1967, Equation 2.39 can be used for two purposes: evaluate radiative flux at any zone if the temperature of all zones of the enclosure are known; or to evaluate the Total Exchange Areas, to be used in the energy balances of the system. Only that second functionality will be analyzed due to its generality and application to solve real problems in furnaces.

The procedure to determine the Total Exchange Area was originally described by McAdams and Hottel, 1954 as a tool to account for all the multiple radiation reflections inside the enclosure, and not just the direct exchange between two zones. The authors proposed an ideal enclosure composed of n source-sink surfaces (A_i, A_j...) with known emissivities (ϵ_i, ϵ_j...). The enclosure also contains a special type of surfaces (A_R, A_S...) named as *Refractory Walls*, which do not exchange net heat flux, reflecting all the radiation received by them. Whenever surface A_i is the taken as the only emitter in the enclosure, it is expected that surface A_j receives a fraction of radiation from A_i, plus the endless multiple reflections from all other surfaces. The concept introduced by Hottel is that all other surfaces, including the refractory ones, "can be thought of as having a partial emissive power due to the presence of each of the source-sink zones, and a total emissive power equal to their sum". After that assumption, the radiant exchange rate $Q_{i \rightleftharpoons j}$ between surfaces A_i and A_j, including their emission and the multiple reflections can be represented in the form of Equation 2.40.

$$Q_{i \rightleftharpoons j} \;=\; A_i \mathbb{F}_{ij} \sigma \left(T_i^4 - T_j^4\right) \;\equiv\; A_j \mathbb{F}_{ji} \sigma \left(T_j^4 - T_i^4\right) \tag{2.40}$$

The term $\mathbb{F}$ brought by Hottel has the meaning of a constant factor which embeds the dependence of the geometry and the radiant properties of the whole enclosure. The procedure proposed by Hottel to determine this factor is based on the premise that it has to be independent on the surfaces temperatures. To do so, all the surfaces in the enclosure are kept at absolute zero temperature, except for A_i, or in other words, $E_n = 0$. Moreover another simplification can be adopted by assuming $E_i = 1$. These boundary conditions allow to solve Equation 2.39 by means of matrix inversion, finding the values of the respective total leaving-flux ${}_nJ_n$. Here a pre-subscript is added, in order to identify which surface is kept with a real emissive power of 1. For example, ${}_iJ_j$ is the total radiant flux per unit of area (surface emission + reflections) that leaves surface A_j, when surface

A_i is set to an emissive power of $E_i = 1$, while all other surfaces has zero emissive power, $E_n = 0$. At the time Hottel published his work, this system had to be solved by matrix determinants, i.e. Cramer's rule, which made the Zonal Method difficult to be employed in complex geometries with a large number of zones. This problem was overcome by the growing computational capacity over the past years and the aid of enhanced libraries and codes. Nonetheless, once the total leaving-flux is determined, the net radiant heat rate ${}_iQ_{net,j}$ from the j-surface may be found by

$$ {}_i\left[Q_{net,j}\right] \;=\; \frac{A_j\epsilon_j}{\rho_j}(E_j - J_j) \;=\; -\frac{A_j\epsilon_j}{\rho_j}{}_iJ_j. \tag{2.41} $$

Once again is important to highlight the difference between J_j which is the radiosity of surface j, and ${}_iJ_j$ that is the total leaving-flux[1] of surface j in the hypothetical situation where only surface i has emissive power of 1. The net exchange presented in Equation 2.41 has limited meaning. It only reveals that the exchange must be proportional to the difference between the emissive power of the surfaces. As they were set to $E_i = 1$ and $E_j = 0$, the proportion constant, given by $-{}_i\left[Q_{net,j}\right]$ is hereafter named the Total Exchange Area - TEA, represented by the capital letter S for surface zones and by the capital letter G for gas zones.

When two surface zones are to be considered, the surface-surface TEA, $\overline{S_iS_j}$, can be calculated by means of the following equation

$$ \overline{S_iS_j} \;=\; \frac{A_j\epsilon_j}{\rho_j}\left({}_iJ_j - \delta_{ij}\epsilon_i\right) \tag{2.42} $$

where the radiant exchange between the surfaces is $Q_{i\rightleftharpoons j} = \overline{S_iS_j}(E_i - E_j)$. By adopting the same procedure presented above, the gas-surface TEA, $\overline{G_iS_j}$, can be determined by Equation 2.43.

$$ \overline{G_iS_j} \;=\; \frac{A_j\epsilon_j}{\rho_j}\,{}_iJ_j \tag{2.43} $$

The last relation regards to the exchange between two volumes of gas dV_i and dV_j. Setting the emissive power of gas-volume $E_i = 1$, and setting all other zones to emissive power equal to zero, the gas-gas TEA, $\overline{G_iG_j}$, can be determined by

$$ \overline{G_iG_j} \;=\; \overline{g_ig_j} + \sum_k \overline{s_kg_j}\;{}_iJ_k \tag{2.44} $$

[1]Several authors present different notations for radiation-related terms. McAdams and Hottel, 1954, for example, uses ${}_iR_j$ for the total leaving-flux, as a reminder that this quantity is normalized to $1 : \sigma T_i^4$, since $E_i = 1$.

Where the first term on the right-hand side of Equation 2.44 is the Direct Exchange Area between the two gas volumes, already calculated by Equation 2.35. The second term is the contribution of the fraction of radiation emitted by V_i and reflected by all other k-surface zones in the enclosure. The definition of these three relations results in two validation-relations. The emission of a given surface per unit of its emissive power equals the sum of all of its Total Exchange Areas.

$$\sum_j \overline{S_j S_i} \; + \; \sum_j \overline{G_j S_i} \; = \; A_i \epsilon_i \tag{2.45}$$

Then, for a gas volume, another verification expression can be stated

$$\sum_j \overline{G_i G_j} \; + \; \sum_j \overline{G_i S_j} \; = \; 4KV_i \tag{2.46}$$

2.4.4 Direct Flux Area

The GG model for participating medium is often an acceptable assumption for many practical situations, leading to reasonable results. However, if a more rigorous characterization of the gas is required, like when the absorption coefficient is dependent on temperature or wavelength, some aspects have to be observed. A possible strategy consists in treating the gas as a Weighted Sum of Gray Gases, as originally proposed by Hottel and Sarofim, 1967. Hence the radiant exchange between two surfaces has to be weighted by each of the absorption coefficients K_n and weight coefficient a_n. When the Total Exchange Areas are weighted by those coefficients, they become Direct-Flux Areas - DFA. Whenever they consider the zone temperature, its nomenclature changes to $\overrightarrow{SS}$, $\overrightarrow{GS}$ and $\overrightarrow{GG}$. Therefore, the net radiant exchange $Q_{A_i \rightleftharpoons A_j}$ between two surface zones will be

$$Q_{A_i \rightleftharpoons A_j} \; = \; E_{s,i} \, \overrightarrow{S_i S_j} \; - \; E_{s,j} \, \overleftarrow{S_i S_j} \tag{2.47}$$

where

$$\overrightarrow{S_i S_j} \; = \; \sum_n \left[a_{s,n}(T_i) \right] \; \left(\overline{S_i S_j} \right)_n \quad \text{and} \quad \overleftarrow{S_i S_j} \; = \; \sum_n \left[a_{s,n}(T_j) \right] \; \left(\overline{S_i S_j} \right)_n \tag{2.48}$$

This approach is specially useful when the temperatures are significantly different, for instance, $T_i \neq T_j$, where i and j are surface zones.

2.4.5 Energy Balances

The final step in the Zonal Method procedure is to set up and resolve the energy balance equation system. The system gathers the contributions to the energy conservation of each zone. Once the equations are written for all zones, the system was solved by iterative numeric methods, such as Gauss-Seidel or Newton-Raphson. All terms in the following energy balances are in watt.

Gas-Volume Zone

According to Hottel and Sarofim, 1967 the energy balance on a gas-volume element dV_i is derived by considering contributions from different mechanisms, that can be observed in Figure 2.5a. It can be stated as the sum of the radiant energy absorbed from all other gas zones Q_{dV_j}, and surface zones Q_{S_j}, in the system, plus the net convection Q_{Conv} from adjacent zones, plus the net enthalpy flux Q_H from the bulk flow. Those terms must equal the rate of emission of dV_i, plus the changes in its enthalpy in time Q_{uns}, if an unsteady state is to be considered. Thus, the balance is given by

$$Q_{dV_j} + Q_{S_j} - Q_{dV_i} + Q_{Conv} + Q_H = Q_{uns}. \tag{2.49}$$

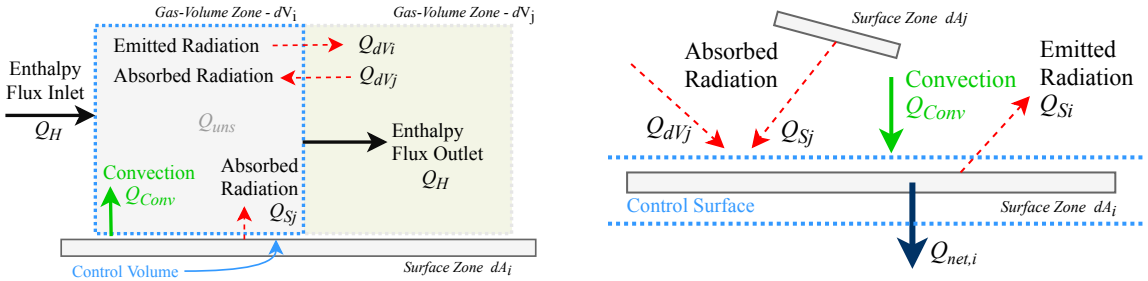

(a) Gas-volume zone

(b) Surface zone

Figure 2.5 – Global energy balance scheme in gas and surface zones.

The first term concerns to the radiation absorbed by the gas volume dV_i, coming from other gas volumes V_j. This absorbed radiant energy by Q_{V_j} can be expressed by

$$Q_{V_j} = \sum_j V_i \int_{\lambda=0}^{\infty} \int_V \frac{4K_{\lambda,j}\, E_{\lambda,j}\, \exp^{-\int_0^{r_{ij}} K_\lambda(r)dr}}{4\pi r_{ij}^2} dV_j\, K_{\lambda,i}\, d\lambda \tag{2.50}$$

where r is the distance along the path line connecting the center of both gas volumes, while r_{ij} is the total length separating both. The gas spectral absorption coefficient is represented by K_λ.

The energy absorbed by the gas volume V_i, coming from all the surface zones, Q_{S_i}, is computed by Equation 2.51.

$$Q_{S_j} = \sum_j V_i \int_{\lambda=0}^{\infty} \int_A J_{\lambda,j} \frac{\exp^{-\int_0^{r_{ij}} K_\lambda(r)dr}}{\pi r_{ij}^2} dA_{n,j}\, K_{\lambda,i}\, d\lambda \tag{2.51}$$

The projected area of the element dA_j normal to r_{ij} is denoted by $dA_{n,j}$. The total leaving-flux density at every area element dA_j, which represents the emitted plus de reflected radiation is represented by $J_{\lambda,j}$, called spectral radiosity.

The next term is the energy exchange due to convection from any adjacent surface with a given area A_k and temperature T_k.

$$Q_{Conv} = hA_k(T_k - T_i) \tag{2.52}$$

The average convection coefficient h in W/(m^{2}K) is estimated with the aid of correlations found in the literature.

The difference between the incoming and outgoing enthalpy flow is also computed in the energy balance. At this point, sensible (i_s) and chemical (i_c) enthalpies are considered having the unit of J/kg.

$$Q_H = \Delta V_i \left[\sum_{inlet} \rho_0 u(i_s + i_c) - \sum_{outlet} \rho_0 u(i_s + i_c) \right] \tag{2.53}$$

Since Equation 2.53 is in per-unit-mass basis, the specific mass ρ_0 in kg/m^3 and the flow average velocity u in m/s are introduced in the equation.

The radiation emitted by the gas-volume dV_i is given by Equation 2.54.

$$Q_{dV_i} = 4V_i \int_0^{\infty} K_{\lambda,i}\, E_{\lambda,i}\, d\lambda \tag{2.54}$$

Finally, if changes unsteady state is to be considered, the rate of energy change can be described by Equation 2.55.

$$Q_{Sto} = V_i \frac{\partial}{\partial t} \left[\rho_0 \left(i_s + i_c\right)\right] \tag{2.55}$$

In the Equations 2.50 to 2.55 subscript i indicates the energy leaving dV_i, while subscript

j represent the incoming energy from other gas volumes and surfaces. All mentioned terms have unit of watt. The sum of Equations 2.50, 2.51, 2.52 and 2.53, when equated to the summation of Equations 2.54 and 2.55, generates an integro-differential equation that describes the total energy conservation for the volume domain. Hottel and Sarofim, 1967 stated the energy balance in a gas volume as:

$$\sum_j \overrightarrow{G_j G_i} E_{g,j} \; + \; \sum_j \overrightarrow{S_j G_i} E_{s,j} \; - \; \sum_j 4a_{g,n} \, K_n \, V_i \, E_{g,i} \; + \; Q_{e,i} \; = \; Q_{u,g_i} \; - \; Q_{c,i} \tag{2.56}$$

where the energy released by a combustion process or any other heat source was include as $Q_{c,i}$. According Hottel's notation Q_{u,g_i} stands for the unsteady state, the same that Q_{uns} in Equation 2.49. Finally, $Q_{e,i}$ comprises the heat transferred convection from the adjacent surfaces and changes in the inlet and outlet fluid enthalpy, i.e. $Q_{e,i} = Q_{Conv} + Q_H$.

Surface Zone

A similar formulation of energy conservation equations can be derived for surface zones. The energy balance for A_i can be described as

$$Q_{S_j} \; + \; Q_{dV_j} \; - \; Q_{S_i} \; + \; Q_{Conv} \; = \; Q_{net,i} \tag{2.57}$$

where Q_{S_j} is the sum of the radiant energy absorbed from all other surfaces in the enclosure, and Q_{dV_j} represent the radiant energy coming from gas zones inside the enclosure. The energy transferred with the adjacent gas zone by convection is accounted by Q_{Conv}. Term Q_{S_i} is the radiative energy emitted by A_i, and all these terms must equal the net energy through the surface $Q_{net,i}$.

The first term to be analyzed is the radiation absorbed by the surface dA_i, named as Q_{dV_j}, and originally emitted by a gas volume

$$Q_{V_j} \; = \; A_i \int_{\lambda=0}^{\infty} \int_V \frac{K_{\lambda,j} \, E_{\lambda,j} \; \exp^{-\int_0^{r_{ij}} K_\lambda(r) dr} \; \cos\theta_{i,j} \; dV_j \; \epsilon_{\lambda,i} \; d\lambda}{\pi r_{ij}^2} \tag{2.58}$$

where the angle $\theta_{i,j}$ is measured between the line r_{ij} and the line normal to the area dA_i.

Radiant energy reaching dA_i, emitted from any other surface zone dA_j, is computed by means of the following equation

$$Q_{S_j} \; = \; A_i \int_{\lambda=0}^{\infty} \int_A \frac{J_{\lambda,j} \; \exp^{-\int_0^{r_{ij}} K_\lambda(r) dr} \; \cos\theta_{i,j} \; \cos\theta_{j,i} \; dA_j \; \epsilon_{\lambda,i} \; d\lambda}{\pi r_{ij}^2} \tag{2.59}$$

where $\theta_{j,i}$ corresponds to the angle between the same line r_{ij} and the line normal to dA_j.

Heat convection is modeled in respect to the adjacent j-gas zone in contact with the surface i, considering the temperature T_j as constant, as

$$Q_{Conv} = h\ A_i\ (T_j - T_i) \tag{2.60}$$

and the radiant energy emitted by surface A_i, in watt, is described by Equation 2.61.

$$Q_{S_i} = A_i \int_0^\infty \epsilon_{\lambda,i}\ E_{\lambda,i} d_\lambda \tag{2.61}$$

Energy transferred to the external medium, $Q_{net,i}$, is related to a global heat transfer coefficient. For furnaces, it is usual to assume a constant temperature boundary condition in the water walls to represent the phase change process of the water. Hottel's description for the energy balance in a surface is presented in Equation 2.62. This is similar to Equation 2.57, with the difference that the terms are in its expanded form.

$$\sum_j \overrightarrow{S_j S_i} E_{s,j} + \sum_j \overrightarrow{G_j S_i} E_{g,j} - A_i \epsilon_i E_{s,i} + h_i A_i (T_{g,k} - T_{s,i}) = Q_{net,i} \tag{2.62}$$

The temperature of a contiguous gas zone is given by $T_{g,k}$. The first and second summations in the left-hand side of the equation are the simplified form of Equations (2.59) and (2.58), respectively. The third term represents the emitted radiation, Equation 2.61, and the last one is the convection heat, presented in Equation 2.60. Equation 2.62 is in energy basis with the unit of watt. The above energy balance equations present dependence on the wavelength λ, following Hottel's deriving. However, in its final form, Equations 2.56 and 2.62, spectral dependence is neglected by considering only variables total quantities.

By implementing the presented calculation routine, it is possible to estimate the energy balance of a furnace given the boundary conditions. The Zonal Method for a GG model can be summarized in the following steps:

a) Define the gas absorption coefficient according to the chosen model.

b) Define a zoning scheme to fit the furnace domain.

c) Calculate the direct exchange areas ($\overline{ss}$, $\overline{sg}$, $\overline{gg}$)[2].

d) Calculate the total exchange areas ($\overline{SS}$, $\overline{SG}$, $\overline{GG}$).

[2]To determine the DEA for each zone, the adopted polynomial correlations are presented in Annex I, [Tucker, 1986].

e) Solve the energy balance equations to find the unknowns (temperature or heat flux).

2.5 Furnace Application

A conceptual furnace application was proposed by Hottel and Sarofim, 1967 in order to highlight some aspects of the Zonal Method, although the authors do not solve the problem up to its end. That same application is solved and detailed in the present work, with the help of the correlations proposed by Tucker, 1986 for the determination of the direct exchange areas. Figure 2.6 presents Hottel's application and its zoning scheme. In the original solution the furnace is divided into 2 gas zones (5 and 6), and 4 surface

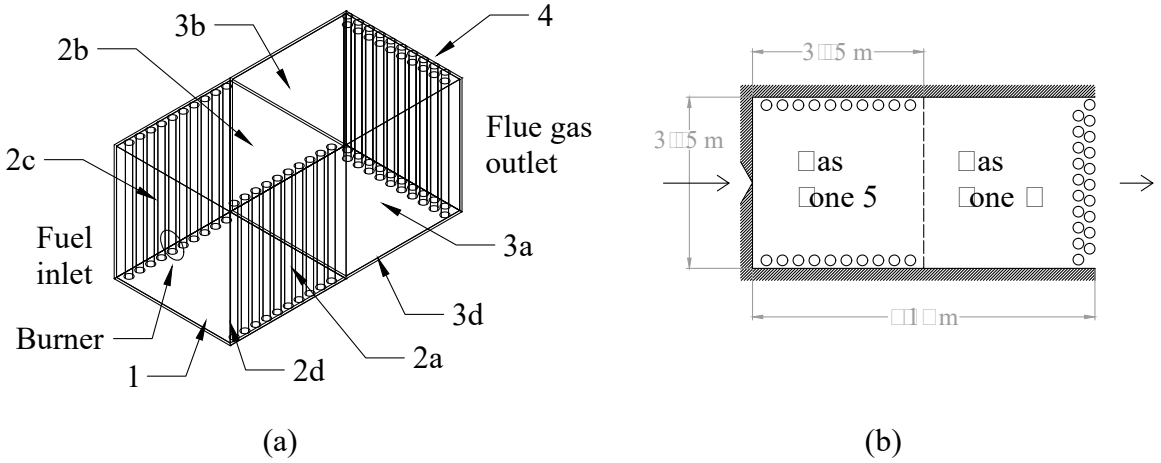

Figure 2.6 – Zonal method applied to a furnace with: (a) Isometric view (b) Top view [adapted from Hottel and Sarofim, 1967].

zones. Surface zone 1 corresponds to the burner wall, zone 2 is composed of four walls (2a to 2d) placed in gas zone 5, zone 3 is similar to the former one at gas zone 6, with four walls (3a to 3d), and zone 4 is the tube wall at the furnace flow outlet. There is no surface zone placed on the interface of gas zones 5 and 6. Original data proposed by the authors are displayed in Table 2.2, followed by their unit conversion to the International System of Units (SI). Tube and refractory walls are considered to be diffuse and gray. Tube temperature was set to a fixed value as a consequence of the phase change process of the working fluid inside the tubes.

The present work proposed the zoning scheme depicted in Figure 2.7, to facilitate the matrix inversion routines in computational codes. A matrix based approach to solve

Table 2.2 – Furnace example data, adapted from Hottel and Sarofim, 1967.

Parameter	Unit (original)	Unit (SI)
Furnace dimensions	10 X 10 X 20 ft	3.05 X 3.05 X 6.1 m
Mass flow rate	836 lb moles/hr	0.10 kg moles/s
Combustion energy release	25x10^6 Btu/hr	7326.77 kW
Tube temperature[1]	922 K	–
Inlet fuel temperature	288 K	–
Gas convection coefficient	2 Btu/ft^2°F hr	11.35 W/m^2°C
Tube emissivity	0.8	–
Refractory walls emissivity	0.5	–

[1] Temperature of the outer-surface of the tube, i.e. inside the furnace. Correspond to zones 2 and 4;

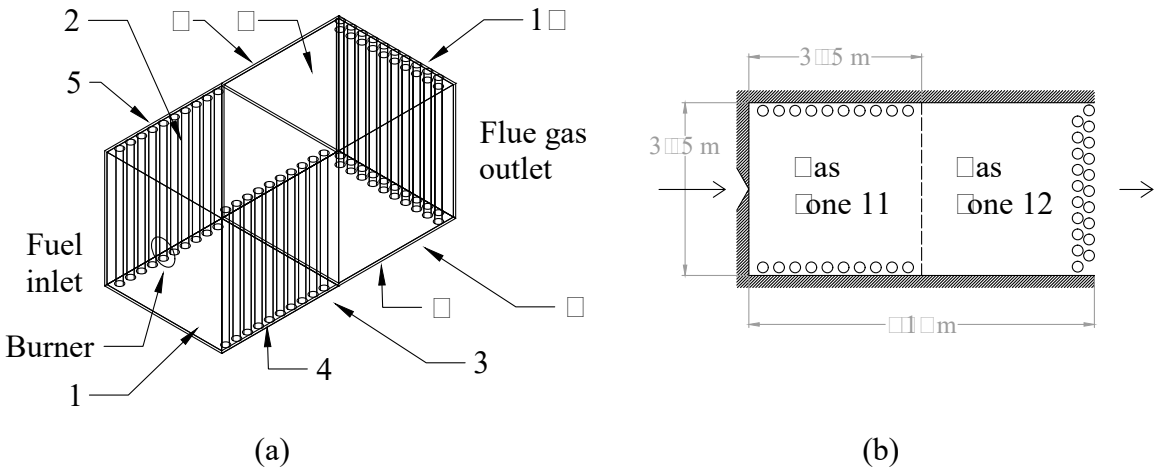

Figure 2.7 – Furnace application, current zoning scheme: (a) Isometric view (b) Top view.

the problem was implemented in a Matlab script [The MathWorks, 2012], allowing to avoid the zoning simplification assumed in the original solution. Direct exchange areas were solved by polynomial correlations from Tucker, 1986, which is a more general and accurate procedure than the graphical solution proposed by Hottel and Sarofim, 1967. The Total Exchange Areas were calculated based on a matrix algorithm, incorporated into the Matlab script.

The WSGG approach, assumed by Hottel and Sarofim, 1967, was switched to a GG model, as a first approach to test the model solution. The original concept of two participant gases and a transparent one, with weighting coefficients of $a_{g,1} = 0.0818$, $a_{g,2} = 0.339$, absorption coefficients of $K_1 = 2.37$ ft^{-1} and $K_2 = 0.0794$ ft^{-1} was simplified

with the adoption of an absorption coefficient mean value of $K = 0.6$, considered to be independent of temperature effect and wavelength. This absorption coefficient was selected as a reasonable value, based on literature review [Ström, 1980; Ebrahimi et al., 2013]. Studies on Zonal Method and imaginary plane method adopted a similar approach [Ström, 1980; Charette et al., 1990; Zhang et al., 2014]. Scattering effects are neglected, given the adopted fuel (methylene).

Hottel's results cover up to the DEA generated from the second gray gas, solved in the present work assuming $K_2 = 0.0794$ ft^{-1} aiming to compare results with the original solution. Comparative results for direct exchange areas are presented in Table 2.3, where zones 1 to 6 correspond to Hottel's zone scheme, Figure 2.6. Most of the differences between the DEA generated by Hottel and the ones calculated in this work have presented deviations below 6%, mainly related to the use of polynomial correlation instead of graphics calculation. Direct exchange areas s_1s_6, s_4s_5 and its symmetric values, s_5s_4 and s_6s_1 presented differences about 24%, what could be also assigned to the chart model accuracy. Nonetheless, the agreement of the results supports the validity of the implemented code. The only Total Exchange Area - TEA calculated by Hottel and Sarofim, 1967 was the one from gas zone 5 to the surface zone 2, reported as $G_5S_2 = 139.6$ ft^{-1}, in contrast to the value of $S_5S_2 = 143.70$ ft^{-1} calculated in the present work, resulting 2.94% relative deviation to Hottel's value. The above mentioned comparison was made to the zone scheme from Hottel's book, hence results from the present work model were correlated to them. The above-mentioned comparison was made to the zone scheme from Hottel's book, hence results from the model were correlated to them in Table 2.3.

As already mentioned, Hottel and Sarofim, 1967 did not present the complete solution to the problem, but results were found by adopting the process parameters from Table 2.2, following the zoning scheme shown in Figure 2.7. The results are presented in Table 2.4 for the radiative heat rate, energy introduced by a combustion process, the net enthalpy flux, the convective heat rate, the net energy rate through the zone and the zones temperature. It was adopted a GG model with $K = 0.6$ based on literature values [Ström, 1980; Ebrahimi et al., 2013].

Results presented in bold text are the ones calculated by the model. The ones in normal text are fixed boundary conditions. The most significant energy input to the system came from the combustion process, restricted to occur in zone 11, with the max-

Table 2.3 – Comparison between direct exchange areas results (m^2).

$Zone_{i,j}$	DEA[1](Original)	DEA (Present work)	Differences[2]
11	0	0.00	–
12	53.6	54.10	0.92%
13	3.9	3.86	-1.05%
14	1.3	1.32	1.92%
15	37.5	38.50	2.68%
16	2.5	3.11	24.46%
21	53.6	54.10	0.92%
22	139.2	141.42	1.59%
23	27.2	27.78	2.14%
24	3.9	3.86	-1.05%
25	150	154.01	2.68%
26	22.6	22.10	-2.23%
31	3.9	3.86	-1.05%
32	27.2	27.78	2.14%
33	137.2	141.42	3.08%
34	53.6	54.10	0.92%
35	22.6	22.10	-2.23%
36	150	154.01	2.68%
41	1.3	1.32	1.92%
42	3.9	3.86	-1.05%
43	53.6	54.10	0.92%
44	0	0.00	–
45	2.5	3.11	24.46%
46	37.5	54.10	2.68%
51	37.5	38.50	2.68%
52	150	154.01	2.68%
53	22.6	22.10	-2.23%
54	2.5	3.11	24.46%
55	92	86.58	-5.89%
56	13.1	13.15	0.39%
61	2.5	3.11	24.46%
62	22.6	22.10	-2.23%
63	150	154.01	2.68%
64	37.5	38.50	2.68%
65	13.1	13.15	0.39%
66	92	86.58	-5.89%

[1] Values from Hottel and Sarofim, 1967.
[2] Relative differences to Hottel's values.

imum gas temperature of T_{11}. As the result of boundary conditions, net heat exchange was only found in zones 3, 5 and 10, the tube-walls. Moreover, it was observed that for the refractory walls, (zones 1, 2, 4, 6, 7, 8 and 9) the net radiative energy is exactly the

Table 2.4 – Model results generated for the conceptual furnace proposed by Hottel and Sarofim, 1967, considering a gray gas model. Results are in bold text.

Zone -	Radiative (W)	Combustion (W)	Enthalpy flux (W)	Convective (W)	Net energy (W)	Temp.[1] (K)
1	**-8.46E+03**	0	**0**	**8.46E+03**	0	**1606**
2	**-9.32E+03**	0	**0**	**9.32E+03**	0	**1598**
3	**2.76E+06**	0	**0**	**8.07E+04**	**2.84E+06**	922
4	**-9.32E+03**	0	**0**	**9.32E+03**	0	**1598**
5	**2.76E+06**	0	**0**	**8.07E+04**	**2.84E+06**	922
6	**1.15E+01**	0	**0**	**-1.15E+01**	0	**1421**
7	**3.27E+02**	0	**0**	**-3.27E+02**	0	**1424**
8	**1.15E+01**	0	**0**	**-1.15E+01**	0	**1421**
9	**3.27E+02**	0	**0**	**-3.27E+02**	0	**1424**
10	**1.47E+06**	0	**0**	**5.27E+04**	**1.53E+06**	922
11	**-6.91E+06**	7.33E+06	**-2.34E+05**	**-1.80E+05**	0	**1687**
12	**-4.51E+04**	0	**4.44E+04**	**6.78E+02**	0	**1421**

[1] Zone temperature.

same as the convective heat transfer, a logical result once these surface zones are adiabatic and, consequently, there is no net energy transferred to the furnace neighborhood through them. Model global energy balance (inlet energy - outlet energy) was calculated to check the calculation routine correctness. 1% normalized deviation was found.

2.6 Conclusions

A comprehensive review of the radiation Zonal Method was presented, combined with a resume of the theory of radiative heat transfer in enclosures. RTE solution methods are discussed and its pros and cons were summarized. Besides, the Zonal Method calculation procedure was synthesized both for Gray Gas - GG model, and the Weighted Sum of Gray Gases - WSGG model. The Zonal Method implementation was exemplified by applying it in a conceptual furnace proposed in the book of Hottel and Sarofim, 1967. Relative deviation up to 24.46% in Direct Exchange Area values denote the accuracy disparity between Hottel's original graphics solution and the values from the adopted polynomial correlations of Tucker, 1986. This work serves mainly as a theoretical background on the Zonal Method allowing for its latter implementation in a boiler furnace from a real coal-fired power plant.

3 INTEGRAL PREDICTION MODEL OF PROCESS PARAMETERS AND POLLUTANT FORMATION FOR A COAL-FIRED THERMAL POWER PLANT

3.1 Introduction

The present work[1] aims to develop a preliminary model of the combustion process of the 360 MW (electrical output) coal-fired boiler from EDP-PECÉM power plant, installed in Ceará, Brazil. The plant operates under a subcritical Rankine cycle originally designed to burn Colombian coal, but economical and logistic issues led to a search for new coal suppliers, resulting in the use of coals of different composition. Changes in fuel composition can cause important operational oscillations, variations in efficiency, pollutant emissions, maintenance, and plant safety. The adoption of off-specification coals and its consequences are highlighted by Xia et al., 2014, showing that this practice is becoming a common reality for coal power plants all around the world. The authors have proposed a Case-Based Reasoning method in order to predict boilers behavior according to the coal characteristics. The method compares on-line data from the server database to well-established operating conditions. Suggested optimized parameters are presented to the plant operator as a decision support information. Although results seem to be coherent to the plant operational needs, this approach requires previous historical data.

More detailed physics description are handled with methodologies as CFD (*Computational Fluid Dynamics*), like in Constenla et al., 2013, who modeled a 350 MW pulverized-coal boiler with ANSYS Fluent commercial software to predict combustion trends along with pollutant formation for different operating conditions. Authors reported simulation results with differences below 10% in comparison with experimental data. Despite the small errors and the compromise with maximum accuracy with minimum computational effort, simulations took over 50 hours to reach convergence, which suggests that CFD still cannot generates fast calculations.

Prediction models aiming to support process control require alternatives with less computational effort. The control-oriented work reported by Zhao et al., 2017 modeled a low-NO_X coal-fired boiler as close as possible to the process physics. Authors modeled

[1] The present Chapter was presented in the ENCIT 2018 - 17th Brazilian Congress of Thermal Sciences and Engineering - November 25th-28th, 2018, under ID-0178

the combustion process by dividing the furnace into N isotherm zones, and solved the radiation exchange by means of the *Imaginary Plane Method* - IPM, derived from the Zonal Method [Hottel and Cohen, 1958], followed by chemical reaction rates along with a post-processed NO_X model. According to the authors, that approach resulted in a reasonably fast model, capable of predicting key-parameters as flue gas temperature and NO concentration. However, in a large-scale coal-fired thermal power plant, other parameters such as SO_X, ash and CO_2 concentrations may be of interest. Thereby, considering the need to estimate boiler operational conditions with little processing time, the present chapter proposes, as a first approach, a zero-dimensional model where the entire furnace domain is represented as a *Perfect Stirred Reactor* - PSR in order to calculate flue gas temperature levels and pollutant concentration under different input conditions.

3.2 Steam Generator Specification

The PECÉM power plant is composed of three groups of 360 MW electric output, and the simulation model presented in this chapter was focused on one independent power system, illustrated in Figure A.2. The superheated steam generator depicted in the figure left side can be divided into three subsystems: the thermohydraulic circuit, the combustion system and the air and flue gas circuit. Liquid water is pressurized by pump P1 to be admitted into the boiler thermohydraulic system, passes through the economizers and arrives the drum. The boiler drum and the furnace walls are part of a subsystem dedicated to promoting water phase change, with saturated water steam as the output, that follows through a sequence of 3 superheaters to finally deliver superheated steam at its higher temperature level to be expanded at the turbine.

The combustion system begins in the grinding mills, that ensures coal granulometry bellow 75 μm. Transport air, also called primary air, carries pulverized coal into the furnace burners. Four burner lines are placed in two opposite walls, in a frontal burn scheme with 24 burners as shown in Figure 3.2. The furnace is 26 m high and displays a 16 m x 13 m cross-section. Flue gas passes along all boiler heat exchangers, and the last one heats the secondary air input of the combustion system. Flue gas is then filtered in a baghouse system for solid matter, and a *Flue Gas Desulfurization* system, FGD, in order to control SO_2 emission. The burning zone is divided into two sections. In the first, coal is burned under substoichiometry condition and then passes through the second one,

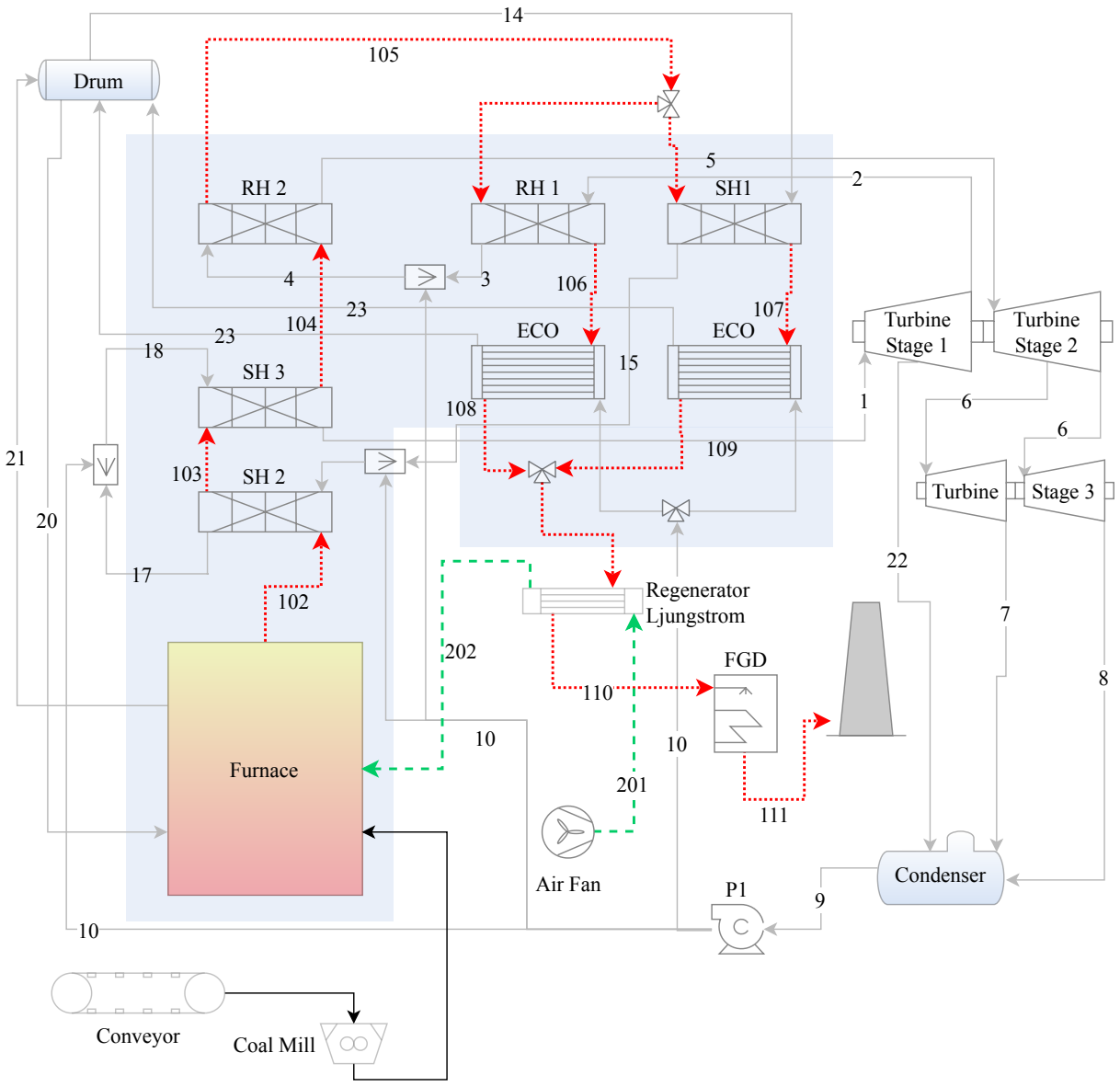

Figure 3.1 – PECÉM boiler process diagram. Devices (SH: Super-Heater, RH: Re-Heater, ECO: Economizer). Boiler streams (solid-line: water and steam system, dashed-line: air feed system, dotted-line: combustion gas system).

called *Over Fire Air* - OFA, which completes the combustion process, preventing flue gas temperature to rise and bringing the combustion process to an excess air condition.

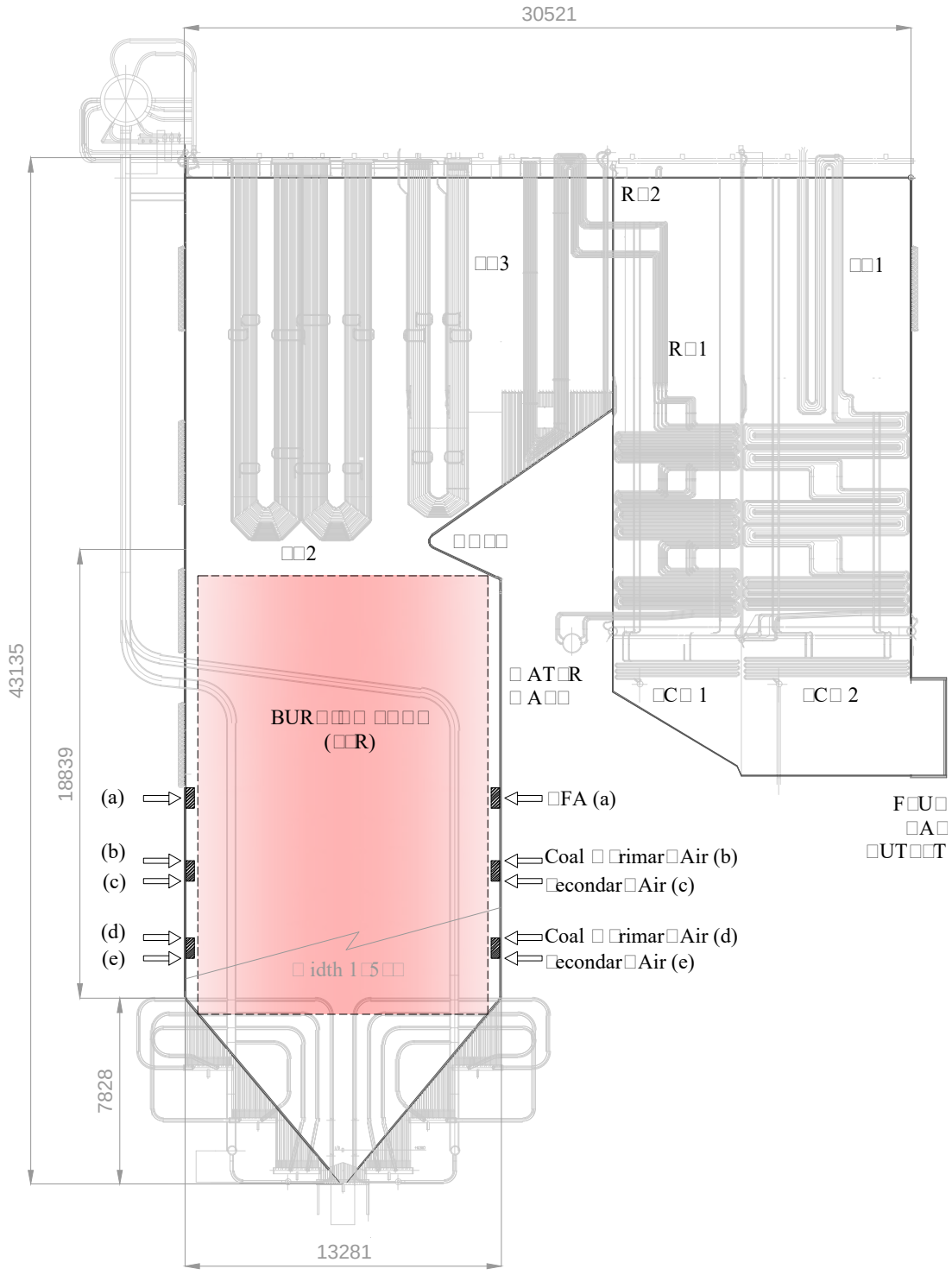

Figure 3.2 – Steam generator arrangement draw (adapted from original power plant design). The entire furnace domain is assumed to be a PSR. Coal and air are introduced in the two burners lines in each side. Dimension presented in millimeters.

3.3 Mathematical Formulation

The main objective of the model is to predict the most important changes in process parameters as a function of coal composition. The present model follows an integral approach, based on mass and energy balances. Energy input is calculated based on a species equilibrium balance.

3.3.1 Combustion Model

A first simplified approach was chosen to estimate the energy released by the combustion process Q_{comb}, calculated by the product $\dot{m}_{fuel}LHV$, (coal mass flow rate and lower heating value), based on data from the fuel ultimate analysis. By considering complete combustion, a set of ideal products is determined by atomic balance. Equilibrium formulation based on coal chemical composition allows predicting product species concentration for stoichiometric condition, as expressed in Equation 3.1 [Coelho and Costa, 2007; Turns, 2013].

$$\left(n_{coal_C}C + n_{coal_H}H + n_{coal_O}O + n_{coal_N}N + n_{coal_S}S + n_{coal_{H_2O}}H_2O\right) + n_{air}(O_2 + 3.76N_2) \rightarrow n_{CO_2}CO_2 + n_{H_2O}H_2O + n_{N_2}N_2 + n_{SO_2}SO_2 \tag{3.1}$$

Combustion process with excess air ($\lambda > 1$) is expressed by Equation 3.2

$$\left(n_{coal_C}C + n_{coal_H}H + n_{coal_O}O + n_{coal_N}N + n_{coal_S}S + n_{coal_{H_2O}}H_2O\right) + \lambda n_{air}(O_2 + 3.76N_2) \rightarrow n_{CO_2}CO_2 + n_{H_2O}H_2O + n_{N_2}N_2 + n_{SO_2}SO_2 + n_{O_2}O_2 \tag{3.2}$$

where n represent the species mole number. A similar procedure was adopted by Asl et al., 2018 to evaluate the retrofit potential of existing power plants.

The high heating value allows for the calculation of the energy released in the combustion process, Q_{comb}, as presented in Equation 3.3. It can be determined by measuring the energy transferred from a steady-state reactor considering that the combustion products are at the same temperature as the inlet reactants. For an adiabatic process, the enthalpy difference between products and reactants results in the Adiabatic Flame Temperature, the maximum value achieved by any combustion processes [Turns, 2013].

$$LHV_{coal} = \frac{Q_{comb}}{\dot{m}_{coal}} \tag{3.3}$$

For coals whose HHV is not known, this parameter can be calculated by the Dulong's relation, suggested by Speight, 2005.

$$HHV_{coal} = 144.4(\%C) + 610.2(\%H) - 65.9(\%O) - 0.39(\%O)^2 \tag{3.4}$$

Considering the HHV previously known, th lower heating value (LHV) in dry basis was determined by

$$LHV_{coal} = HHV_{coal} - Y_{H_{db}} h_{evap,H_2O}, \tag{3.5}$$

where $Y_{H_{db}}$ is the coal nitrogen mass fraction in dry basis, and water evaporation heat h_{evap,H_2O}= 2257.03 kJ/kg was assumed [Van Wylen et al., 2003]. The HHV and LHV relations presented in Equations 3.4 and 3.5 are approximations. In the present work, combustion heat was estimated adopting LHV values declared in the coal analysis report.

In view of the solid state of coal elements such as carbon and hydrogen, an alternative approach is proposed. The energy due to the enthalpy difference between inlet and outlet, considering only products species (CO_2, H_2O, N_2 and O_2) is assumed to be the energy released in the combustion. This approach overlooks the changes in elements enthalpy, due to the formation of new species. Hence, the adiabatic flame temperature was determined by Equation 3.6, illustrated in Figure 3.3a, where the subscripts indicate the process location depicted in Figure A.2.

$$Q_{comb} = Q_{Prod,T_{[202]}} - Q_{prod,T_{af}} \tag{3.6}$$

The flue gas temperature is then determined by estimating the energy removed from the

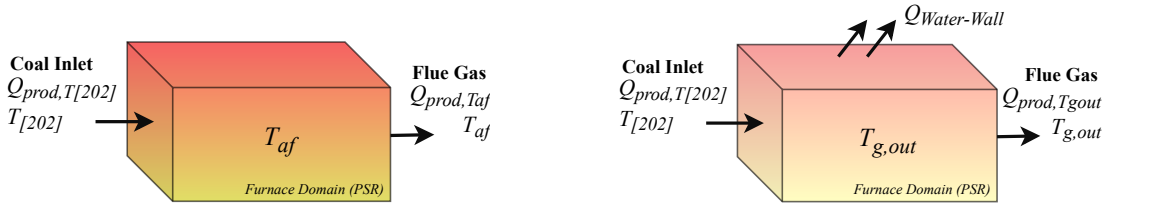

(a) Energy balance for the adiabatic flame temperature

(b) Energy balance for the flue gas temperature

Figure 3.3 – Energy balance diagrams for determination of the adiabatic flame temperature and flue gas temperature. Steady-stated reactors.

system by the furnace water-walls, where a significant amount of heat is transferred to

promote fluid phase change. The heat transferred on that process, $Q_{Water-Wall}$, can be estimated by Equation 3.7 from measured data, such as water flow rate $\dot{m}_{[20]}$, inlet and outlet water enthalpy $h_{[23]}$ and $h_{[24]}$, as referred to in Figure A.2.

$$Q_{water-wall} = \dot{m}_{[23]} \left(h_{[14]} - h_{[23]} \right) \tag{3.7}$$

The flue gas temperature inside the furnace can then be approximated by a single value for the global zone, calculated by means Equation 3.8

$$Q_{comb} = Q_{Prod,T_{[202]}} - Q_{Prod,T_{fg}} - Q_{water-wall} \tag{3.8}$$

where $Q_{Prod,T_{[202]}}$ and $Q_{Prod,T_{fg}}$ are the energies due to the temperature of above-mentioned species at the furnace inlet and outlet, respectively. Despite the approach simplicity, results may be of great value whenever the actual temperature measurement is not available.

3.3.2 *NO* Formation Model

Nitric oxides, or NO_X, are important industrial pollutants as they contribute to several environmental impacts. To control its emission has become an important concern in industrial combustion processes [Warnatz et al., 2006]. Among all nitric oxides, *NO* stands for the most important species, which demand strategies to prevent its formation. Its formation can be described by three well-established chemical paths, namely *NO-Thermal*, also known as Zeldovich mechanism; *NO-Prompt* and the *NO-Fuel* which is important in fuel-rich regions [Turns, 2013].

Generally, the amount of active NO_X reactants is small enough to assume that its formation has no impact on the entire combustion calculations, allowing to consider exclusively the *NO-Thermal* and *NO-Fuel* mechanisms. The *NO-Thermal* formation rate is given by Equation 3.9 [Zhao et al., 2017]

$$\frac{\partial R_{NO-Thermal}}{\partial t} = 3.6 \times 10^{11} exp\left(\frac{-38370}{T_{fg}}\right) C_{N_2} C_O \tag{3.9}$$

where T_{fg} is the furnace homogeneous temperature, C_{N_2} is the nitrogen concentration in molar basis, and the O-radical mole fraction C_O, defined as:

$$C_O \approx 12.567 \times 10^3 T_{fg}^{-0.5} exp\left(\frac{-31096}{T_{fg}}\right) \sqrt{C_{O_2}} \tag{3.10}$$

with C_{O_2} the oxygen molar fraction. Regarding the *NO-Fuel* mechanism, it is assumed

that all coal-N is converted into HCN immediately, and then oxidized into NO at the rate of Equation 3.11

$$\frac{\partial R_{NO-HCN}}{\partial t} = 10^{10} C_{HCN} C_{O_2}^{b} exp\left(\frac{-33713}{T_{fg}}\right) \tag{3.11}$$

where $b = 0$ for $C_{O_2} > 0.018$ and $b = 1$ for $C_{O_2} < 0.0025$ [Hill and Douglas Smoot, 2000]. Equations 3.9 and 3.11 are presented in derivative form, and must be integrated over the residence time t, estimated for an imaginary particle.

3.4 Methodology

The proposed Zero-Dimensional model aims to predict process parameters and pollutant formation of a coal-fired power plant that operates under a sub-critical Rankine cycle. Table 3.1 presents the model inputs and calculated variables. Coal composition is based on immediate and ultimate analysis, which gives the elementary composition (carbon, hydrogen, sulfur, oxygen, nitrogen, ash and moisture content). Table 3.1 resumes the input variables used in the code and its average values for the design operational condition at 360 MW output power. All simulations were performed with fixed boundary conditions.

Table 3.1 – Input variables list for the design operational condition of PECÉM boiler at 360 MW output power.

Symbol	Variable	Figure A.2 Index	Standard Values[1]	Unit
-	Coal composition	-	-	%
$\dot{m}_{coal}$	Coal flow rate	-	36.89	kg/s
$\dot{m}_{air}$	Total air flow rate	$\dot{m}_{[202]}$	356.76	kg/s
$\dot{m}_{Steam}$	Steam mass flow rate	$\dot{m}_{[1]}$	343.86	kg/s
$\dot{m}_{Water}$	Water mass flow rate	$\dot{m}_{[23]}$	340	kg/s
T_{air}	Inlet air temperature	$T_{[202]}$	370	°C
T_{Steam}	Steam temperature	$T_{[1]}$	530	°C
P_{Steam}	Steam pressure	$P_{[1]}$	182	bar
$h_{water,in}$	Drum inlet water enthalpy	$h_{[23]}$	1233	kJ/kg
$h_{steam,out}$	Drum outlet steam enthalpy	$h_{[14]}$	2473	kJ/kg

[1] Average values for a standard operating condition of 360 MW output.

The calculation procedure employed in the solution script is presented in Table 3.2 and was implemented with the aid of EES (Engineering Equation Solver) software [F-

Chart Software, 2019]. The proposed integral model is mostly a straight-forward sequence,

Table 3.2 – Coal combustion calculation procedure.

Step	Description	Equation	Table
1	St[1] Combustion: calculating of molar fractions (from coal composition)	-	3.5, 3.6
2	St[1] Combustion: element conservation balance	3.1	-
3	St[1] Combustion: calculating of equivalence ratio	-	3.3
4	EA[2] Combustion: calculating of molar fractions (from coal composition and flow rates)	-	3.5, 3.6, 3.3
5	EA[2] Combustion: element conservation balance	3.2	-
6	EA[2] Combustion: calculating of equivalence ratio	-	3.3
7	EA[2] Combustion: Estimation of LHV[3]and HHV	3.4 and 3.5	3.6
8	EA[2] Combustion: adiabatic flame temperature	3.3, 3.6, 3.7	-
9	EA[2] Combustion: heat exchange with water-wall	3.7	3.3
10	EA[2] Combustion: flue gas temperature	-	-
11	EA[2] Combustion: calculating of molar and mass fractions	-	-
12	EA[2] Combustion: calculating of NO	3.9, 3.10, 3.11	-

[1] Stoichiometric condition;
[2] Excess air condition;
[3] LHV from laboratory report was adopted;

however, it requests a numeric interactive routine to solve the involved equations. The stoichiometric condition (St) is determined in steps 1 to 3 for the given coal composition. The excess air operational condition (EA) is considered by recalculating molar fractions and performing an element balance in steps 4 and 5. The LHV was determined by means of Equation 3.5 and it is independent of process conditions, while the adiabatic flame temperature T_{af} and the flue gas temperature $T_{g,out}$ are strongly dependent on process parameters. The first temperature is calculated by Equation 3.6, and the last one, after the energy balance, on Equation 3.8. The total NO concentration is the summation of the Thermal NO, Equation 3.9, and Fuel NO, Equation 3.11, contributions.

A reference case assembled to validate the model is presented, considering the input values from Table 3.3, with coal composition in wet and dry basis from *Sample 1* coal, in addition to actual operational flow rates. Simulation results were compared to PECÉM power plant measured data in Table 3.4. LHV and HHV were calculated by means of Equations 3.4 and 3.5, and compared with laboratory reported values, reaching normalized deviations below 2%. NO formation was predicted below the actual measured

Table 3.3 – Model validation coal *Sample 1*- Elemental composition and average process parameters.

Variable	Dry basis	Wet basis	Process setup	Unit
Carbon	72.36	61.4	-	%
Hydrogen	5.13	4.35	-	%
Nitrogen	1.48	1.26	-	%
Sulphur	0.68	0.58	-	%
Oxigen	12.25	10.39	-	%
Ash	8.1	6.87	-	%
Moisture	-	15.15	-	%
$\dot{m}_{coal}$	-	-	37.26	kg/s
$\dot{m}_{air}$	-	-	362.15	kg/s
$\dot{m}_{steam}$	-	-	343.86	kg/s

Table 3.4 – Model validation coal *Sample 1* - results.

Parameter	Simulation (SP 1)	Measured data[1]	Unit	Deviation[1]
LHV	28844	28333	kJ/kg	1.82%
HHV	28954	29343	kJ/kg	-1.32%
NO	1.63E-06	1.57E-05	kmol/m^3	-89.61%
SO_2	1008	1059	mg/m^3	4.82%
O_2	3.4	2.21	%	53.85%
CO_2	14.03	12.23	%	14.72%
$T_{g,out}$	1373	1159	°C	18.46%

[1] Relative deviation to measured data.

data indicating the necessity of further developments. NO formation is strongly dependent on temperature and species-concentration, and could be more accurately predicted if temperature profile along burnout zone was available. SO_2 prediction presented good agreement, while CO_2 14.72% normalized deviation to measured data is quite reasonable. The O_2 deviation could be related to analyzer accuracy, or delay time of the control system. Although predictions showed some relevant biases, the model can be considered a reasonable first approach to the combustion process, with respect to a common magnitude order. Still, the model requires further analysis to mitigate the presented deviations.

Flue gas temperature at the furnace outlet, $T_{g,out}$, was choose as main comparison variable. As temperature was note physically measured at the furnace outlet, it was estimate by considering an energy balance in SH2. It was assumed that SH2 has an

efficiency of 1, hence $T_{g,out}$= 1159°C was found. Simulated result for that temperature deviates from 18.46% with respect to measured data. However, if efficiency of 0.8 is assigned to SH2 (more realistic value) the reference temperature would be about $T_{g,out}$= 1226°C, and the model normalized deviation would become 11.9%, indicating the model relative capacity to reproduce furnace behavior. Figure 3.4a displays the temperature profile provided by the CFD model of the 600 MW tangentially coal-fired boiler studied by Chen et al., 2017. The flue gas temperature at the furnace outlet is about 1327°C. Likewise, Figure 3.4b indicates 1427°C as a suitable flue gas temperature for coal-fired furnaces [Babcock and Wilcox, 1992]. Nonetheless, CFD models from different boilers can only give a clue to the temperature profile. Accurate results could be achieved by means of CFD model applied to PECÉM furnace, validated with real measurements.

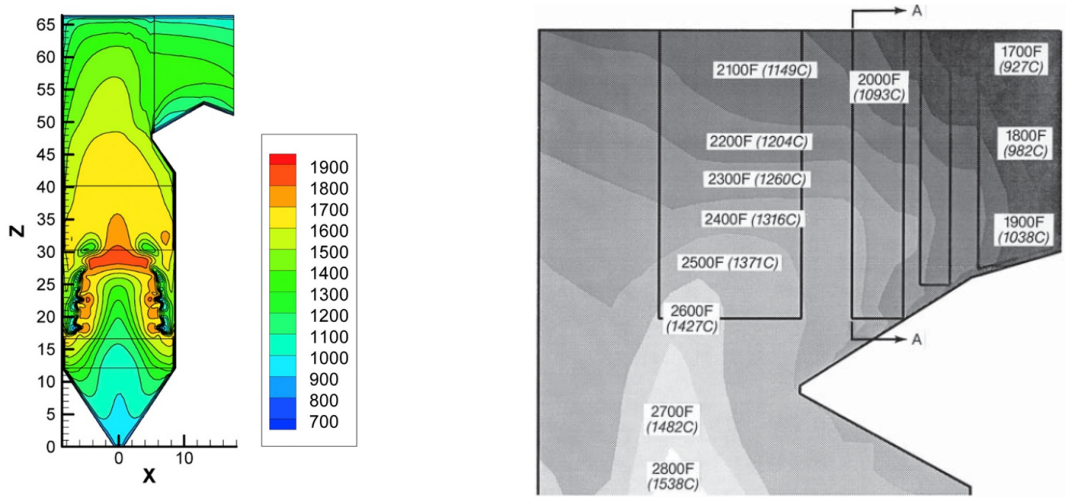

(a) (b)

Figure 3.4 – Literature reported values for flue gas temperature in coal-fired boiler furnaces. (a) Contours of the temperature on the central vertical cross-section *Case 7: FF-WTFB*, in a coal furnace CFD model [Chen et al., 2017]; (b) Numerical modeling results - flue gas temperature profile at coal-fired furnace outlet [Babcock and Wilcox, 1992].

3.5 Analysis of Different Coals

Simulation model was tested for three coal samples, from plant data history, namely Sample 1, 2 and 3. Their immediate and ultimate analysis in wet and dry basis are

compiled in Tables 3.5 and 3.6. In addition, coals from four different regions of the globe were used to feed the model, and its composition was gathered from different literature works, as Bhowmick et al., 2017 for Indian coal, [Trent et al., 1982] for American coal, [Silva et al., 2010] for Brazilian coal and [Wütscher et al., 2017] for Colombian coal. Simulations were performed for the process operational parameters, previously presented in Table 3.3.

Table 3.5 – Chemical and physical properties of coals from different regions - Wet basis [Trent et al., 1982; Silva et al., 2010; Wütscher et al., 2017; Bhowmick et al., 2017].

Origin[1]	COL.	IND.	USA	BR	SP1	SP2	SP3
Carbon (%)	63.15	51.72	69.54	27.74	61.50	61.45	61.55
Hydrogen (%)	4.29	3.32	4.26	1.95	4.13	4.27	4.17
Nitrogen (%)	1.09	1.10	1.24	0.51	1.26	1.25	1.28
Sulphur (%)	0.40	0.88	0.71	0.95	0.50	0.67	0.62
Oxigen (%)	11.40	19.06	12.95	6.62	10.74	10.51	10.66
Ash (%)	10.64	22.16	9.20	45.76	6.80	8.00	6.00
Moisture (%)	10.10	1.76	2.10	16.47	15.03	14.34	15.54

[1] COL= Colombia, IND= India, USA = United States of America, BR= Brazil, SP= Samples;

Table 3.6 – Chemical and physical properties of coals from different regions - Dry basis [Trent et al., 1982; Silva et al., 2010; Wütscher et al., 2017; Bhowmick et al., 2017].

Origin[1]	COL.	IND.	USA	BR	SP1	SP2	SP3
Carbon (%)	69.42	52.65	71.03	33.21	72.41	71.33	73.03
Hydrogen (%)	4.72	3.38	4.35	2.33	4.86	4.96	4.95
Nitrogen (%)	1.20	1.12	1.27	0.61	1.48	1.45	1.52
Sulphur (%)	0.44	0.90	0.72	1.14	0.59	0.78	0.74
Oxigen (%)	12.53	19.40	13.23	7.93	12.65	12.20	12.65
Ash (%)	11.70	22.56	9.40	54.78	8.01	9.29	7.12
C/H ratio (-)	14.7	15.6	16.3	14.3	14.9	14.4	14.8

[1] COL= Colombia, IND= India, USA = United States of America, BR= Brazil, SP= Samples;

As the elemental composition changes from coal to coal, comparisons must be done on a normalized basis to avoid discrepancies. A steady 346 MW electric production was chosen as the baseline for all simulations, whose results for general operating parameters are presented in Table 3.7, while predicted flue gas composition are in Table 3.8. As expected, different coal LHV lead to variable coal consumption and air mass flow rates.

Table 3.7 – Model results: Process parameters for simulations with generation power fixed in 346 MW and excess air $\lambda = 1.19$.

Origin[1]	COL	IND	USA	BR	SP1	SP2	SP3	Unit
LHV	27846	19090	27746	13136	29455	28881	29359	kJ/kg
$\dot{m}_{coal}$	39.57	57.73	39.72	83.89	37.41	38.16	37.54	kg/s
$\dot{m}_{air}$	382.2	430.5	419.6	358.6	359.9	364	359.4	kg/s
$\dot{m}_{Fluegas}$	421.8	488.2	459.4	442.5	397.3	402.1	397	kg/s
Res.Time	1.799	1.677	1.497	2.115	2.007	1.978	2.033	s
T_{af}	2106	2031	2123	1912	2098	2097	2094	°C
$T_{g,out}$	1422	1298	1597	1101	1340	1344	1321	°C

[1] COL= Colombia, IND= India, USA = United States of America, BR= Brazil, SP= Coal Samples from PECÉM

Table 3.7 shows that higher rank coals, i.g., USA and COL, require lower quantities to generate the same output power, due to its higher levels of Carbon and Hydrogen, and consequently higher LHV. Higher flue gas temperature is also a consequence of coal carbon and hydrogen content. Although the $\dot{m}_{coal}$ varies significantly as a function of the LHV, the air mass flow rate $\dot{m}_{air}$ does not, as presented in Figure 3.5. For low-rank coals, such as Brazilian, greater $\dot{m}_{coal}$ is required. However, since the carbon and hydrogen contents are lower, and the output power is fixed at 346 MW, the necessary air to ensure excess air, $\lambda = 1.19$, is not much different from other coals, as observed in the air mass flow rate, Figure 3.5. Nonetheless, those differences impact on other parameters such as the particles residence time, NO formation, ash concentration, and total pollutant emission.

More evident deviation were found in Figure 3.6 where the adiabatic flame temperature and the final flue gas temperatures are presented. Although the adiabatic flame temperature T_{af} was found to be around 1159°C, the so-called real flue gas temperature can display higher deviations, as for the USA coal with 1597°C, and the Brazilian coal with 1101°C. Flue gas temperature is affected directly by the coal LHV, which is determined by Equation 3.4 being dependent on the coal composition (carbon, oxygen, and hydrogen). Aside from its impact on the furnace overall heat exchange, gas temperature highly influences NO formation mechanisms.

Addressing pollutant emission, Table 3.8 brings the model prediction for the mass flow rate of the species in the flue gas (CO_2, H_2O, N_2, O_2, SO_2, Ash) along with the respectively mass fractions and the oxygen concentration X_{O_2}. The ratio C/H is presented

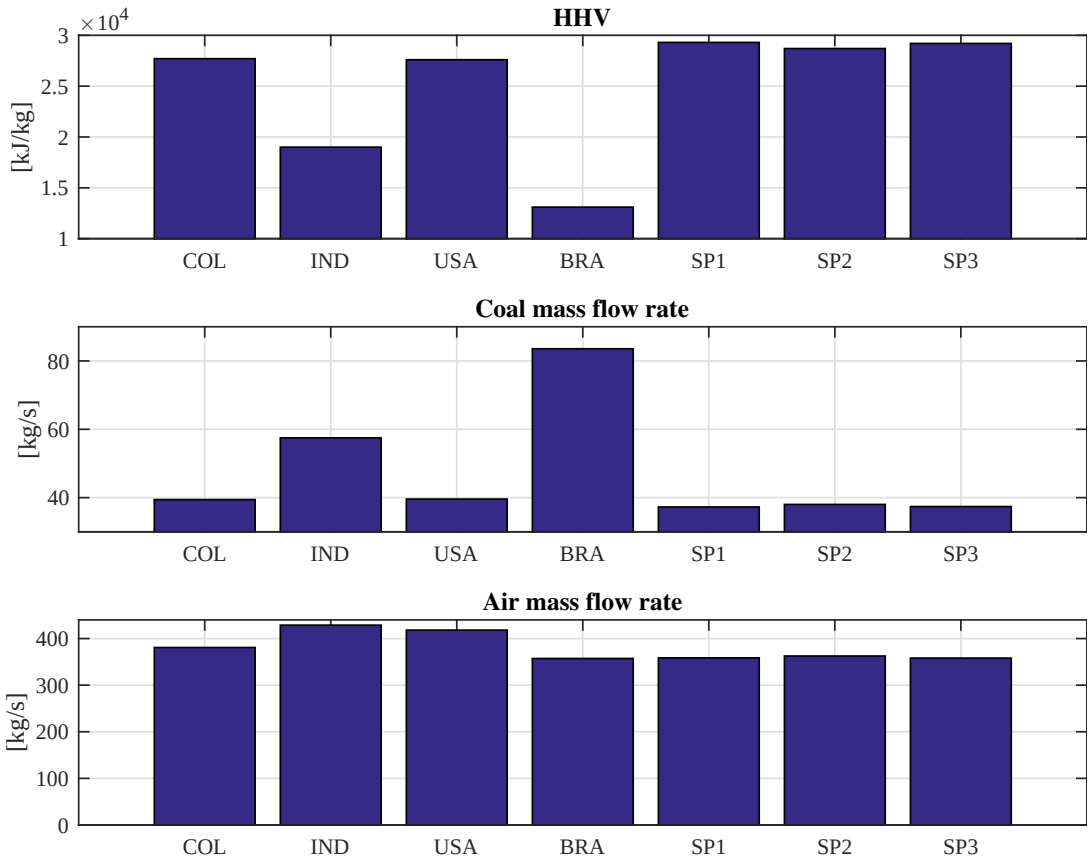

Figure 3.5 – Mass flow rates as a function of coal composition for a fixed 346 MW power generation.

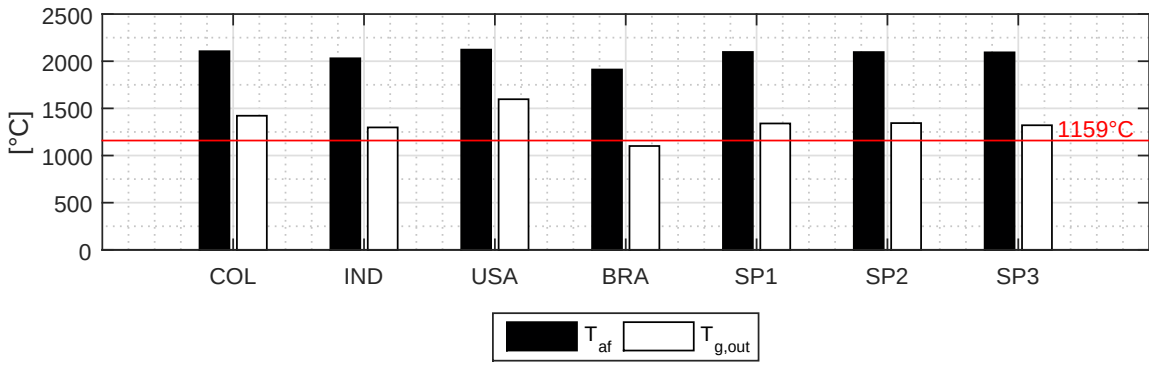

Figure 3.6 – Model result for furnace temperature: Adiabatic flame temperature T_{af} and real temperature $T_{g,out}$ for coals with different composition. $T_{g,out} = 1159°C$ is the measured temperature for the simulated operating condition.

in Figure 3.7, and is related to the amount of air required to promote the combustion. In this analysis the American coal presented the highest value. One of the most important species formed in combustion processes is the carbon dioxide, and its relation with the

Table 3.8 – Model results: Flue gas composition for simulations with generation power fixed in 346 MW and excess air $\lambda = 1.19$.

Origin[1]	COL	IND	USA	BR	SP1	SP2	SP3	Unit
CO_2	90.49	109.40	101.20	85.27	84.17	85.42	84.83	kg/s
H_2O	19.00	18.15	15.95	28.41	20.22	19.96	19.86	kg/s
N_2	293.60	330.80	322.40	275.50	276.50	279.60	276.20	kg/s
O_2	14.25	16.04	15.64	13.37	13.41	13.56	13.40	kg/s
SO_2	0.31	1.02	0.56	1.60	0.43	0.51	0.47	kg/s
ASH	4.16	12.79	3.66	38.39	2.57	3.04	2.26	kg/s
X_{O_2}	3.16	3.13	3.21	2.90	3.13	3.14	3.14	%
Y_{SO_2}	0.0007	0.0021	0.0012	0.0036	0.0011	0.0013	0.0012	kg/kg
Y_{H_2O}	0.0451	0.0372	0.0347	0.0642	0.0509	0.0496	0.0500	kg/kg
Y_{N2}	0.6960	0.6776	0.7017	0.6226	0.6959	0.6954	0.6957	kg/kg
Y_{CO_2}	0.2145	0.2241	0.2203	0.1927	0.2118	0.2124	0.2137	kg/kg

[1] COL= Colombia, IND= India, USA = United States of America, BR= Brazil, SP= Coal Samples from PECÉM;

mass of coal burned is given by the metrics $\text{kg}_{CO_2}/\text{kg}_{coal}$, also presented in Figure 3.7. CO_2

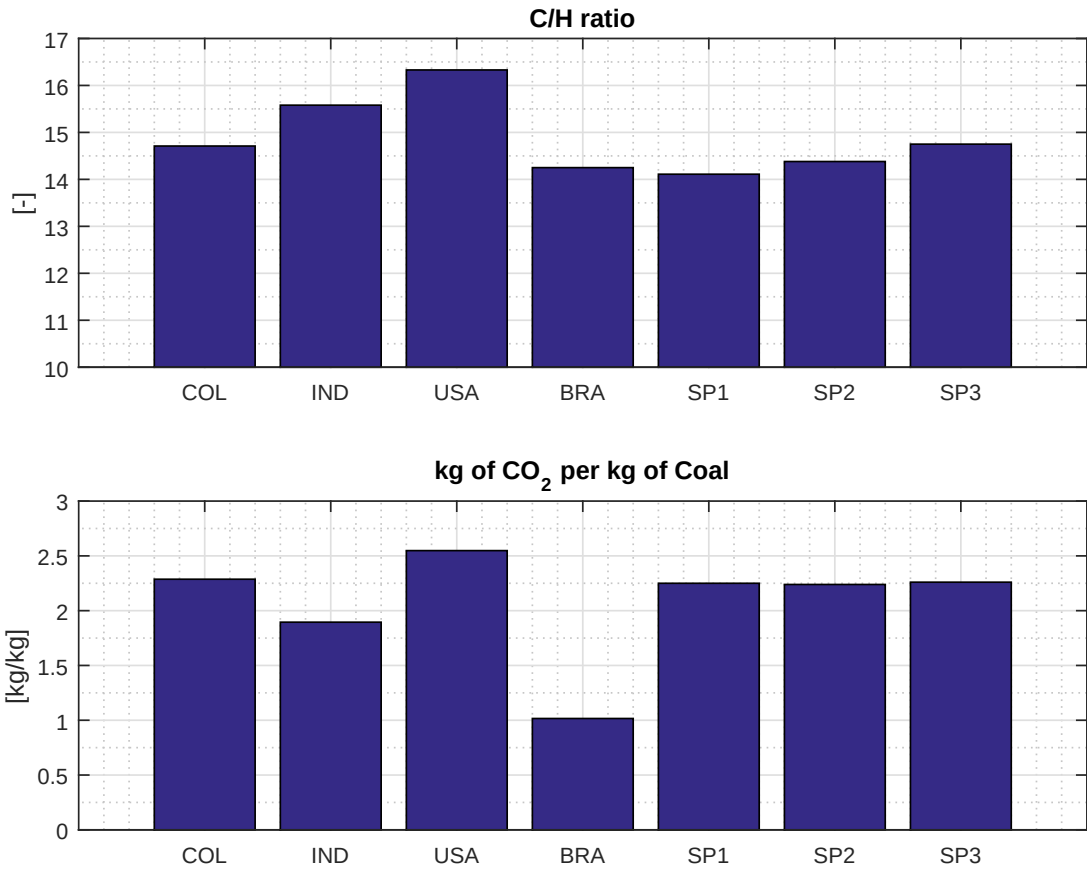

Figure 3.7 – Model result for Carbon and Hydrogen ratio and kg of CO_2 per kg of coal.

concentration is associate with combustion completeness, and it is possible to observe that coal from India and Brazil generate less quantities of CO_2 per kg of coal. At first sight, it appears that these coals produce lower emission rates. Nonetheless, total flow rates must be taken into consideration in order to evaluate the total quantities of pollutants.

Therefore, pollutant formation in kg/s is presented in Figure 3.8 for each species, according to coal composition, for a 346 MW power output. This allows for assessing the effect of various coal and air flow rates in total pollutant emission. Despite the fact that

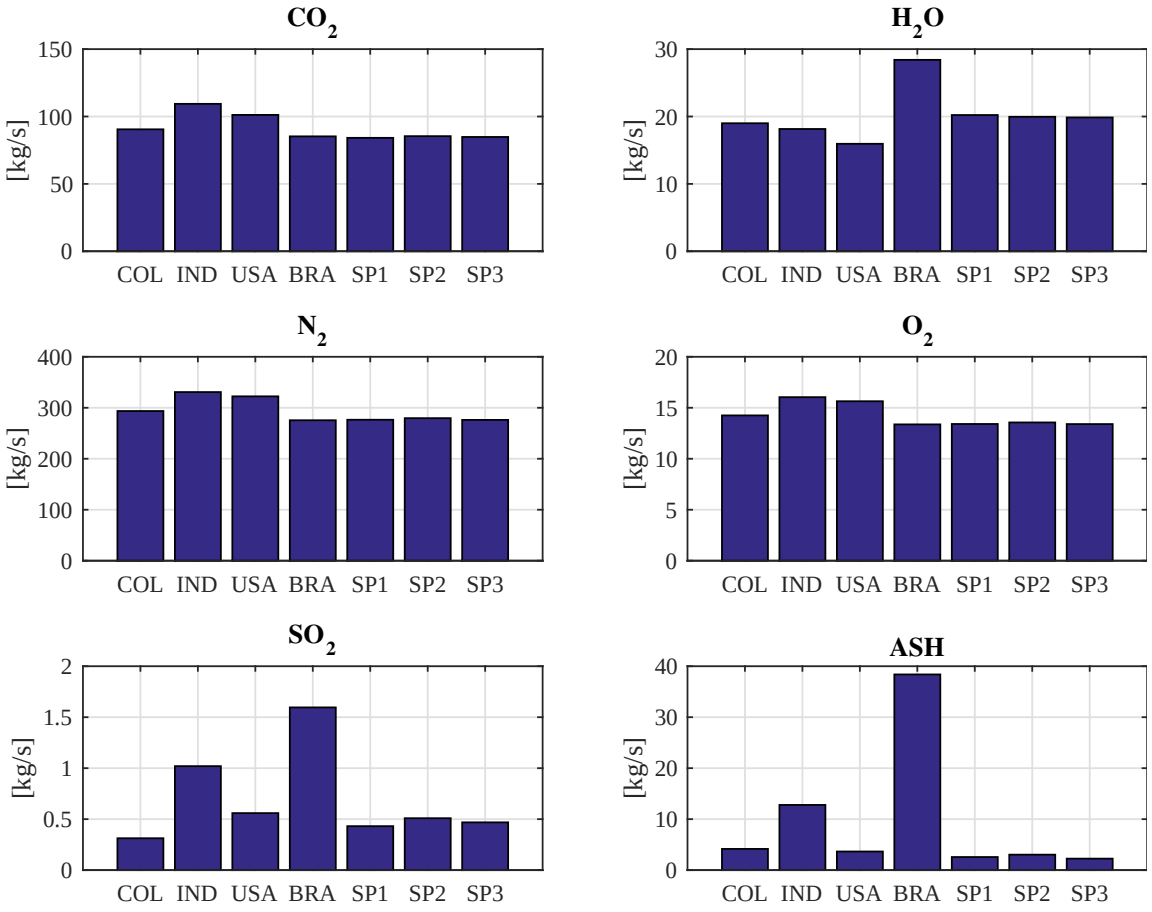

Figure 3.8 – Model results for total pollutant formation in kg/s, for a power generation of 346 MW.

coals with lower LHV demand a higher mass flow rate for the same 346 MW power output, their pollutant emission do not follow the same trend. The American coal, for instance, presents a lower CO_2 total emission than Indian coal, despite showing the highest amount of kg of CO_2 per kg of coal burned. Sulfur dioxide formation, in turn, is mostly dependent on coal sulfur content. This can be observed as the produced amount of SO_2 per second for the USA coal is 45% higher than for the Colombian coal, even though their coal flow

rates are practically equal, and flue gas flow rate differs only 8%. Brazilian coal presents the highest amount of SO_2 emission, due to the coal composition (high level of sulfur). In practical terms, these higher levels could represent problems to the boiler FGD system.

Parallel to gas pollutant control, ash content is also a pressing issue, since it can cause fouling and slag encrustation on water-wall tubes, leading to less-effective heat transfer and tube temperature raising, becoming a real safety problem [Bazzo, 1992; Restrepo et al., 2015]. The proposed model considers ash as inert matter, estimating its amount in the flue gas as a function of coal composition. Outline, the proposed model, despite its accuracy limitation, is able to give an overall picture of pollutant formation and process trends as a function of coal composition, even though it does not solve chemical reaction rates.

3.5.1 Results for NO Formation

The model response regarding NO formation for coals with different compositions is presented in Table 3.9. Table data shows that NO_{Fuel} was the most significantly NO formation mechanism, within the range of 10^{-7} to 10^{-3}, while $NO_{Thermal}$ was between 10^{-14} to 10^{-6}. NO_{Fuel} calculated with Equation 3.11 depends on flue gas temperature, O_2 concentration and HCN converted from coal nitrogen, and becomes the predominant mechanism in fuel-rich regions. For $NO_{Thermal}$, Equation 3.9 shows that O_2 and N_2 concentration are also important in that mechanism, together with flue gas temperature. The NO formation was similar to all coal types, with the exception of USA coal, whose

Table 3.9 – Model results: NO formation.

Origin[1]	$NO_{Thermal}$	NO_{Fuel}	NO_{Total}	Unit
COL	1.75E-08	3.11E-04	2.66E-06	kmol/m^3
IND	1.58E-10	3.03E-05	2.85E-07	kmol/m^3
EUA	2.98E-06	4.07E-03	3.11E-05	kmol/m^3
BR	1.35E-14	1.58E-07	1.75E-09	kmol/m^3
SP1	9.78E-10	9.29E-05	8.46E-07	kmol/m^3
SP2	1.16E-09	9.90E-05	8.98E-07	kmol/m^3
SP3	4.82E-10	6.76E-05	6.24E-07	kmol/m^3

[1] COL= Colombia, IND= India, USA = United States of America, BR= Brazil, SP= Coal Samples from PECÉM;

concentration is much higher, Figure 3.9c. According to Table 3.5 and 3.6, American

coal and samples SP1, SP2 and SP3 share similar chemical composition, differing only in moisture content, and should behave similarly as suggested in Equation 3.9 and 3.11.

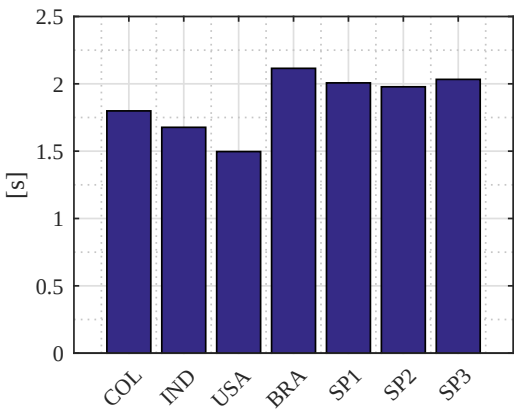

(a) Residence time

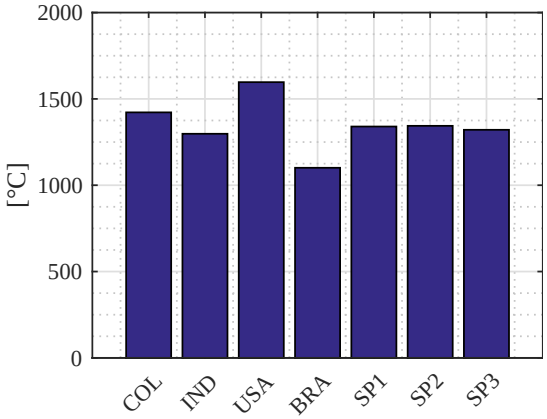

(b) Furnace temperature

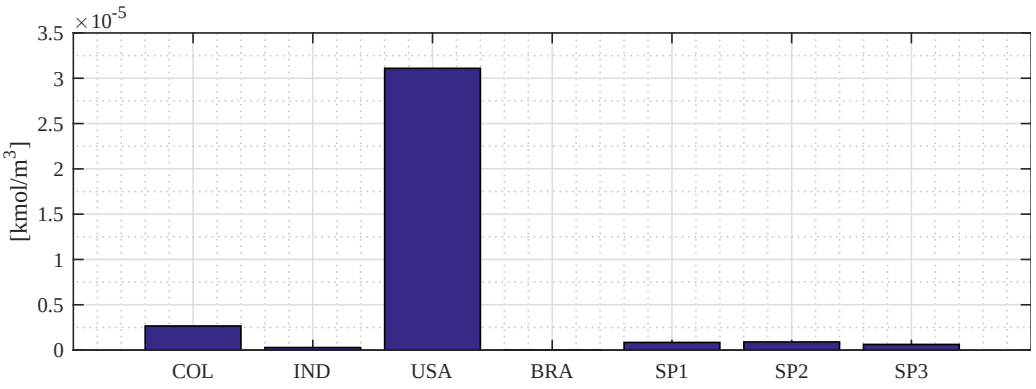

(c) NO Concentration in the flue gas

Figure 3.9 – Model results regarding NO formation for fixed output power of 346 MW.

Another important parameter in NO formation is the residence time, calculated for an imaginary coal particle within the furnace domain, presented Figure 3.9a. The residence time vary for each type of coal due to the coal and air flow rates, $\dot{m}_{coal}$ and $\dot{m}_{air}$, which compose the flue gas flow rate $\dot{m}_{Fluegas}$. The NO formation equations are integrated over the residence time, which varies according to the fuel composition (LHV). Hence, lower flow rates imply greater times leading to higher amounts of NO.

Although the residence time has influence in the NO formation, the flue gas temperature inside the exponential term has greater weight in Equations 3.9 and 3.11. Therefore the discrepancy in the NO generated by USA coal can be related to the furnace higher temperature, and ultimately, to the coal composition including moisture content.

Aside from the NO concentration in kmol/m^3, the total nitrogen oxide formation, kg/s, was also evaluated. The NO total formation results are presented in Figure 3.10, considering a fixed operating condition of 346 MW generation power. Once more the

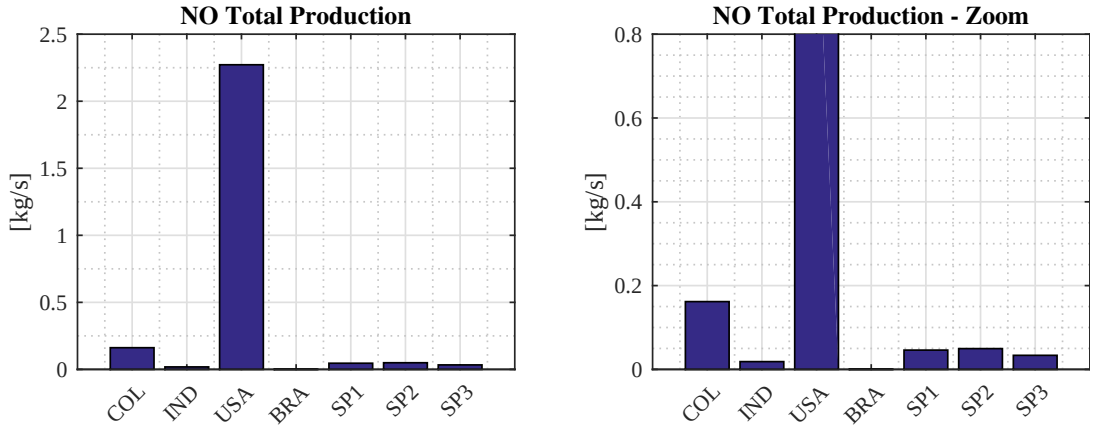

Figure 3.10 – Model results regarding NO total production, in kg/s, for fixed output power of 346 MW.

USA coal presented the highest rate of NO formation. Actually, the total NO formation followed the tendency found for the nitrogen oxide concentration, Table 3.9. In the present analysis, the furnace gas temperature was also the predominant factor for the NO emission. Brazilian coal kept its propensity to produce low amounts of NO, as observed in Figure 3.9c. For this specific coal the low gas temperature combined with low grades of nitrogen in coal composition, justify the result.

3.6 Conclusions

The integral combustion model presented in this chapter allows for a first approach to predict the behavior of the combustion process of a coal-fired boiler. The process output Flue Gas Temperature and fuel LHV and HHV were calculated and compared with measured data from the 360 MW PECÉM power plant, with relative deviations of 18.46%, 1.82% and -1.32%, respectively. Deviations for calculated pollutant species were found to be 4.82% for SO_2, 14.72% for CO_2, -89.61% for NO and 53.85% for O_2. Nitrogen oxide and oxygen presented the highest differences. NO results came out to be relatively far from actual data because the model considers a unique isotherm volume, far from the gas temperature profile along the furnace. It is worth noticing that nitrogen oxide formation is strongly dependent on the flue gas temperature. Oxygen molar fraction

also presented an important relative deviation, but still within an acceptable scale of uncertainty.

Although simple, the proposed approach presented an interesting agreement with process and fuel parameters but showed to be limited for predicting species concentration. The PSR assumption as a uniform and isotherm domain, combined with the lack of reaction rates for each species reflected in results relative inaccuracy. Nonetheless the model still can be used as a guideline for furnace combustion modeling. Further development of the proposed model is required, looking for more accurate predictions allied to low processing effort. Boiler domain discretization into different isotherm zones may be an interesting option to improve accurateness, keeping a reasonably fast processing model oriented to control and decision support.

4 COAL FIRED FURNACE MODELING WITH THE ZONE METHOD

4.1 Introduction

Despite the global migration to renewable energy sources, such as wind and solar, fossil fuels will remain on the basis of the world energy matrix in the near future. Forecast scenarios for developed countries as Germany, where clean energy is fostered, indicate that coal will occupy 25% of the country energy matrix in 2030 and will remain as a relevant option at least until 2050 [Hübel et al., 2017]. China relied on coal to supply 64% of its energy matrix in 2016 [Zhang et al., 2018], within a scenario of continuous energy demand growth. Despite any radical change in energy and environmental policies, coal-fired power plants will be kept operating for longer, reason why it is so important to improve efficiency and mitigate environmental impacts. Among several distinct methods to improve efficiency, control emissions, and ensure safe operation in variable loads, process computational modeling is an attractive approach.

Power plant steam generators can be modeled by several methods, for different purposes. Basically, the furnace models can be divided into two groups: i) Complete mathematical models based on Computational Fluid Dynamics (CFD) and ii) Reactor Network Models (RNM) [Sankar et al., 2019]. Recently, statistical approaches based on large data amount have been explored as well. Computational Fluid Dynamics is a detailed approach to model transport phenomena with high accuracy that has been widely used in recent years. Literature review indicates that accuracy improvement cames prior than response time [Mahmoodi et al., 2017]. CFD models usually demand high computational capacity, and even nowadays with powerful processing devices, the simulations of real scale boilers and furnaces easily take hours or days to converge [Constenla et al., 2013; Crnomarković et al., 2016; Sankar et al., 2019]. From a different point of view, statistical modeling based on artificial intelligence (AI) algorithms uses large amounts of data in order to estimate process behavior. Although fast and powerful, they depend on both reliable data and specialist knowledge about the process. There are situations where this type of model cannot foresee unusual process conditions, moreover, data acquisition is a challenge once it depends on complex control systems, and the accuracy of measurement instruments [Wang et al., 2018].

Reactors Network Models (RNM) can be conceived as control-oriented tools to

model industrial steam generators, composed by simplified descriptions, without losing track of the physics of the problem. This type of approach is based on dividing the domain into a set of reactors, creating a solution mesh not as refined as CFD approaches. Concerning the combustion process, some strategies can be adopted in order to improve calculation routines, avoiding expensive solution times. The same precaution must be respected when solving radiative heat exchange balances, whose non-linearities can easily be time-consuming, even for simple geometries [Zhang et al., 2014]. In this context, the zonal method [Hottel and Cohen, 1958] is an effective alternative for modeling thermal performance of enclosures with participating media like industrial furnaces [Ebrahimi et al., 2013], combining accuracy to solution time.

After ZM became popular by the work of Hottel and Cohen, 1958, reactor network models approaching the radiative heat exchange by means of the zonal method were proposed by different authors. Johnson and Beer, 1973 explored the zonal method in industrial furnaces applications by proposing an emissivity model for clouds of soot particles as a weighted sum of gray gases. Experimental data were gathered in the small scale furnace of the International Flame Research Foundation (IFRF) at IJmuiden, Netherlands. Authors reported small deviations for the model results of gas temperature and heat flux when compared to measured data.

Smith and Smoot, 1980 modeled the combustion and gasification process of pulverized coal, accounting for moisture evaporation, devolatilization, and char combustion. The research focused on the detailed phenomena description despite the limited processing capacity at the time the study was carried out.

A simpler radiation model recast from the zonal method, that neglects the direct radiative interaction of a gas zone with others within the enclosure, was proposed by Ström, 1980. In this alternative approach, named Imaginary Plane Method (IPM) the interface between the zones is made by considering an imaginary plane with unit emissivity. This approach was adopted by several authors when computational effort mattered [Charette et al., 1989, 1990; Zhang et al., 2014].

Zonal method and IPM are still suitable approaches for radiation in industrial furnaces nowadays, especially if current computational processing capacity is taken into consideration. Zhao et al., 2017, for instance, modeled a Low-NO_X utility boiler furnace by subdividing the furnace domain into slab zones, where energy balances allow for the

calculation of gas temperature and heat fluxes. The combined application of the RNM with a gray box model assessed by the authors suggests the suitability of ZM and IPM to control-oriented models.

In the present chapter, a coal-fired steam generator furnace was modeled with the aid of the zonal method. Code accurateness was primarily compared to both calculated and experimental data published by Ström, 1980, which allowed to simulate the steam generator furnace from PECÉM power plant. Outputs as flue gas temperature, heat flux, and chemical species formation were compared with PECÉM records and the computational processing time was also evaluated.

4.2 Mathematical Formulation

The zonal method was first proposed by McAdams and Hottel, 1954 and consists in subdividing the non-isothermal and inhomogeneous furnace domain into isotherm and homogeneous surface and gas-volume zones. The method is based on the calculation of the Direct Exchange Areas - DEA, that relate all domain zones, and represent the fraction of radiant energy that leaves a given zone and directly reaches other given ones, as a function of their geometry and the medium radiant characteristics. DEA can be determined by means of the following relations [Hottel and Sarofim, 1967]:

$$\overline{s_i s_j} = \int_{A_i}\int_{A_j} \tau(r)\frac{\cos\theta_i \cos\theta_j}{\pi r^2} dA_j dA_i, \tag{4.1}$$

$$\overline{g_i s_j} = \int_{V_i}\int_{A_j} \frac{\tau(r) K_i \cos\theta_j}{\pi r^2} dA_j dV_i, \tag{4.2}$$

$$\overline{g_i g_j} = \int_{V_i}\int_{V_j} \frac{\tau(r)\ K_i}{\pi r^2} dV_j dV_i. \tag{4.3}$$

Term $\tau(r)$ is the fraction of radiant energy that is transmitted, described as $\tau(r) = exp^{-\int_0^r K dr}$, with r the straight line that connects the center of two selected zones, and $\cos\theta_i$ and $\cos\theta_j$ the angles between r and the respective normal direction of zones i and j, and K_i is the gas absorption coefficient[1]. Equation 4.1 indicates the DEA between two surface zones, Equation 4.2 the exchange between a surface zone and a gas-volume zone and Equation 4.3 the exchange between two gas-volume zones. The DEA were determined by the polynomial correlations proposed by Tucker, 1986, presented in Annex I. Next step

[1]In this chapter, K stands for the gas absorption coefficient integrated over the entire spectrum.

concerns the computation of the simultaneous effect due to the incident radiation coming from all zones, with multiple reflections inside the enclosure, solved by means of the Total Exchange Area TEA concept, which allows simplifying the solution of the energy balance equations. The TEA calculation procedure, presented by McAdams and Hottel, 1954 and Hottel and Sarofim, 1967, consists in setting to zero the emissive power of all zones but one, and accounting the multiple reflections for this condition. This operation is performed until all zones contributions are computed, and an overall relation is found.

Finally, one energy equation must be stated for each zone, leading to a closed system of **N** equations and unknowns. For a surface zone, considering the boundary condition of unknown temperature, the energy balance equation is

$$\sum_j \overrightarrow{S_j S_i} E_{s,j} + \sum_j \overrightarrow{G_j S_i} E_{g,j} - A_i \epsilon_i E_{s,i} + h_i A_i (T_{g,k} - T_{s,i}) = Q_{net,i} \tag{4.4}$$

with $T_{g,k}$ the adjacent gas-volume temperature. The first and second terms in the left-hand side of the equation stand for the radiation received from other surfaces and gas zones, respectively. The third term represents the emitted radiation. Convection is accounted for the relation $h_i A_i (T_{g,k} - T_{s,i})$, and the energy through the surface is represented by $Q_{net,i}$. The gas-volume zone balance requires a different energy equation, stated as

$$\sum_j \overrightarrow{G_j G_i} E_{g,j} \; + \; \sum_j \overrightarrow{S_j G_i} E_{s,j} \; - \; \sum_j 4 a_{g,n} \, K_n \, V_i \, E_{g,i} \; + \; Q_{e,i} \; = \; Q_{u,g_i} \; - \; Q_{c,i} \tag{4.5}$$

that comprehends the radiant heat received from all surface and gas zones (first and second terms in the left-hand side of the equation) and the radiation emitted to them, represented by the third term. Additionally, three terms of energy source/sink are included: the energy rate release by combustion $Q_{c,i}$, the transient term Q_{u,g_i}, and the rate of change in the sensible enthalpy of a gas between the control volume inlet and outlet, plus the convection from any surface adjacent to the gas-volume $Q_{e,i}$. Gas-volumes are modeled like Perfect Stirred Reactor (PSR). The energy released in the combustion process is estimated by the coal LHV and its mass flow rate.

The energy balance in the furnace domain is depicted in Figure 4.1, where the application of the first law, in steady-state regime, is expressed by Equation 4.6.

$$\Delta Q \; = Q_{outlet} \; - Q_{inlet} \tag{4.6}$$

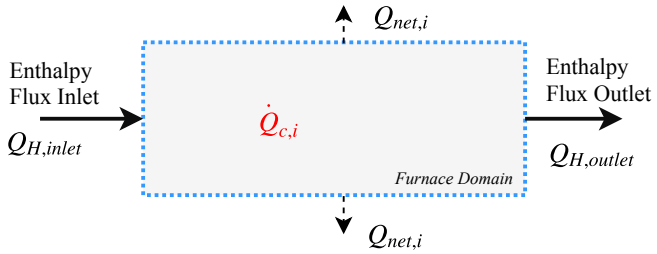

Figure 4.1 – Furnace domain global energy balance.

$$Q_{outlet} = \sum_{i=1}^{N} Q_{net,i} + Q_{H,outlet} \tag{4.7}$$

$$Q_{inlet} = \sum_{i=1}^{N} Q_{comb,i} + Q_{H,inlet} \tag{4.8}$$

Outgoing energy Q_{outlet}, Equation 4.7, is composed by the sum of the net outgoing energy of each of the N zones, plus the enthalpy term $Q_{H,outlet} = \dot{m}\, C_p\, T_{outlet}$, assuming positive values when energy leaves the control volume. Q_{inlet} from Equation 4.8 is composed by the sum of the heat released by the combustion process associated to the N gas zones plus the incoming fuel enthalpy, represented by $Q_{H,inlet} = \dot{m}\, C_p\, T_{inlet}$.

Species are calculated, by element balance, for each of the gas volumes under excess air condition presented in Equation 4.9,

$$\left(n_{coal_C}C + n_{coal_H}H + n_{coal_O}O + n_{coal_N}N + n_{coal_S}S + n_{coal_{H_2O}}H_2O\right) + \lambda n_{air}(O_2 + 3.76N_2) \rightarrow n_{CO_2}CO_2 + n_{H_2O}H_2O + n_{N_2}N_2 + n_{SO_2}SO_2 + n_{O_2}O_2, \tag{4.9}$$

and although soot is an important matter in coal combustion, no model to considering its formation was implemented in the present chapter. The NO formation was adapted from Zhao et al., 2017, with Equation 4.10 for the Zeldovich mechanism

$$\frac{\partial R_{NO-Thermal}}{\partial t} = 3.6 \times 10^{11} exp\left(\frac{-38370}{T_{fg}}\right) C_{N_2} C_O \tag{4.10}$$

with T_{fg} being the furnace homogeneous temperature, C_{N_2} the nitrogen concentration in molar basis, and C_O the O-radical mole fraction, defined as:

$$C_O \approx 12.567 \times 10^3 T_{fg}^{-0.5} exp\left(\frac{-31096}{T_{fg}}\right) \sqrt{C_{O_2}} \tag{4.11}$$

with C_{O_2} the oxygen molar fraction. Regarding the Fuel-NO mechanism, it was assumed that all coal-N is converted into HCN immediately, and then oxidized into NO at the

rate of Equation 4.12.

$$\frac{\partial R_{NO-HCN}}{\partial t} = 10^{10} C_{HCN} C_{O_2}^{b} exp\left(\frac{-33713}{T_{fg}}\right) \tag{4.12}$$

Assuming $b = 0$ for $C_{O_2} > 0.018$ and $b = 1$ for $C_{O_2} < 0.0025$, according to Hill and Douglas Smoot, 2000. Equations 4.10 and 4.12 are presented in derivative form, and are integrated over the residence time t estimated for an imaginary particle.

Heat convection correlations for water walls of pulverized-coal furnaces are scarce in the literature. Cantrell and Idem, 2010 proposed convective correlations for several furnace devices, but none for the water wall area. The authors presented convection heat transfer coefficients that go from 62.5 W/(m^{2}K) for reheaters, and up to 97.7 W/(m^{2}K) for economizers. Nusselt correlations for a flat plane of length X under laminar flow conditions [Bejan, 2004] can be expressed by:

$$\overline{Nu}_x = 0.664\ Re_x^{1/2}\ Pr^{1/3} \tag{4.13}$$

with Re_x the characteristic Reynolds number and Pr the Prandtl number, limited to $Pr \geq 0.6$. The convection heat transfer coefficient $\overline{h}_x$ is determined by $\overline{Nu}_x = \frac{\overline{h}_x X}{k_f}$, where k_f is the thermal conductivity of the fluid, evaluated at the film temperature, in W/(m K). Moreover, for turbulent flow over an isotherm plate, the Nusselt number can be estimated by

$$\overline{Nu}_x = 0.0296\ Re_x^{4/5}\ Pr^{1/3} \tag{4.14}$$

for a Prandtl number range of $0.6 \leqslant Pr \leqslant 60$. Another correlation can be adopted for flat planes submitted to constant heat flux and turbulent flow:

$$\overline{Nu}_x = 0.0308\ Re_x^{4/5}\ Pr^{1/3} \tag{4.15}$$

valid for the same Prandtl number range of Equation 4.14. Flow regime (laminar or turbulent) can be determined by evaluating the flow Reynolds number by two approaches. First furnace internal cross-section can be thought of as a rectangular duct with hydraulic diameter calculated as $D_h = 4A_c/P$, where A_c corresponds to the duct cross-sectional area, and P is the wet perimeter. Another approach is to treat the gas flow as a boundary layer flow over a flat plate (water wall), neglecting buoyancy effects due to high temperatures and velocities. Transition values are: $Re = 2{\times}10^4$ - 10^6 for boundary layer flow, and $Re = 2000$ for duct flow [Bejan, 2004]. Comparisons denote that both approaches

lead to much similar results.

4.3 Method Validation: Strom's Problem

The work presented by Ström, 1980 was chosen to validate the furnace heat exchange model accuracy and reliability. That author was the first to propose the Imaginary Plane Method, which is a simplification of the zonal method. Ström modeled an experimental scale furnace, designed to operate with natural gas and oil in a horizontal burner, as presented in Figure 4.2. This furnace conveniently can be described as a composition of

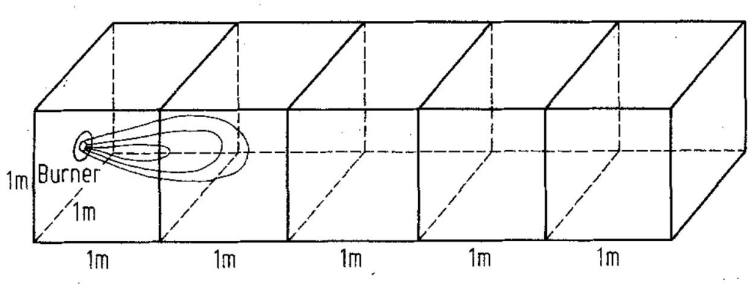

Figure 4.2 – Studied oil/gas furnace [Ström, 1980].

several squares and cubes, which leads to a straightforward application of Tucker's correlations. Figure 4.3 shows the furnace boundary conditions and its geometric description.

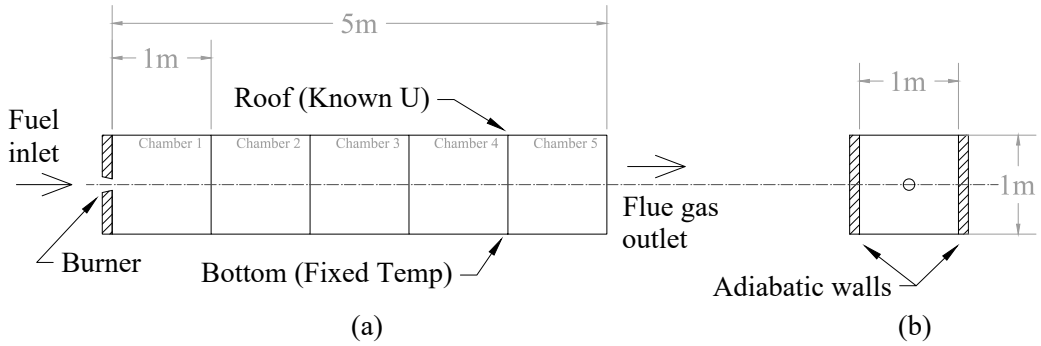

Figure 4.3 – Ström furnace geometry and boundary conditions. a) Right and b)Front views.

The burner was placed in an isolated wall. All side walls are adiabatic (Neumann condition), bottom surfaces were at a prescribed temperature (Dirichlet condition) and roof surfaces exchanged heat to the environment (Robin condition) with an overall heat transfer coefficient of $\overline{U} = 5$ W/(m^{2}K). Different absorption coefficients were associated

with each chamber, both for gas and oil operation. In the present work, average absorption coefficients were adopted for gas and oil ($\overline{K}_{gas}$ =0.26; $\overline{K}_{oil}$ =0.46), based on Ström's values. Additionally, a gas specific heat of 1.674 kJ/(kg K) was adopted, and the ambient temperature was set at T_{amb} =303 K. The fuel inlet temperature was $T_{gas,inlet}$ =1550 K. Emissivities, combustion energy release and other boundary conditions reproduced from Ström's work are shown in Table 4.1.

Table 4.1 – Input parameters adopted to simulate Ström's furnace [Ström, 1980].

Location	K_{gas} (m^{-1})	K_{oil} (m^{-1})	ϵ	Temp. (K)	$\overline{U}$ (W/(m^2K))	Q_{comb} (kW)
Zone 23[2]	0.3	0.8	-	-	-	500[1]
Zone 24[2]	0.2	0.6	-	-	-	500[1]
Zone 25[2]	0.2	0.3	-	-	-	0
Zone 26[2]	0.3	0.3	-	-	-	0
Zone 27[2]	0.3	0.3	-	-	-	0
Roof	-	-	0.5	-	5	-
Floor	-	-	0.87	1798	-	-
Inlet wall	-	-	0.5	-	-	-
Outlet wall	-	-	1	-	-	-

[1] Ström, 1980 considered a fixed combustion energy released only in the two first chambers;
[2] The simulations were performed considering averaged absorption coefficients for all gas zones ($\overline{K}_{gas}$ =0.26; $\overline{K}_{oil}$ =0.46);

No details were mentioned about the fluid exit plane, so it was assumed a free outlet, without any heat exchanger or tube wall, modeled as a near black body at T_{amb}, with $\epsilon_{oulet} = 0.99$, [Incropera et al., 2007], as also adopted by Díez et al., 2005. For the convection heat transfer coefficient a reference value of 1 W/(m^2K) was adopted after Ström, 1980.

4.3.1 Zoning Scheme

The Ström's furnace thermal behavior was solved by means of the zonal method in the present work. In order to do that, the zoning scheme presented in Figure 4.4a and 4.4b was adopted. The burner wall was labeled as zone 1, and then an organized sequence was set for all surface zones placed on the furnace sides, bottom and roof, with surface zone 22 at the furnace outlet. Gas-volume chambers 1 to 5 were labeled as zones 23 to 27.

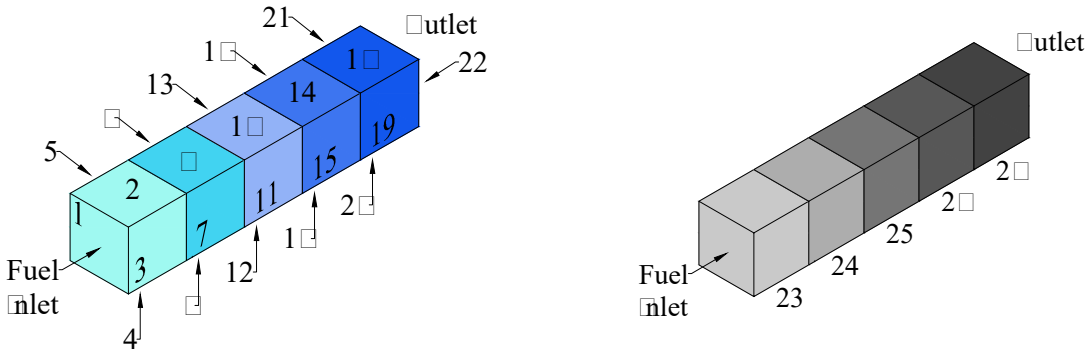

(a) Ström's furnace zoning: surface zones

(b) Ström's furnace zoning: gas zones

Figure 4.4 – Proposed zoning scheme for the simulation of Ström's furnace.

4.3.2 Solution Strategy

The solution strategy presented in Figure 4.5 with the Gray Gas model (GG model) as the choice to simulate the participating media, implemented in a tandem development with Matlab and EES codes. The process starts by declaring the simulation parameters (Process Setup) in order to run the direct exchange area and the Total Exchange Area calculation procedures. At that point, the TEA matrix is transferred to the EES code, which solves the energy balance equations with an improved Newton-Raphson method set to convergence criteria of 10^{-6}. Calculated temperatures and heat fluxes are then handled by Matlab to be displayed on their final form. Calculations are run from Matlab only, who remotely operates EES connection.

4.3.3 Results

Results obtained from the developed code were compared with the ones presented by Ström, 1980 for the two fuel types: natural gas, and oil. Each fuel feeding led to the mass flow rates $\dot{m}_{gas} = 0.3842$ kg/s and $\dot{m}_{oil} = 0.3972$ kg/s, and different gas absorption coefficient, shown in Table 4.1. Figure 4.6 presents roof temperature for zones 2, 6, 10, 14 and 18, and gas temperatures for zones 23, 24, 25, 26, and 27, with natural gas as fuel.

Results from the present work approached the ones reported by Ström, with an -0.36% average deviation for roof temperatures, and -0.87% for flue gas temperatures, which indicates the accuracy of the implemented computational code. Despite the small

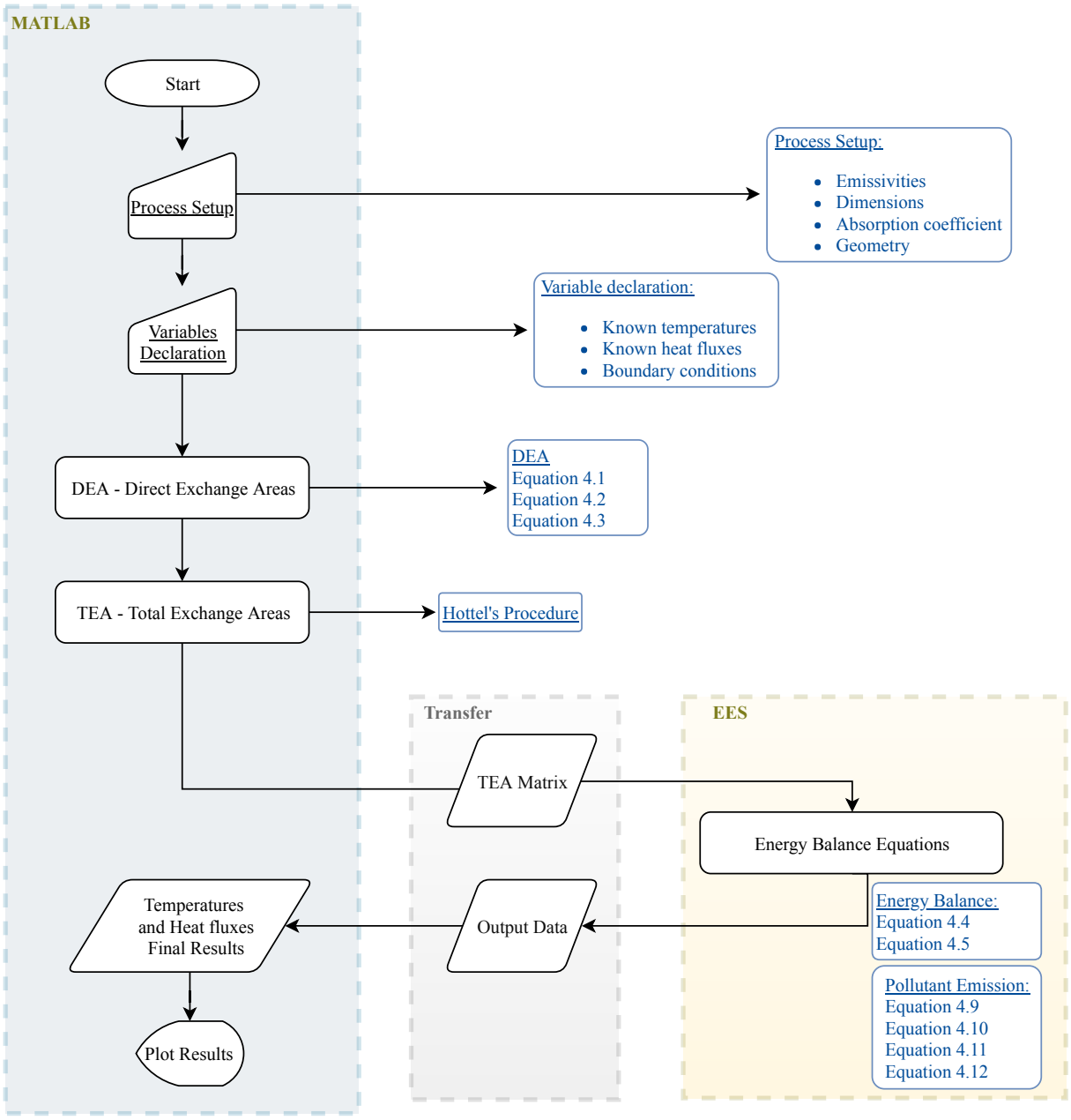

Figure 4.5 – Zonal method gray gas model solution strategy.

average differences of all zones, the 10^{th} surface zone presented a -1.38% deviation that does not seem to be significant at first sight, however, it appears to influence the temperature of its adjacent gas zone. Gas zone 25 displayed a -5.79% deviation, that could probably be explained by the use in the present model of a different gas absorption coefficient. Ström used an individual gas constant for each zone, while the present work assumes a constant average coefficient.

A similar behavior was found when simulations were performed considering oil as fuel, as shown in Figure 4.7.

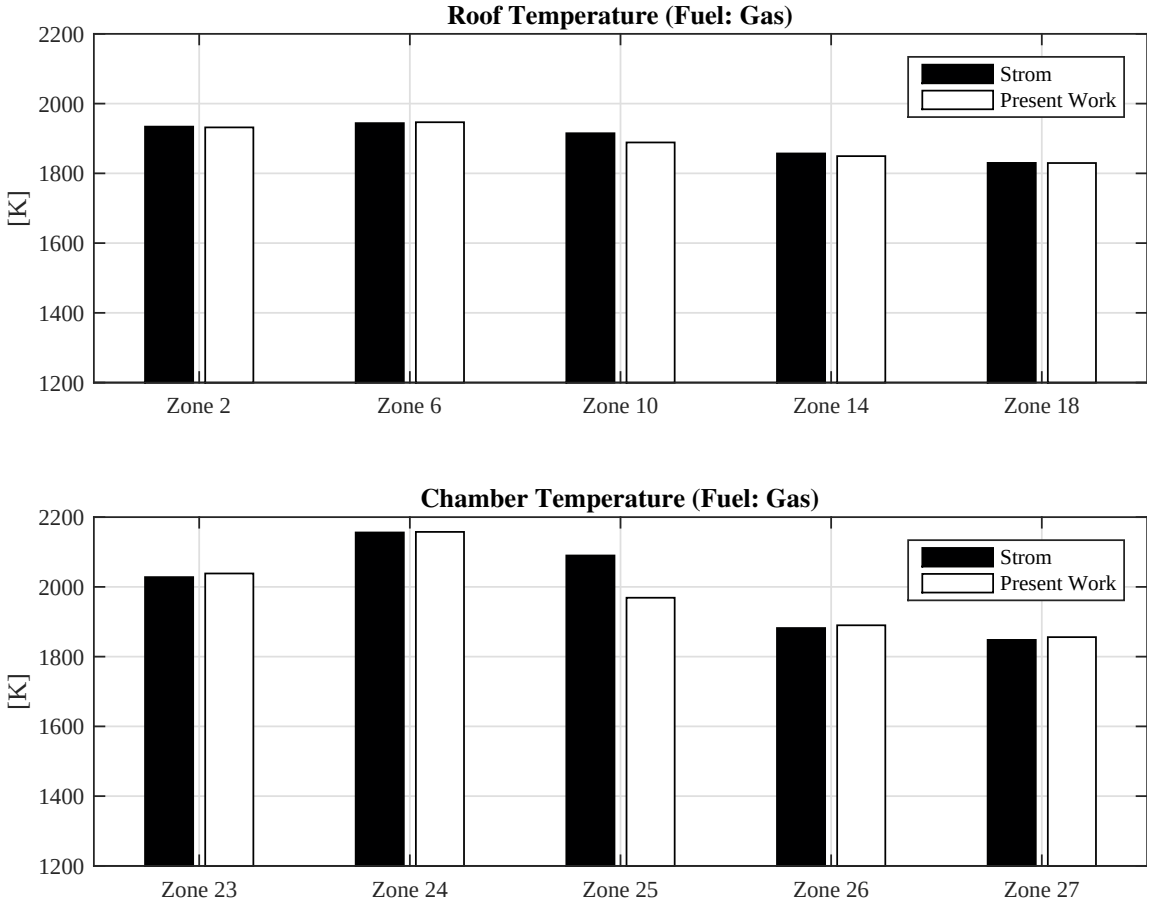

Figure 4.6 – Simulated temperatures in respect to Ström's reported values and model results for natural gas. Zones 2, 6, 10, 14 and 18 are the roof wall. Zones 23, 24, 25, 26 and 27 are the gas zones.

The average deviation remained in the same order as for the former case, with -0.22% for roof temperatures, and -2.53% for gas temperatures. Once again, the highest deviation was found for zone 25 (-7.57%) when compared to Ström's results, which is higher than the deviation found in the gas simulations. In order to test this tendency of higher differences as a function of the absorption coefficient, an alternative simulation was carried out with $\overline{K}_{alt} = 0.6$. Zone 25 deviation reached -8.04%, confirming the tendency, but that observation does not allow for stating that the absorption coefficient is the only discrepancy source, once the DEA correlations were also different of the ones used by Ström.

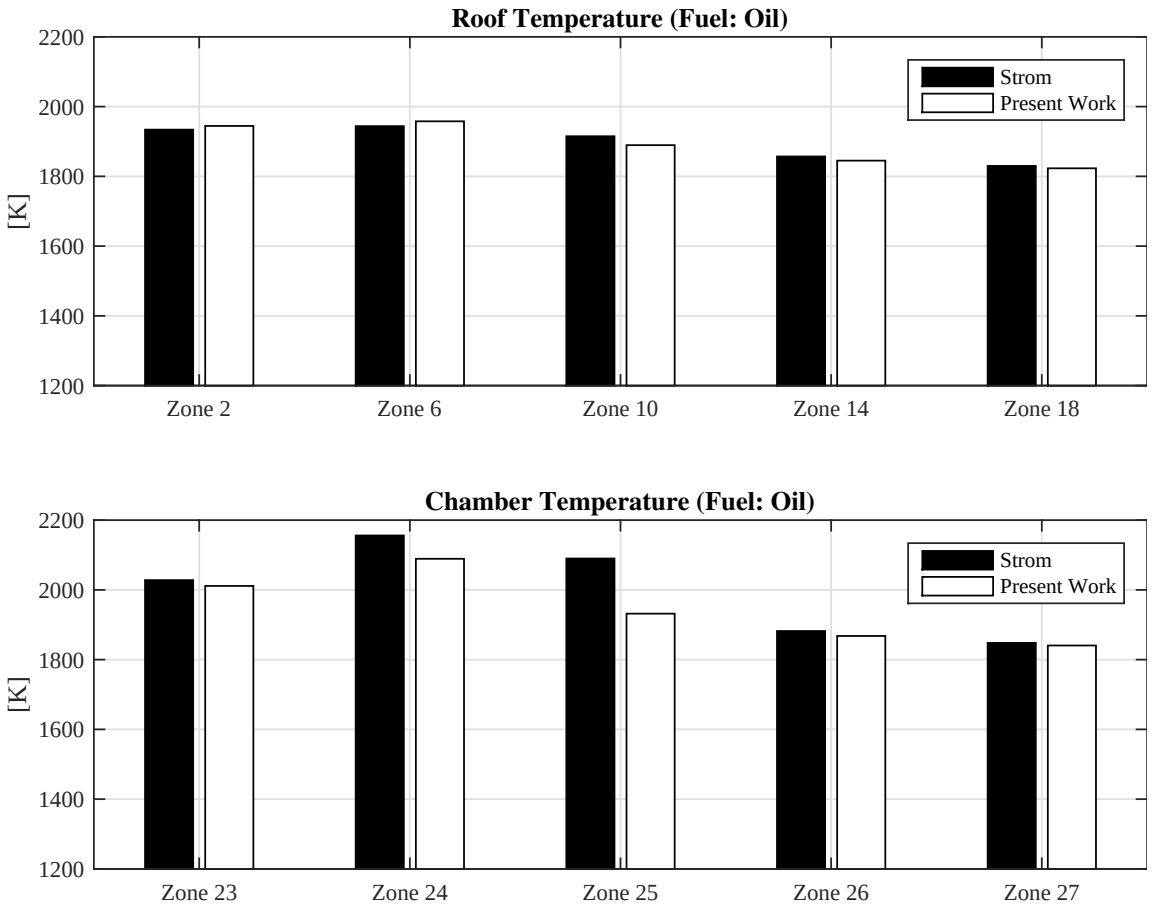

Figure 4.7 – Simulated temperatures in respect to Ström's reported values and model results for oil. Zones 2, 6, 10, 14 and 18 are the roof wall. Zones 23, 24, 25, 26 and 27 are the gas zones.

4.3.4 Sensitivity Analysis

The model sensitivity in respect to input and process parameters was assessed by means of a One-Factor-at-a-Time approach OFaT. The procedure consists in establishing a set of baseline levels for all the chosen input factors, followed by swiping each one of then at a time, along its range, while the remaining factors are kept at their baseline level [Montgomery, 1997]. Five selected parameters were assessed, namely: fuel and air mass flow rates, convection heat transfer coefficient, inlet gas temperature, gas absorption coefficient, and wall emissivity. Baseline values for these parameters, also called factors, are presented in Table 4.2. Fuel type was not assessed at this point, because their influence was already embedded on some of the former factors. Ten different values were selected within each factor range.

Table 4.2 – OFAT baseline factor values and correspondent ranges.

Factor	Value	Unit	Range
Mass flow rate - $\dot{m}$	0.3842	kg/s	$1e^{-20}$ - 0.3842
Convective coefficient - h_{conv}	1	W/(m^{2}K)	0.5 - 100
Gas inlet temperature - $T_{gas,inlet}$	1550	K	1000 - 2000
Absorption coefficient - K	0.5	m^{-1}	0.1 - 0.9
Wall emissivity - ϵ_w	0.5	-	0.1 - 0.95

The first sensitivity result concerns to zone 2 temperature (Figure 4.8), which is the first roof zone starting from the inlet section. Flat horizontal lines indicate factor small influence on the model output.

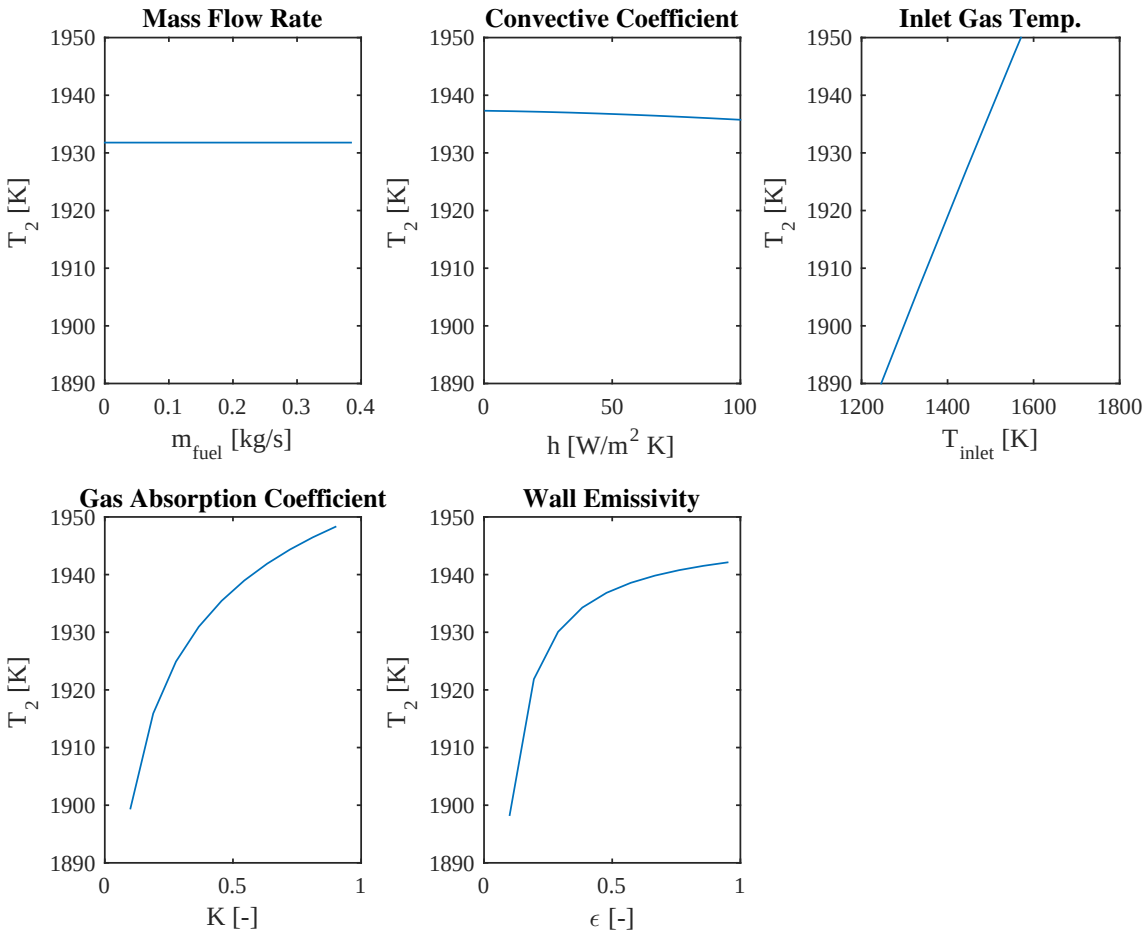

Figure 4.8 – Sensitivity analysis for Ström's furnace simulation. Results for the temperature of first chamber roof, T_2.

Air mass flow rate and fuel did not generate any impact in zone 2 temperature. Although this result seems to be unexpected, it is reasonable according to the model

construction, since it considers a fixed combustion heat release of 500 kW in gas zones 23 and 24, which is not affected by the fuel mass flow rate. Changes in the convection heat transfer coefficient also presented small influence in T_2. Though convection plays a minor role compared to radiation, physical behavior occurs as expected, i.e. higher coefficient means higher convective heat transfer and consequently, lower roof surface temperature.

Ström's furnace operates with their inlet sources at $T_{gas,inlet} = 1550$ K, which influences zone 2 temperature. That impact, although significant, cannot be overestimated, based on physical and practical limits of real furnace preheating systems. Gas absorption coefficient and wall emissivities forced T_2 to behave in a non-linear way and along a similar output range. The span of the factors within their range resulted in T_2 changes up to 2.63% for gas absorption coefficient and 2.1% for wall emissivity. Gas absorption coefficient directly impacts the direct exchange areas and consequently, the energy balances. The higher the K value, lower will be the gas absorption allowing the increase of the radiative heat exchange. The roof temperature intends to rise along, as observed in Figure 4.8. Concerning the wall emissivity, the model behavior is straightforward inferred, once higher emissivities mean the intensification of the radiative heat transfer, and then rising of the surface temperature.

The same sensitivity analysis was performed for gas temperature, T_{27}, at the output of the last furnace chamber. The same factors of the previous analysis were evaluated, over the same range. Results for temperature T_{27} were significantly distinct from the ones presented in Figure 4.8, except for mass flow rate and the convective heat transfer coefficient, that conserved similar behavior. The inlet gas temperature, although keeping the tendency to increase T_{27}, displayed smaller influence in that case. Wall emissivities seemed to have no impact in T_{27} since it remained almost constant over the entire range of ϵ.

Perhaps the most interesting result in this second sensitivity analysis lied on the behavior of T_{27} as a function of the gas absorption coefficient. With decreasing K, the gas transmissivity, $\tau(r) = exp^{-\int_0^r K dr}$, decreased as well and the emitted and absorbed radiation in Equation 4.5 led the gas temperature to decrease, also in a non-linear way. Gas absorption coefficient generated changes of 5.46% in the gas temperature of the last chamber, T_{27}.

The above results indicates that the zonal method procedure was correctly imple-

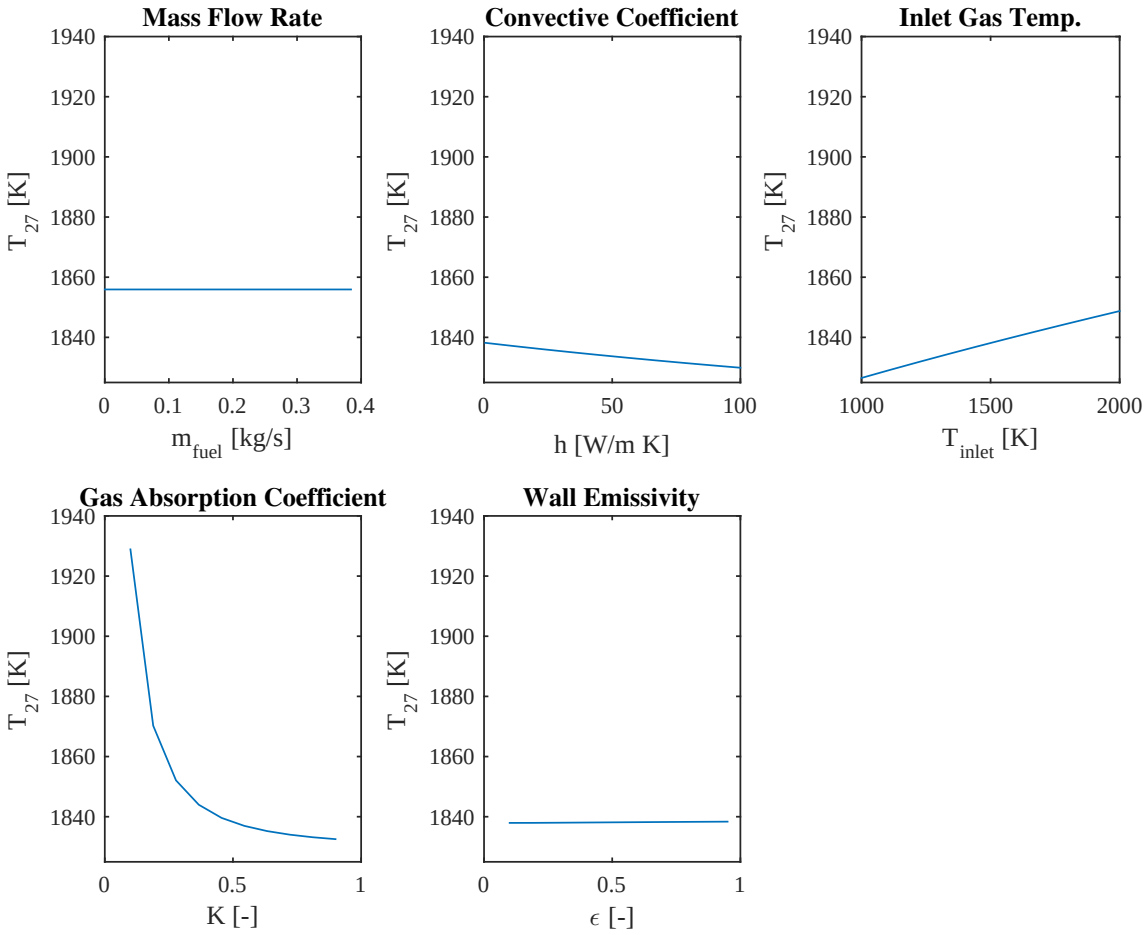

Figure 4.9 – Sensitivity analysis for Ström's furnace simulation. Results for the temperature of the last gas chamber T_{27}.

mented for a gray gas approach, generating outputs with small relative deviations to the values presented by Ström. Moreover, sensitivity analysis indicates that gas absorption coefficient and wall emissivities are the most relevant parameters to be observed in further developments.

4.4 Zonal Method Applied to PECÉM Furnace

In this section simulations were performed with actual operational data from one of the three 360 MW electric generation boilers of EDP PECÉM power station, located in São Gonçalo do Amarante in Ceará - Brazil. Two assessments were developed. First, a 5-chamber zoning scheme was fed with operational data from PECÉM power plant, aiming to produce data to a response surface method (RSM) analysis. Secondly, a 2-chamber model was implemented in order to describe PECÉM boiler operation. Next two subsec-

tions present the combustion model and wall temperature calculations, common to both 5 and 2-chamber zoning schemes. Finally, simulation results for these zone approaches are discussed.

4.4.1 Combustion Process

The adopted combustion model takes as inputs the coal composition and the coal to air rate. Higher heating value and lower heating value are informed in laboratory reports from PECÉM power station. The energy introduced in the system by the fuel Q_{comb} is then calculated by Equation 4.16.

$$Q_{comb} = LHV_{coal}\,\dot{m}_{coal} \tag{4.16}$$

The magnitude order of the main chemical species in the flue gases was estimated by the element balance presented in Equation 4.17.

$$\begin{aligned}&\left(n_{coal_C}C + n_{coal_H}H + n_{coal_O}O + n_{coal_N}N + n_{coal_S}S + n_{coal_{H_2O}}H_2O\right) + \lambda n_{air}(O_2 + 3.76N_2)\\ &\rightarrow n_{CO_2}CO_2 + n_{H_2O}H_2O + n_{N_2}N_2 + n_{SO_2}SO_2 + n_{O_2}O_2\end{aligned} \tag{4.17}$$

4.4.2 Flow Pattern

As each gas volume was treated as a PSR, receiving coal and air from the burners, complete combustion hypothesis was assumed, and each chamber presented its own input parameter relations, boundary conditions, and consequently, gas temperature and species concentration as Figure 4.10 depicts. The unburned fuel is not considered in the present model. One dimensional flow pattern was assumed. Each zone receives only a fraction f_i of the total coal and air mass flow rate entering the furnace domain, $\dot{m}_{coal,total}$ and $\dot{m}_{air,total}$. Inlet mass flow rate for zone i, in kg/s, is presented by Equation 4.18 while outlet flow rate is expressed by Equation 4.19.

$$\dot{m}_{i,inlet} = f_i(\dot{m}_{coal,total} + \dot{m}_{air,total}) \tag{4.18}$$

$$\dot{m}_{i,outlet} = \dot{m}_{i,inlet} \tag{4.19}$$

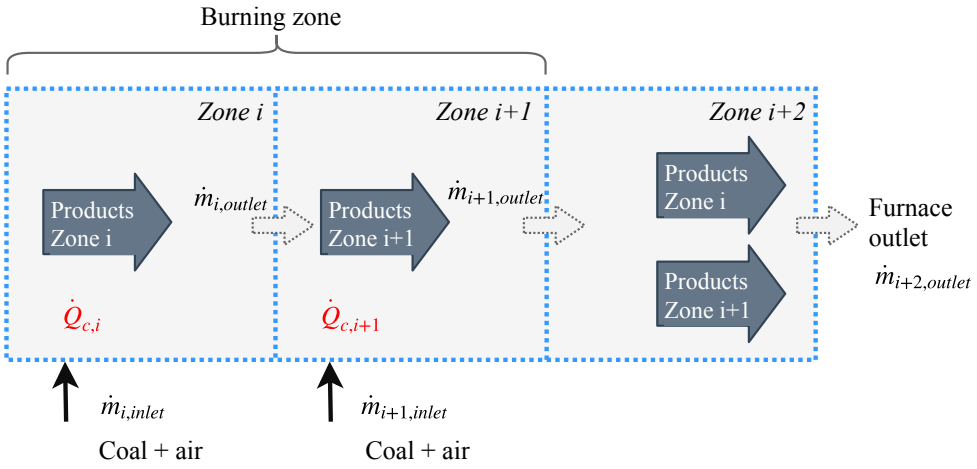

Figure 4.10 – Flow pattern in Furnace domain and outlet weighting.

When OFA is active, zone $i+1$ has its inlet flow rate described by Equation 4.20. Its outlet flow rate is described by Equation 4.21.

$$\dot{m}_{i+1,inlet} = f_{i+1}(\dot{m}_{coal,total} + \dot{m}_{air,total}) + \dot{m}_{OFA} \tag{4.20}$$

$$\dot{m}_{i+1,outlet} = \dot{m}_{i+1,inlet} + \dot{m}_{i,outlet} \tag{4.21}$$

The concentration of a given species at the furnace outlet is weighted by the respective zone flow rate. CO_2 concentration, for instance, was calculate by means of Equation 4.22.

$$CO_{2(outlet)} = CO_{2(i)}\left(\frac{\dot{m}_{i,inlet}}{\dot{m}_{i+2,outlet}}\right) + CO_{2(i+1)}\left(\frac{\dot{m}_{i+1,inlet}}{\dot{m}_{i+2,outlet}}\right) \tag{4.22}$$

Where $\dot{m}_{i+2,outlet} = \dot{m}_{i+1,outlet} = \dot{m}_{i,inlet} + \dot{m}_{i+1,inlet}$. The same procedure was carried out for other species.

4.4.3 Water Wall Temperature

The following model was proposed to estimate the external temperature of PECÉM furnace water-wall, based on the assumption that the power plant working fluid (water) that flows along these walls operates under phase change condition. Water at liquid phase is admitted at the bottom drum, boils along the water-walls to be finally collected as saturated vapor at the upper drum. A simplified description of the conductive heat transfer across a cylinder section is shown in Figure 4.11.

The steady state, one dimensional heat flux q_{wall} can be represented by Equation

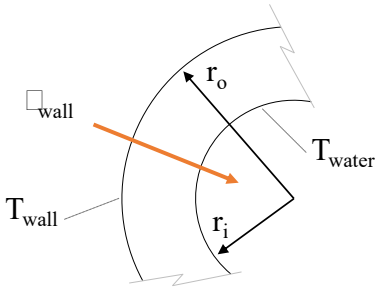

Figure 4.11 – Conductive heat transfer across a cylinder section.

4.23 [Arpaci, 1966] for constant thermal conductivity.

$$Q_{wall} = N_{tubes} \frac{2\pi\, L\, k_{cond}\, (T_{wall} - T_{water})}{2 \ln\left(\frac{r_o}{r_i}\right)} \tag{4.23}$$

with L the furnace height, and N_{tubes} is the total number of water-wall tubes. Since the tubes are disposed very close to each other, it was considered that heat exchange occurs only through tubes half area. The half facing the furnace exterior is covered with isolating material, so it is considered to be adiabatic. Wall temperatures were calculated by prescribing Q_{wall}, with the aid of Equation 4.24.

$$Q_{wall} = \dot{m}_{water}\, (h_{steam} - h_{liquid}) \tag{4.24}$$

Wall heat flux was found to be Q_{wall} = 3.5 x 10^8 W for water flow rate $\dot{m}_{water}$ =318.3 kg/s, steam and liquid water specific enthalpies h_{steam} =2473 kJ/kg and h_{liquid} =1372 kJ/kg, obtained from the plant measured operational data at constant approximated 360 MW electric power output. At boiler drum inlet, compressed liquid water pressure and temperature are P_{liquid} = 196.6 bar and T_{liquid} = 580 K. At drum outlet, the saturated steam pressure and temperature are P_{steam} = 188.1 bar, and T_{steam} = 633.8 K, respectively.

The wall temperature T_{wall} was estimated as 686 K, by assuming L =18.8 m, r_o =33.35 mm, r_o =27 mm. PECÉM water-walls are composed of 894 parallel 66.7 mm outer diameter tubes. Tubes are built with ASME SA-209 T1a, thermal conductivity k = 50 W/(m K) [MakeItFrom, 2019], however, Babcock and Wilcox, 1992 also indicates a similar alloy, SA-213 T11 ($1\frac{1}{4}Cr\frac{1}{2}MoSi$), as a common material for furnaces-walls tubes, with k = 26.7 W/(m K) [Incropera et al., 2007]. Although the alloys displayed different thermal conductivities, the impact on wall temperature was not significant. Simulations with both values found a 4% deviation in wall temperature, and thereafter the reference

value of k =26.7 W/(m K) was assumed. The wall temperature can be highly affected by ash deposits in the tube outer side, which add a thermal resistance that reduces heat transfer and make wall temperature at the furnace side raises [Mendes et al., 2017]. In the water side (tube inner region) oxide layers can increase tube thickness and thermal conductive, affecting the heat exchange as well [Corrêa et al., 2008]. Both phenomena can reduce boiler efficiency, and lead to the increasing of tube temperature, harming its structural integrity, therefore compromising operational safety. Despite its importance, they were not considered in the present model due to its complexity.

Tube thickness nominal value of 6.35 mm was taken from the plant data sheets, and a sensitivity analysis on that parameter showed that ranging it from 50% up to 90% affected a maximum 5.3% of the wall temperature. The estimated wall temperature agrees in magnitude with the reported value of 600 K from Vuthaluru and Vuthaluru, 2006 in a CFD- modeling of a 500 MW wall-fired utility boiler. The higher value of 783 K was found by Chen et al., 2017, who performed numerical investigations for tangential burner arrangements of a 600 MW (electric) utility boiler. Both literature examples concern to sub-critical Rankine cycle coal power stations, where reported water-wall temperature ranges from 600 to 783 K. The wall temperature calculated in the present work, T_{wall} = 686 K, is within this range, and comes closer to the water phase-change temperature inside the tubes, T_{steam} = 633.8 K, correspondent to the saturated steam temperature at the operating pressure of P_{steam} = 188.1 bar.

4.4.4 5-Chamber Zoning Scheme

Ström's furnace geometry (Section 4.3.3) was slightly adapted to simulate PECÉM operational data, as shown in Figure 4.12. The reference length B (squares and cubes side length) was set to 4 meters, and the 5-chamber arrangement was placed vertically in the furnace domain, horizontally centered. Zoning scheme and the five chambers division were kept the same, as Figure 4.12b depicts the inlet flows arrangement. The 5-chamber model is not meant to literaly represent PECÉM operation, once its volume differs up to 70% from PECÉM furnace volume. However, the present subsection aims to generates data to the RSM analysis presented in subsection 4.4.6, instead describing the real boiler operation.

Although PECÉM furnace operates under sub-stoichiometric combustion condi-

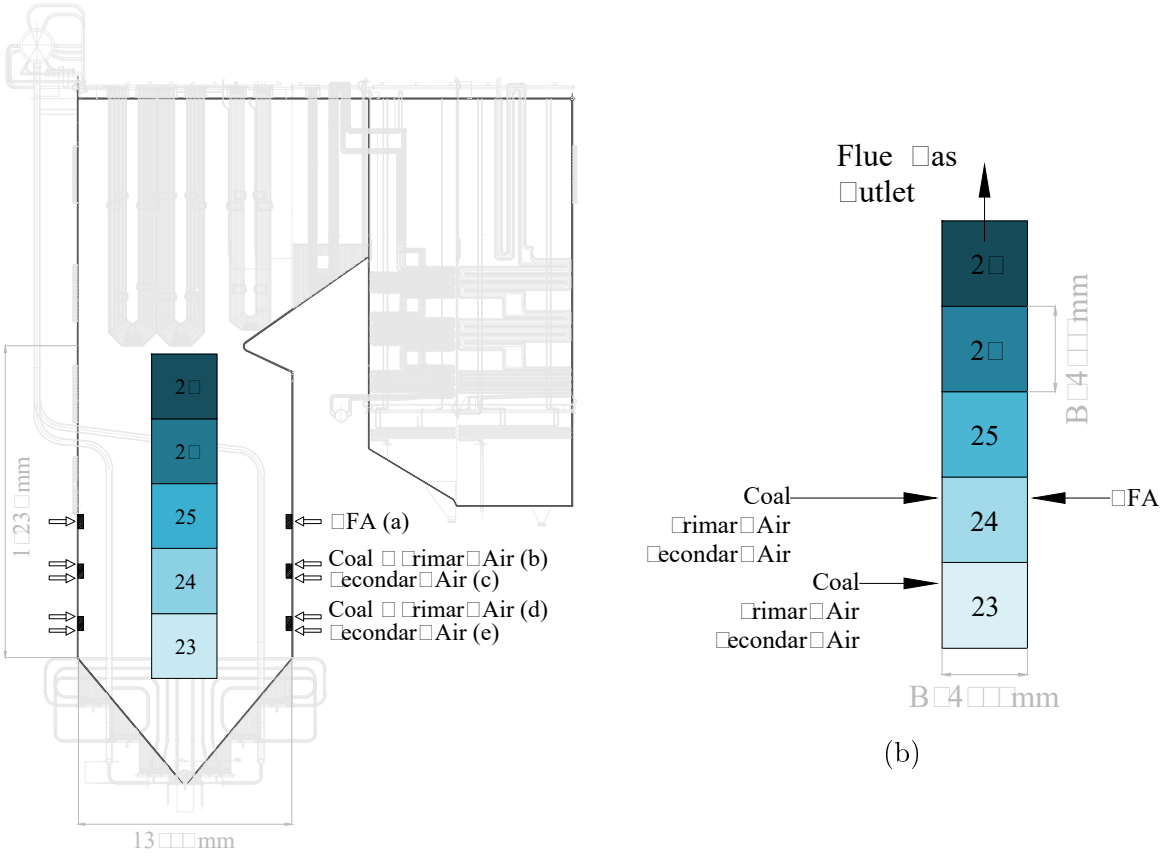

Figure 4.12 – Adapted 5-chamber scheme to perform the zonal model at PECÉM boiler. a) The positioning of the adopted geometry in PECÉM boiler. b) Flow arrangement in the proposed model.

tions, followed by the injection of Over Fire Air (OFA), that decreases the process temperature, aiming to reduce NO_X formation. That scheme was modeled in the present work as presented in Figure 4.12b in a simpler way, only considering stoichiometric combustion and excess air $\lambda \geq 1$. Hence, coal stream, primary and secondary air were assigned to the first two chambers, zones 23 and 24, and OFA to the second one, zone 24. The primary and secondary air inlet were shown separately due to the data format of the power plant control system, but the model only accounts for the total amount of inlet air, as each chamber is treated as a PSR. That PSR assumption also implies that all the combustion process is completed within a single chamber, and the downstream adjacent chamber receives heat input from the incoming flue gas. Furthermore, different inlet flow fractions were assigned for each combustion chamber, namely, $f_{23} = 0.4$ for zone 23 and $f_{24} = 0.6$

for zone 24.

Surface emissivity changes under real operational conditions, and can range from 0.5 and 0.95 [Cañadas et al., 1990] as a function of ash deposit and temperature. In cases such as burner walls or tubes highly-covered with ash, the assumption of $\epsilon_w = 0.9$ and even 1, can be adopted [Constenla et al., 2013; Chen et al., 2017]. The present work assumed $\epsilon_w = 0.5$, as suggested by Lowe et al., 1975 and Ström, 1980, due to the scheduled maintenance of the furnace surfaces.

The gas absorption coefficient was assumed to be $K = 0.5$ m^{-1}, a reasonable choice considering the range of 0.3 to 0.8 for oil, and 0.2 to 0.3 for natural gas, adopted by Ström, 1980. Ebrahimi et al., 2013 also employed $K = 0.5$ m^{-1} in its zonal method implementation on industrial furnaces. Lockwood et al., 1987 assessed the burning process of two types of coal in a hypothetical cylindrical furnace, where an absorption coefficient of 0.5 m^{-1} was adopted.

Reynolds number of flue gas flow was $Re = 1.6{\times}10^6$, confirming a turbulent flow regime inside the furnace [Bejan, 2004]. A mean convection heat transfer coefficient of $\overline{h} = 43.4$ W/(m^{2}K) was determined by means of Equation 4.14, which is indicated for turbulent flow regimes over isotherm flat planes.

4.4.4.1 Results for the 5-chamber zoning scheme

Simulation was performed adopting data displayed in Table 4.3 which are the original operational data from PECÉM. Simulating the operation with these process parameters was intentional, even though the model geometry is much smaller than the real furnace domain. This strategy was adopted to assess model behavior instead of reaching PECÉM boiler output results. Gas volume zone temperature is depicted in Figure 4.13, and shows a monotonic decrease along the adjacent zone. Although zones 23 and 24 experience heat released by combustion, the last one displayed a lower temperature due to air injection from the OFA system. Temperature ranges of 2000 K to 2250 K indicate the distance between the model results and real operational data from PECÉM furnace.

Evaluation of pollutant emission was also carried out to understand how the model behaves with respect to the fuel-air ratio in each zone. Table 4.4 shows simulated results for gas zones 23, 24 and furnace outlet, determined as presented in Section 4.4.2.

Measured excess air coefficient was calculated from total air and coal inlet, and

Table 4.3 – 5-chamber zoning scheme: PECÉM original operational parameters and boundary conditions.

Parameter	Value	Unit
Coal flow rate	36.89	kg/s
Primary air flow rate	74.56	kg/s
Secondary air flow rate	238.28	kg/s
Over fire air flow rate	43.92	kg/s
Inlet coal/air temperature	623	K
Absorption coefficient	0.5	m^{-1}
Wall emissivity	0.5	-
Wall temperature (zone: 2 to 21)	686	K

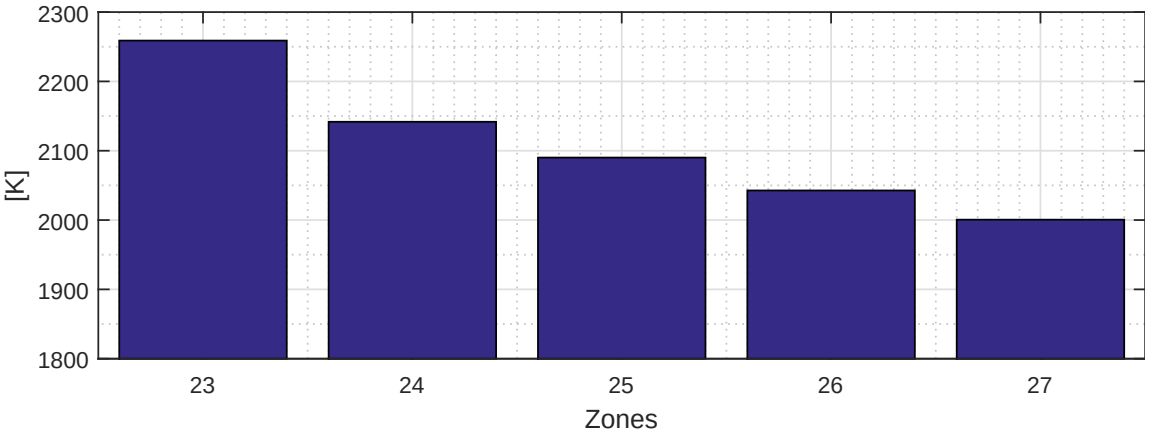

Figure 4.13 – Simulated gas zone temperatures for the 5-chamber zoning scheme with PECÉM operational data (Table 4.3).

Table 4.4 – 5-chamber model results relative deviation to PECÉM real process parameters and emissions.

Parameter	Zone 23	Zone 24	Outlet	Measured data[1]	Units	Deviation[2]
λ	1.049	1.295	-	1.203	-	-
T_{gout}	2258	2141	2000	1432	K	39%
NO	5.23E-06	5.37E-06	5.33E-06	1.57E-05	$kmol/m^3$	-66.1%
SO_2	-	-	1193	1447	mg/m^3	-17.6%
CO_2	16.78	16.65	16.7	12.23	%	36.5%
O_2	0.162	0.96	0.641	2.21	%	-71.0%

[1] Data from EDP-PECÉM power plant;
[2] Relative deviation of furnace outlet result to PECÉM measure data;

differences were not evaluated once outlet λ is not calculated. Nonetheless, overall behavior evaluation is pertinent, as zone 23 present a burning condition closer to ($\lambda = 1$). The real furnace was designed to operate in a sub-stoichiometric condition in zone 23, however, the proposed model only predicts burning conditions $\lambda \geq 1$. Zone 24, in turn, due to over fire air injection present excess air about 20%.

Although the 5-chamber model was not design to represent PECÉM operational data, comparisons are displayed in Table 4.4. Model result for flue gas temperature was 38.6% far from measured data, an expected relative deviation considering the small geometry simulated in front of operational process parameters designed for the real furnace of PECÉM. As well as for the flue gas temperature, the model prediction for pollutant emissions displayed significant deviation to measure data. NO was 66.1% under-predicted, which is a curious result since the gas temperature was almost 40% higher than the real condition. The relative deviations to PECÉM records denote the 5-chamber model inability to represent the real furnace process outputs, however, those results are further analyzed from an alternative point of view, as the RSM assessment allows to understand the model behavior as a function of the input parameters, and moreover, the interdependence among these parameters.

4.4.5 2-Chamber Zoning Scheme

The 5 Chamber furnace model was an easy to adapt solution of the Ström model and there was no expectation to find accurate results out of it but to explore its potentialities. A newer zoning scheme was then proposed, composed by two chambers (gas volumes) and 10 surface zones, as close as possible to PECÉM furnace domain, presented in Figure 4.14. The characteristic length was switched to B= 11.5 m. Although that zoning scheme achieved a much better dimensional coverage, there were some overlapping at the nose and bottom regions, as shown in Figure 4.14a, with an extra volume of 2.6%. Zone 1 was associated with the inlet mass flow rate and zone 10 the furnace flue gas outlet. All burner lines were positioned at zone 11 and the over-fire-air inlet OFA at zone 12. Most of the burning process was meant to occur within zone 11 ($f_{z11} = 0.7$) and the complementary combustion at zone 12. Table 4.5 presents the considered mass flow rates.

The same physical modeling and hypothesis assumed for the 5-chamber zone

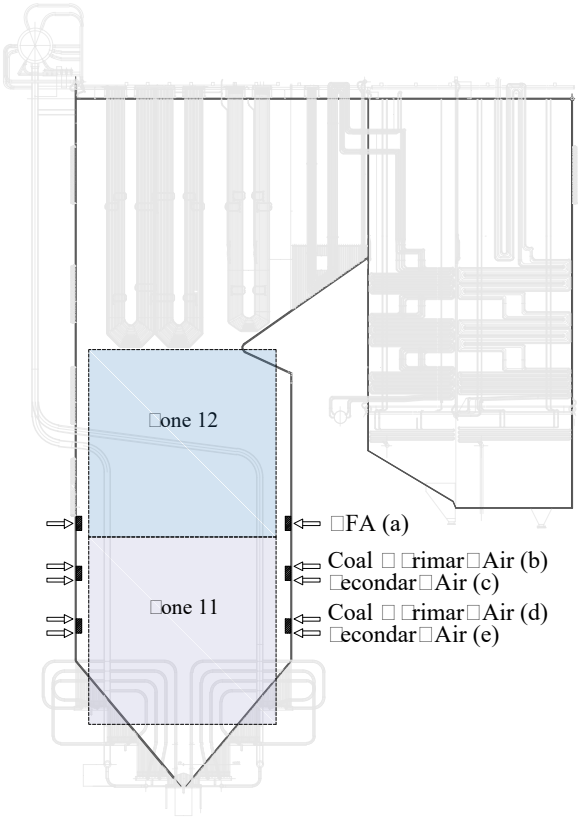

(a) Model domain in PECÉM furnace draw

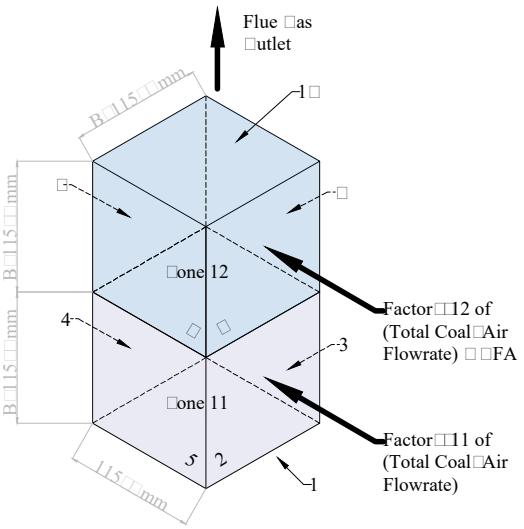

(b) Proposed model: zoning scheme and flow arrangement

Figure 4.14 – 2-Chamber model: positioning of the proposed model in PECÉM furnace. Zoning scheme and flow rates arrangement.

Table 4.5 – 2-chamber model input operational parameters.

Parameter	Zone 11	Zone 12	Real data[1]	Unit
$\dot{m}_{coal}$	25.82	11.07	36.89	kg/s
$\dot{m}_{air}$	218.99	137.77	356.76	kg/s

[1] Data from EDP - PECÉM power plant;

scheme were adopted here, and operational data were the ones presented in Table 4.3. The water wall prescribed temperature of 686 K was assumed for zones 2 to 9. Zone 10 is an imaginary plane placed at the interface of the furnace outlet and the boiler superheaters, and it was assumed the same temperature of the surface zones, which was a conservative hypothesis. A mean convective heat transfer coefficient of $\overline{h} = 6.5$ W/(m^{2}K) was calculated by means of Equation 4.14. The turbulent flow condition was verified as the calculated Reynolds number was $Re = 5.5{\times}10^5$ for boundary layer flow. Based on

literature references cited in subsection 4.4.4, and considering that PECÉM operational data was gathered six months before the annual periodic maintenance, the walls emissivities were assumed to be $\epsilon = 0.7$. The absorption coefficient was set equal to one of the 5-chamber model, $K = 0.5\ \mathrm{m}^{-1}$.

4.4.5.1 Results for the 2-chamber zoning scheme

Simulated results for output process parameters are presented in Table 4.6. Flue

Table 4.6 – 2-chamber model output process parameters.

Variable	Zone 11	Zone 12	Outlet	Measured Data[1]	Unit	Deviation[2]
$T_{g,out}$	1723	1620	1620	1432	K	13.12%
LHV	-	-	28844	28333	kJ/kg	1.82%
HHV	-	-	28954	29343	kJ/kg	-1.32%
Res. Time	2.26	1.68	-	-	s	-
λ	1.05	1.54	-	1.2	-	-

[1] Data from EDP - PECÉM power plant;
[2] Relative deviation of furnace outlet result to PECÉM measure data;

gas temperature, $T_{g,out}$, at furnace outlet presented a 13.12% relative deviation to PECÉM measured data if the efficiency of the SH2 is considered to be 1. For efficiency equal to 0.8, as presented in Appendix A, this normalized deviation becomes 8% as the temperature in the furnace outlet turns to 1499 K. Although the reference temperature is uncertain within the presented range, comparison results indicate that the model could represent the furnace real behavior at this region, with reasonable accuracy for a fast calculation model. Gas temperature in zone 11 was higher than in zone 12, due to the larger amount of coal received by the first one (70% of the feeding coal) and also due to the energy absorbed in the water walls. HHV does not depend on the model zoning scheme, so prediction made for the 2-chamber model was exactly the same as the one found in the 5-chamber model, with 1% relative deviation.

In the present model, where 1D flow is assumed, residence time depends solely on the particle speed and ultimately on the mass flow rate of each zone, as depicted in Figure 4.10. Therefore, particles presented lesser residence time in zone 12 than in zone 11, due to the higher mass flow rate. Although λ results are not the same for the 2-chamber model and the 5-chamber model, the behavior is similar. Technical reports from

PECÉM indicated that the first burning stage occurs at a sub-stoichiometric condition, but that condition was changed in the model, as it only deals with $\lambda \geqslant 1$ ($\lambda = 1.05$ in zone 11). Nonetheless, excess air coefficient was set to a much higher value in zone 12 (which receives the OFA), probably approximating to the operation condition for the respective regions in the real furnace.

Figure 4.15a presents the simulated temperatures for all zones. The only calculated temperatures were the ones for gas zones 11 and 12, as the zones 1 to 10 were assigned at a prescribed temperature. The model predicted T_{11}=1723 K for the combustion region and T_{12}=1620 K for the adjacent one. Zone 12 receives alone the total air flow rate from the OFA system which represents 12.3% of the total inlet air. The air, introduced at 623 K, absorbs part of the energy released by the combustion. The model is capable of capture this effect by the changes in the fluid enthalpy when the energy balance equations are solved. Power plant reports indicated that the average flue gas temperature in the nose region was about 1159°C (1432 K), relatively close to T_{12}.

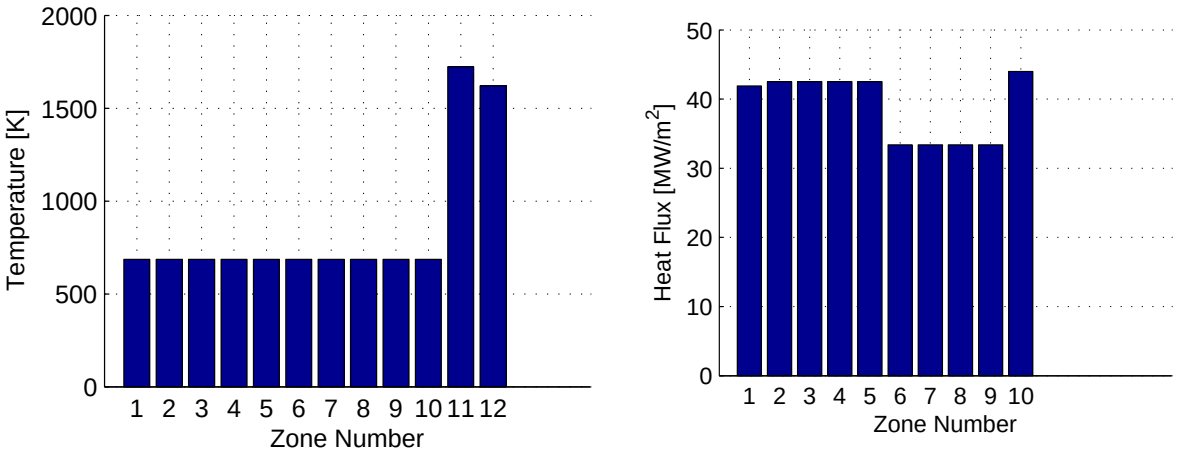

(a) Temperature in the zones

(b) Zoning Scheme: Proposed Model

Figure 4.15 – 2-Chamber zonal method model results for a steady-state condition, at PECÉM nominal operation parameters.

The calculated heat flux is presented for each zone in Figure 4.15b. As gas zone 11 is at a higher temperature, it is expected that its bounding walls (zones 1 to 5) present higher heat flux, than the surfaces bounding gas zone 12. The outlet plane (zone 10) presents the highest heat flux which was anticipated since the regions afterward the furnace outlet are at lower temperature, resulting in higher radiative heat flux.

Overall convective heat transfer was $Q_{conv} = 8.9{\times}10^6$ W, representing only 3% of total exchanged energy in the surface zones $Q_{net} = 2.9{\times}10^6$ W, confirming the behavior reported in the literature [Charette et al., 1990; Bazzo, 1992]. The calculated total energy absorbed by the water-walls in the furnace region (zones 1 to 10) corresponds to approximately 33% of the total energy introduced by the combustion process. Hajebzadeh et al., 2019 states that about 40.71% of the energy introduced in the boiler is absorbed in the furnace region, so the fractions are similar. Results coherency was verified by calculating the global energy balance, Equation 4.6, which delivered a 0.12% error.

The 2-chamber model results for pollutant emissions are presented in Table 4.7. In the power plant of PECÉM, pollutant emissions are continuously measured by online

Table 4.7 – 2-chamber model results for pollutant emissions.

Variable	Zone 11	Zone 12	Outlet	Measured data[1]	Unit	Deviation[2]
SO_2	1151	811	1049	1008	mg/m^3	4.04%
CO_2	16.08	11.22	14.61	12.23	%	19.46%
O_2	0.91	6.98	2.73	2.21	%	23.53%
$NO_{Thermal}$	3.84E-10	6.82E-11	2.89E-10	-	kmol/m^3	
NO_{Fuel}	4.12E-06	3.07E-06	3.81E-06	-	kmol/m^3	
NO_{Total}	4.12E-06	3.07E-06	3.81E-06	1.57E-05	kmol/m^3	-75.75%

[1] Data from EDP - PECÉM power plant, measured in the chimney inlet;
[2] Relative deviation of furnace outlet result to PECÉM measure data;

analyzers, as an environmental safety strategy. Most of the pollutants are measured in mg/Nm^3, so the readings have to be converted to mg/m^3. Real data used to assess model accurateness were measured at the chimney inlet, whereas the model predicted them at the furnace outlet (nose region). Comparisons were made by assuming no changes in gas composition along these two locations.

The normalized deviation in the SO_2 calculation was about 4.04%. Model results for CO_2 and O_2 also predicted values relatively closer to the real process condition. Despite the reported differences, the fact that the analyzers are not located in the same place where the gas composition is calculated, adds uncertainty to the comparison, leading to the acceptance of the model results as a good indicator of process behavior.

An interesting result is the model prediction of nitrogen oxide. Model result for NO_{Total} presented a -75.75% relative deviation to measured data. In the face of this difference, the model capability in predicting NO concentration is questioned. It is necessary,

however, to observes that NO formation is considered by means of complex post-processed calculation, strongly dependent on the gas composition, residence time and temperature. The proposed model possess only two chambers, so the temperature profile coarseness has an important impact on the calculated values. Moreover, gas composition is assumed to be constant, which is not the real process condition. Nonetheless, despite the simplicity of the proposed model, the results are reasonable concerning the magnitude order and physical behavior tendency. In zone 11, which has a higher temperature and fuel concentration, is found higher $NO_{Thermal}$ and NO_{Fuel} concentrations, than in zone 12.

Despite not simulating sub-stoichiometric combustion, the model suggests the role of the over-fire-air, in decreasing the gas temperature, and consequently reducing the NO emission, even though the O_2 and N_2 levels are higher. Furthermore, concerning the formation mechanisms, the model suggests that fuel NO is the predominant formation path, in both gas zones. Results lead to believe that more refined zoning schemes could result in a more accurate NO prediction since the temperature profile becomes more detailed.

Regarding the computational effort, the processing time of the entire script was less than 10 s. The proposed model achieved its initial requirement of being a fast response model, suitable to be incorporated in a decision support tool for a coal-fired power plant.

4.4.6 DoE - Response Surface Methodology

The One-Factor-at-a-Time approach (OFAT) provides a sensitivity analysis based on the influence that each factor alone has on a given response factor. The interdependence between the input factors ranges at different levels, and understanding how their combination can affect the output, requires a different approach. Design of Experiments DoE can perform planned exploitations with simulated or experimental data and is a suitable tool to identify the coupled sensitivity of multi-input factors on the model output [Montgomery, 1997]. Among the known techniques, the Box-Behnken method with central composition generates a smaller number of combinations when compared to regular 3^k factorial design [Ferreira et al., 2007], but prevents to simultaneously overlap factor maximum values. An alternative to that restriction is the Response Surface Methodology (RSM) for the three selected input factors, namely, Flow rate factor, Gas absorption coefficient, and Wall emissivity, ranged as presented in Table 4.8. The 5-chamber model

was chosen to perform a response surface analysis due to its higher resolution, compared to the 5-chamber model, although their results for the output factor were less accurate.

Table 4.8 – Input factors in the DoE performed for the 5-chamber model: first trial.

Input factor	Description	Minimum	Maximum	Unit
Flow	Coal and air inlet fraction[1]	0.5	1.5	-
Emiss	Wall emissivities	0.1	0.95	-
Abs	Gas absorption coefficient	0.1	1	m^{-1}

[1] Flow = 1 is the design mass flow rates for PECÉM power plant operating at 360 MW electric output;

PECÉM power plant has the characteristic of operates most of the time in two base levels. As observed in Figure 4.16, the power plant generates 240 MW when operating in low load condition, or it generates its maximum power output of 350 MW. Intermediary measures represent transient operation between the two power levels. This operational behavior is due to the coal feed system, and the coal grinding mills limitations. Even

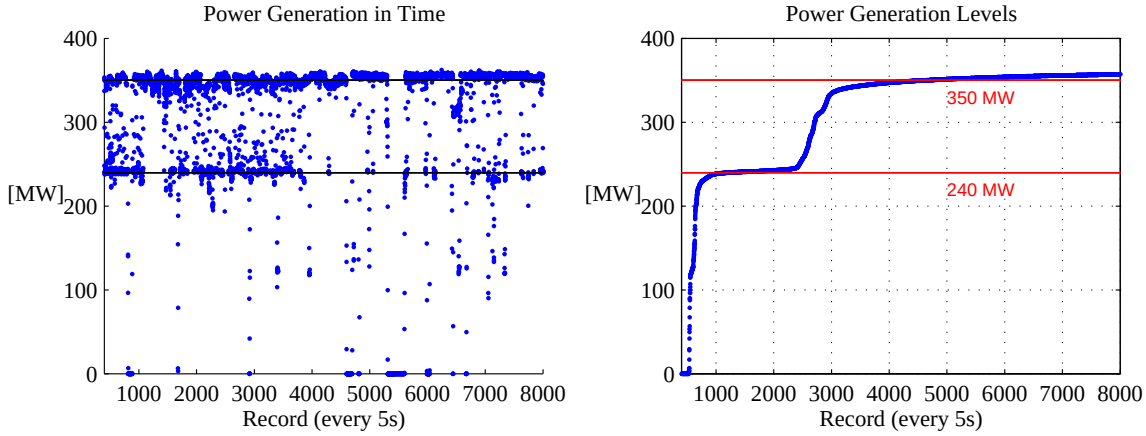

Figure 4.16 – PECÉM's Power generation trend (one year operation). The *Power Generation in Time* graphic shows the control system records. The *Power Generation Levels* graphic represents the system records, in ascending order, to emphasize the two levels of generation: 240 MW and 360 MW.

though a real power plant presents this operation behavior regarding the power generation level, in the present analysis a wider range was tested to enhance the visualization of flow rate influence in the flue gas temperature, T_{27}. Logically, it is expected that the power generation is closely related to the inlet coal and air flow rates. Operational data from

the power plant shows that the for the decrease in power generation from 350 MW to 240 MW (approximately 70% of the maximum power) the coal and air inlet flow tends to decrease up to 26%, keeping proportionality. Therefore, it was considered the inlet flow rates varying from 50% up to 150% of the nominal flow rate at 350 MW. This is obviously not a real operation condition, instead, this analysis tries to observe and extrapolates the zonal method response to the influence of flow rates in a larger range of values.

DoE helped to identify one important issue while running the following combination: Flow rate factor = 0.5, Absorption coefficient = 0.1 and Wall emissivity = 0.1 when the model was not able to reach convergence. Deeper analysis showed that that combination generated inconsistencies in the energy-balance equation solver block, in the EES code. Although these input values were far from actual operation condition, considering that ϵ will most likely be closer to 1 [Lowe et al., 1975; Lockwood et al., 1980; Carvalho and Farias, 1998; Chen et al., 2017], that model limitation could not be predicted by running a simple parametric sensitivity analysis. To overcome the problem, a new range was proposed for wall emissivity as $0.3 \leq \text{Emiss} \leq 0.95$, and assessed ranges are displayed in Table 4.9. The validation parameter *P-value* was employed, set to a significance level of 0.95, $\alpha = 0.05$. The response surface results are presented in Figure 4.17.

Table 4.9 – Input factors in the DoE performed for the 5-chamber model: assessed ranges.

Input factor[1]	Description	Minimum	Maximum
Flow	Coal and air inlet fraction	0.5	1.5
Emiss	Wall emissivities	**0.3**	0.95
Abs	Gas absorption coefficient	0.1	1

[1] Flow = 1 is the design mass flow rates for PECÉM power plant operating at 360 MW electric output;

Results suggest a linear relation of T_{27} with the inlet mass flow rate, which comes from Equation 4.16. The combined effect of the flow rate and the absorption coefficient on zone 27 gas temperature is presented in Figures 4.17a and 4.17b. Similar results were found for the combination of the flow rate fraction (Flow) and the walls emissivities (Emiss). The same linear trend is observed in Figures 4.17c and 4.17d, but with a slight different slope.

A non-linear trend was observed for the absorption coefficient (Abs) and wall emis-

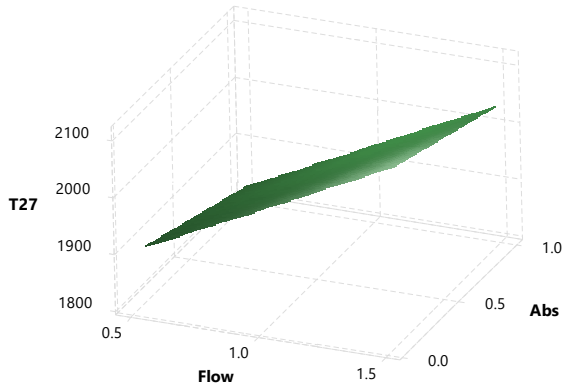

(a) Surface: Flow-Absorption

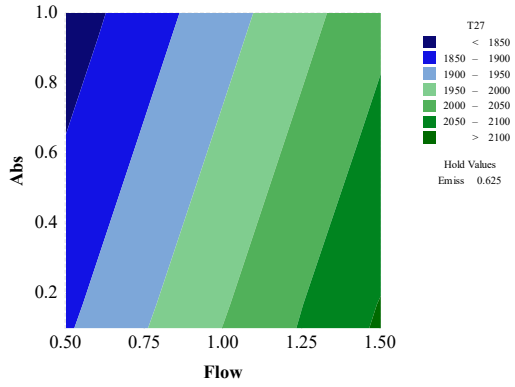

(b) Contour: Flow-Absorption

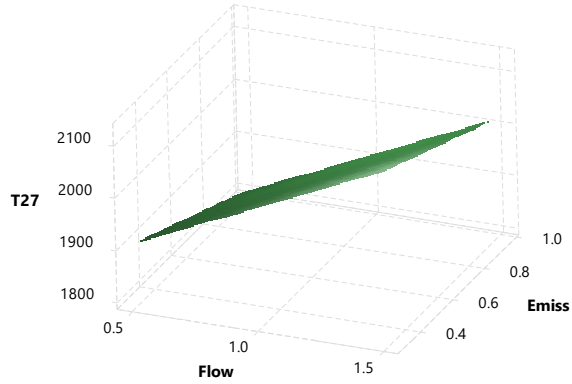

(c) Surface: Flow-Emissivity

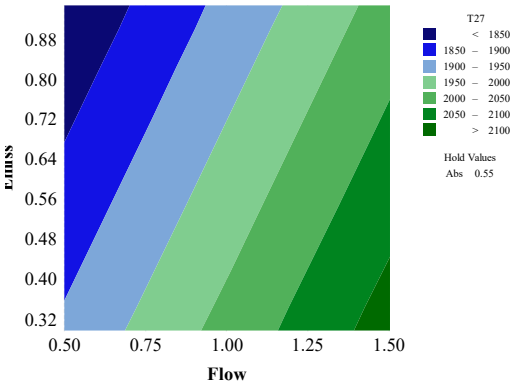

(d) Contour: Flow-Emissivity

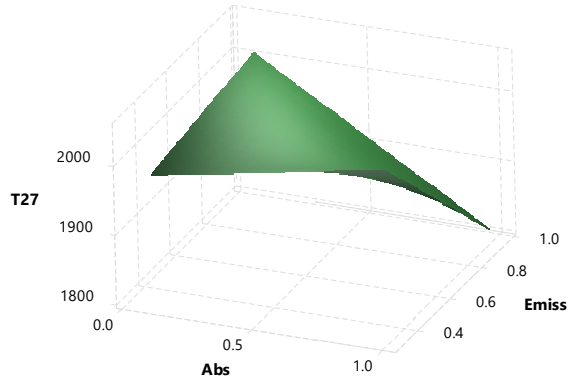

(e) Surface: Absorption-Emissivity

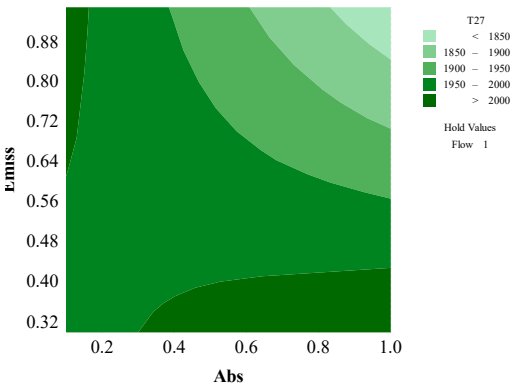

(f) Contour: Absorption-Emissivity

Figure 4.17 – Response Surface Method (RSM) results for the 5-chamber furnace model. Flow-wall emissivity and flow-absorption coefficient presented a linear inter-relation. Emissivity-absorption coefficient displays a non-linear relation.

sivities (Emiss) response curve, displayed in figures 4.17e and 4.17f. Figure 4.17f, particularly denotes the difference between a sensitivity analysis and the RSM. From the first

one it could be inferred that T_{27} tends to decrease as *Abs* and *Emiss* grows independently from each other. The RSM, yet, unveils the interrelation surface between wall emissivity and gas absorption coefficient, displaying in which ranges they could result in T_{27} maximum or minimum values. Figure 4.17f highlight that maximum gas temperature would only be achieved when one of the factors was set to its maximum, whereas the other closer to its minimum value.

4.5 Conclusions

The present chapter developed an approach strategy in the modeling of an actual pulverized-coal-fired furnace of a 360 MW power plant. The complete calculation procedure was based on the zonal method [Hottel and Cohen, 1958], adopting Tuckers correlations for determining the direct exchange areas, and solving the energy equation system for the one-dimensional description of the furnace. As a basic requirement, the model cannot be time-expensive such as traditional CFD models, which justified the choice of simplified modeling of the combustion process.

Model validation was based on experimental and simulated results from Ström, 1980 for a 5-chamber furnace, fueled with natural gas or oil. Maximum relative deviations on surface and gas zones temperatures were found below 5.7% for natural gas and 8.0% for oil. A parametric sensitivity analysis was performed for that model in order to evaluate the influence of the mass flow rate, convective coefficient, inlet gas temperature, gas absorption coefficient, and wall emissivities, highlighting the direct relation of wall emissivities to wall temperature, and the influence of the gas absorption coefficient on flue gas temperature.

The 5-chamber zoning scheme was tested with real boundary conditions from PECÉM power plant. Although the geometry did not correspond to the real furnace, the model behavior was assessed by means of a Response Surface Method (RSM), planned in the Minitab software [Minitab, 2018]. Three input factors were evaluated to assess the last chamber temperature. RSM results highlighted the interaction between gas absorption coefficient and wall emissivity. The response surface also revealed the model convergence limitation when wall emissivity was set to values below 0.3 at specifics operation conditions.

A 2-chamber zoning scheme was simulated as an effort to model the real PECÉM furnace with the zonal method. This scheme was better fitted in the real furnace domain,

and real operation condition was adopted. Each gas zone, treated as a perfect stirred reactor, had its temperature and composition determined as a function of the prescribed flow rate. Results concerning to the flue gas temperature were relatively satisfactory where a 13.2% normalized deviation was found. Pollutant emission, although not accurate, presented consistency with the order of magnitude of the recorded values from the power plant control system. Prediction of NO appears as an interesting result since even with a coarse discretization of the domain, relative order of magnitude concordance with real data was observed (75.75% deviation).

The code was developed in Matlab, linked to EES subroutines, and displayed a processing time of about 10 s, which is at the same order than fast-response prediction models such as gray-box models, neural networks and simplified analytical models. CFD models can take hours and even days to be processed, despite its accuracy, and cannot be compared to the proposed model when processing time is a crucial aspect.

The proposed model presented very interesting results, as it brought together important features of both types of modeling approaches (CFD and AI). From the process physics point of view, the model was capable of predicting some selected furnace parameters, as many CFD models do. On the other hand, the model proved to be a fast-response procedure, such as some machine learning approaches. Outline, the presented model can deliver a fast prediction of process parameters without losing track of basics physical phenomena involved in the combustion process.

5 CONCLUSIONS

In the present work, a comprehensive study on Hottel's zone method was developed. Chapter 2 brought a detailed review on the method basis and how it can be applied to industrial furnaces. Mathematical radiation methods such as Spherical Harmonics, Monte Carlo, DOM and DTRM were introduced, and a summary synthesized the main advantages and disadvantages of each one. The theoretical background was provided by presenting the methodology for direct exchange area and total exchange area calculations. Energy balance equations were explored, and the complete calculation procedure was depicted both for gray gas and WSGG applications. A computational code was developed to solve an example proposed by Hottel and Sarofim, 1967 for a hypothetical furnace. Complete results for the mentioned example were not provided by the authors, and the problem was solved for a gray gas condition for simplicity. The only partial comparison was made for the direct exchange areas reported on the book, which indicated a deviation of 3.28%. Nevertheless, the step-by-step solution for the complete example was presented in this chapter.

The main object of the present work was to produce options for the simulation the PECÉM power plant boiler, respecting the balance between accuracy and computational time. Two models were assembled and discussed: Chapter 3 presents a fast response routine based on stoichiometric coal combustion and element balance and chapter 4 presents a zonal method based model for the heat exchange simulation of the boiler furnace.

The fast response routine was meant to estimate coal combustion based on a general energy balance applied to the boiler furnace, modeled as a Perfect Stirred Reactor (PSR). A post-processed NO_X formation model as a function of the flue gas outlet temperature was implemented. Differences between model results and real data reached 18.46% for the flue gas temperature, 1.82% for coal LHV and -1.32% for coal HHV. Regarding pollutant emission, relative deviations for calculated species were found to be 4.82% for SO_2, 14.72% for CO_2, -89.61% for NO and 53.85% for O_2. These last differences, although apparently high, can be acceptable for a simplified model. The model was fed with coals with distinct chemical compositions from the United States, Colombia, India, and Brazil in order to assess boiler efficiency and pollutant formation. Such a database can be used as support for future analysis and decisions regarding coal supply for PECÉM power plant.

The Zonal model presented in chapter 2 was adapted to simulate PECÉM boiler with the aid of the combustion model from chapter 3 and results are discussed in 4. Prediction for flue gas temperature, CO_2, O_2, SO_2, NO_X and ash concentrations were presented. The model was implemented in a Matlab and coupled to EES subroutines. Experimental and simulated data from a furnace modeled by [Ström, 1980] were used to verify the code accuracy and coherency. An assessment of Zonal method behavior as a function of the input parameters and operational conditions was carried out, and the sensitivity analysis showed the impact from mass flow rate, gas absorptivity coefficient and wall emissivity on the model output flue gas temperature. However, only the response surface method revealed the non-linear interdependence of emissivity and absorption coefficient, and confirmed the small contribution of the convection inside the furnace, mentioned in the literature. Simulations indicated that the convective heat transfer corresponded to 3% of the overall heat transfer in the furnace. Participant media was modeled as a gray gas and the maximum differences found were about 7.6% while average differences between model results and real data were 1.7%. The same code developed to reproduce Strom problem was adapted to simulate the PECÉM furnace, with two geometric approaches: a 5-chamber and a 2 chamber discretization. The last one designed to represent PECÉM furnace predicted flue gas temperature 13.12% distant from the measured value. The calculated Coal Higher Heating Value HHV showed a -1.32% difference to the one burned in the power plant while LHV was 1.82% far from laboratory report. Higher deviations were found regarding flue gas species concentration, as follows: 4.04% for SO_2, 19.46% for CO_2 and 23.53% for O_2. The model was sensitive to changes in the zoning scheme and showed results in the same order of magnitude of real measurement of NO concentration. A consistency assessment was performed in the calculation procedure and computational code implementation, by checking the global energy balance, which found a 0.12% deviation. Processing time took less than 10 seconds, a reasonable time for an online prediction model, much faster than CFD models.

The above-reported results indicated that the zonal method is an interesting choice to simulate control-oriented coal-fired furnaces. If a sufficiently-detailed combustion model was to be employed, a good agreement could be achieved, within a feasible processing time. Although CFD models can better detail physical phenomena with accuracy, its computational effort could be prohibitive when decision-support is the goal. Zonal method,

however, can deliver a fast response by using matrices in the determination of DEA and TEA, and adopting a coarser domain discretization. Therefore, it was concluded that coal combustion can be represented by zonal method models, with acceptable accuracy and processing time, and they can be attached to decision support tools for boiler furnace simulation.

5.1 Future works

Future works could be developed by applying a more detailed gray gas model, dependent on temperature, for instance, or a non-gray gas model, such as the WSGG model. Soot formation model could be also considered since coal usually present high levels of it in its combustion process. Regarding coal combustion description, chemical reaction rate equations could be employed in order to bring model results closer to reality, improving pollutant emission prediction. The NO formation can be enhanced by means of a finer zoning scheme. This would generate a more defined temperature profile along furnace height, which would be better for the post-processed NO formation model. It is suggested as well, that more detailed temperature measurements be carried out in the furnace of PECÉM, both in cross-sectional direction and along the furnace height, in order to confront the model results.

REFERENCES

Alobaidd, X., Mertensd, X., Starkloffd, X., Lanzd, X., Heinzed, X., and Eppled, X. Progress in dynamic simulation of thermal power plants, **Progress in Energy and Combustion Science journal**, vol. 59, p. 79–162, 2016.

Arpaci, V. S. **Conduction Heat Transfer**. Addison-Wesley Publishing Co., Reading, Massachusetts, 1 edition, 1966.

Asl, S. S., Tahouni, N., and Panjeshahi, M. H. Energy benchmarking of thermal power plants using Pinch Analysis, **Journal of Cleaner Production**, vol. 171, p. 1342–1352, 2018.

Babcock and Wilcox. **Steam its Generation and Use**. The Babcock & Wilcox Company, Ohio, 41 edition, 1992.

Banks, J. **Handbook of Simulation: Principles, Methodology, Advances, Applications, And Practice.** John Wiley & Sons, Inc., Danvers, 1 edition, 1998.

Bazzo, E. **Geração de Vapor**. Editora da UFSC, Florianópolis, 1 edition, 1992.

Bejan, A. **Convection Heat Transfer**. John Wiley & Sons, Inc., 3 edition, 2004.

Bhowmick, T., Nayak, B., and Varma, A. K. Chemical and mineralogical composition of Kathara Coal, East Bokaro Coalfield, India, **Fuel**, vol. 208, p. 91–100, 2017.

Biel, K. and Glock, C. H. Systematic literature review of decision support models for energy-efficient production planning, **Computers & Industrial Engineering**, vol. 101, p. 243–259, 2016.

BP. **67th BP Statistical Review of World Energy**. Technical report, 2018.

Callon, M., Courtial, J.-P., Turner, W. A., and Bauin, S. From Translations to Problematic Networks: An Introductino to co-Word Analysis, **Social Science Collections**, vol. 22, p. 191–235, 1983.

Cañadas, L., Salvador, L., and Ollero, P. Radiative Heat-Transfer Model in the Interior of a Pulverized Coal Furnace, **Industrial and Engineering Chemistry Research**, vol. 29(4), p. 669–675, 1990.

Cantrell, C. and Idem, S. On-line performance model of the convection passes of a pulverized coal boiler, **Heat Transfer Engineering**, vol. 31(14), p. 1173–1183, 2010.

Carvalho, M. G. and Farias, T. L. Modelling Of Heat Transfer In Radiating And Combusting Systems, **Trans IChemE**, vol. 76, p. 175–184, 1998.

Centeno, F. R. **Modelagem da Radiação Térmica em Chamas Turbulentas da Combustão de Metano em Ar**. PhD thesis, UFRGS, 2014.

Centeno, F. R., Brittes, R., França, F. H., and da Silva, C. V. Application of the WSGG model for the calculation of gas–soot radiation in a turbulent non-premixed methane–air flame inside a cylindrical combustion chamber, **International Journal of Heat and Mass Transfer**, vol. 93, p. 742–753, 2016.

Chandrasekhar, S. **Radiative Transfer**. Dover Publications Inc., Toronto, Canada, 1 edition, 1960.

Charette, A., Erchiqui, F., and Kocaefe, Y. S. The imaginary planes method for the calculation of radiative heat transfer in industrial furnaces, **The Canadian Journal of Chemical Engineering**, vol. 67(3), p. 378–384, 1989.

Charette, A., Larouche, A., and Kocaefe, Y. Application of the imaginary planes method to three-dimensional systems, **International Journal of Heat and Mass Transfer**, vol. 33(12), p. 2671–2681, 1990.

Chen, S., He, B., He, D., Cao, Y., Ding, G., Liu, X., Duan, Z., Zhang, X., Song, J., and Li, X. Numerical investigations on different tangential arrangements of burners for a 600 MW utility boiler, **Energy**, vol. 122, p. 287–300, 2017.

Cho, J., Kim, Y., Song, J., Lee, T. K., and Song, H. H. Design of dynamic plant model and model-based controller for a heat recovery system with a swirling flow incinerator, **Energy**, vol. 147, p. 1016–1029, 2018.

Coelho, P. and Costa, M. **Combustão**. Rolo & Filhos II, 1 edition, 2007.

Constenla, I., Ferrín, J., and Saavedra, L. Numerical study of a 350 MWe tangentially fired pulverized coal furnace of the As Pontes Power Plant, **Fuel Processing Technology**, vol. 116, p. 189–200, 2013.

Corrêa, R., Carlos, A., and Bazzo, E. **Surface Temperature Monitoring on Boiler Tube Bundles**. In Proceedings of ENCIT 2008 - 12th Brazilian Congress of Thermal Engineering and Sciences, p. 1–11, Belo Horizonte, MG. ABCM, 2008.

Crnomarković, N. D., Belošević, S. V., Tomanović, I. D., and Milićević, A. R. Influence of the gray gases number in the weighted sum of gray gases model on the radiative heat exchange calculation inside pulverized coal-fired furnaces, **Thermal Science**, vol. 20(January), p. s197–s206, 2016.

Cui, M., Chen, H.-g., and Gao, X.-w. Mathematical Models Developed by Zone Method Considering Non-Gray Radiation Properties of Gas in Combustion Chamber, **Journal of Iron and Steel Research, International**, vol. 17(11), p. 13–18, 2010.

da Silva, C. V. **Simulacao Numerica Da Combustao Turbulenta De Gas Natural Em Camara Cilindrica**. PhD thesis, UNIVERSIDADE FEDERAL DO RIO GRANDE DO SUL, 2005.

Díez, L. I., Cortés, C., and Campo, A. Modelling of pulverized coal boilers: review and validation of on-line simulation techniques, **Applied Thermal Engineering**, vol. 25(10), p. 1516–1533, 2005.

Dorigon, L. J., Duciak, G., Brittes, R., Cassol, F., Galarça, M., and França, F. H. WSGG correlations based on HITEMP2010 for computation of thermal radiation in non-isothermal, non-homogeneous H2O/CO2 mixtures, **International Journal of Heat and Mass Transfer**, vol. 64, p. 863–873, 2013.

Ebrahimi, H., Zamaniyan, A., Soltan Mohammadzadeh, J. S., and Khalili, A. A. Zonal modeling of radiative heat transfer in industrial furnaces using simplified model for exchange area calculation, **Applied Mathematical Modelling**, vol. 37(16-17), p. 8004–8015, 2013.

Echi, S., Bouabidi, A., Driss, Z., and Abid, M. S. CFD simulation and optimization of industrial boiler, **Energy**, vol. 169, p. 105–114, 2019.

ExxonMobil. **2018 Outlook for Energy: A View to 2040**. Technical report, Exxon Mobil Corporation, Irving, Texas, 2018.

F-Chart Software, L. **EES - Engineering Equation Solver**, 2019.

Ferreira, S., Bruns, R., Ferreira, H., Matos, G., David, J., Brandao, G., da Silva, E., Portugal, L., dos Reis, P., Souza, A., and dos Santos, W. Box-Behnken design: An alternative for the optimization of analytical methods, **Analytica Chimica Acta**, vol. 597, p. 176–186, 2007.

Fiveland, W. A. Discrete-Ordinates Solutions of the Radiative Transport Equation for Rectangular Enclosures, **Journal of Heat Transfer**, vol. 106(4), p. 699–706, 1984.

Gielen, D., Boshell, F., Saygin, D., Bazilian, M. D., Wagner, N., and Gorini, R. The role of renewable energy in the global energy transformation, **Energy Strategy Reviews**, vol. 24, p. 38–50, 2019.

Hajebzadeh, H., Ansari, A. N., and Niazi, S. Mathematical modeling and validation of a 320 MW tangentially fired boiler: A case study, **Applied Thermal Engineering**, vol. 146(June 2018), p. 232–242, 2019.

Herman, E. **Radiant Heat Exchange in Gas-Filled Slabs and Cylinders**. PhD thesis, Massachusetts Institute of Technology, 1959.

Hill, S. and Douglas Smoot, L. Modeling of nitrogen oxides formation and destruction in combustion systems, **Progress in Energy and Combustion Science**, vol. 26(4-6), p. 417–458, 2000.

Hottel, H. C. and Cohen, E. S. Radiant heat exchange in a gas-filled enclosure: Allowance for nonuniformity of gas temperature, **AIChE Journal**, vol. 4(1), p. 3–14, 1958.

Hottel, H. C. and Sarofim, A. F. **Radiative Transfer**. McGraw-Hill Book Co, 1 edition, 1967.

Howell, J. R. and Perlmutter, M. Monte Carlo Solution of Thermal Transfer Through Radiant Media Between Gray Walls, **Journal of Heat Transfer - ASME**, vol. 86(1), p. 116, 1964.

Hübel, M., Meinke, S., Andrén, M. T., Wedding, C., Nocke, J., Gierow, C., Hassel, E., and Funkquist, J. Modelling and simulation of a coal-fired power plant for start-up optimisation, **Applied Energy journal**, vol. 208, p. 319–331, 2017.

Incropera, F. P., DeWitt, D. P., Bergman, T. L., and Lavine, A. S. **Fundamentals of Heat and Mass Transfer**. vol. 6th. John Wiley & Sons, Inc., 7 edition, 2007.

International Energy Agency. **World Energy Outlook 2017**, 2017.

Jeans, J. The Equations of Radiative Transfer of Energy, **Royal Astronomical Society - NASA Astrophysics Data System**, vol. 1, p. 28–36, 1917.

Johnson, T. and Beer, J. Radiative heat transfer in furnaces: Further development of the zone method of analysis, **Symposium (International) on Combustion**, vol. 14(1), p. 639–649, 1973.

Kothari, C. **Research Methodology - Methods ans Techniques**. New Age International (P) Ltd, Publishers, New Delhi, second edition, 2004.

Liua, F., Becker, H., and Bindar, Y. A comparative study of radiative heat transfer modelling in gas-fired furnaces using the simple grey gas and the weighted-sum-of-grey-gases models, **International Journal of Heat and Mass Transfer**, vol. 41(22), p. 3357–3371, 1998.

Lockwood, F., Salooja, A., and Syed, S. A prediction method for coal-fired furnaces, **Combustion and Flame**, vol. 38, p. 1–15, 1980.

Lockwood, F. and Shah, N. A new radiation solution method for incorporation in general combustion prediction procedures, **Symposium (International) on Combustion**, vol. 18(1), p. 1405–1414, 1981.

Lockwood, F. C., Rizvi, S., and Shah, N. Comparative predictive experience of coal firing, **Journal of Mechanical Engineering Science**, vol. 200, p. 79–87, 1987.

Lowe, A., Wall, T. F., and Stewart, I. M. A zoned heat transfer model os a large tangentially fires pulverized coal boiler, **Symposium (International) on Combustion**, vol. 15(1), p. 1261–1270, 1975.

Ma, L., Fang, Q., Yin, C., Wang, H., Zhang, C., and Chen, G. A novel corner-fired boiler system of improved efficiency and coal flexibility and reduced NOx emissions, **Applied Energy**, vol. 238, p. 453–465, 2019.

Madejski, P. Numerical study of a large-scale pulverized coal-fired boiler operation using CFD modeling based on the probability density function method, **Applied Thermal Engineering**, vol. 145, p. 352–363, 2018.

Mahmoodi, B., Hosseini, S. H., Ahmadi, G., and Raj, A. CFD simulation of reactor furnace of sulfur recovery units by considering kinetics of acid gas (H2S and CO2) destruction, **Applied Thermal Engineering**, vol. 123, p. 699–710, 2017.

MakeItFrom. **ASTM A209 Grade T1a C-Mo Steel**, 2019.

McAdams, W. H. and Hottel, H. C. **Heat Transmission**. In Chemical Engineering Series, chapter 4 - Radian, p. 553. McGraw-Hill Inc., New York, NY, 3 edition, 1954.

McCain, K. W. Mapping Authors in Intellectual Space: A Technical Overview, **Journal of the American Society for Information Science**, vol. 41(6), p. 433–443, 1990.

Mendes, N., Bazzo, E., and Azevedo, J. Thermal conductivity analysis of an ash deposit on boiler superheater, **Powder Technology**, vol. 318, p. 329–336, 2017.

Minitab, I. **Minitab**, 2018.

Modest, M. F. **Radiative Heat Transfer**. McGraw-Hill Inc., New York, NY, 1 edition, 1993.

Montgomery, D. C. **Design and Analysis of Experiments**. John Wiley & Sons, Inc., 5 edition, 1997.

Noble, J. J. The zone method: Explicit matrix relations for total exchange areas, **International Journal of Heat and Mass Transfer**, vol. 18(2), p. 261–269, 1975.

Oko, E. and Wang, M. Dynamic modelling, validation and analysis of coal-fired subcritical power plant, **Fuel**, vol. 135, p. 292–300, 2014.

Raithby, G. D. and Chui, E. H. A Finite-Volume Method for Predicting a Radiant Heat Transfer in Enclosures With Participating Media, **Journal of Heat Transfer**, vol. 112(2), p. 415, 1990.

Restrepo, Á., Bazzo, E., and Miyake, R. A life cycle assessment of the Brazilian coal used for electric power generation, **Journal of Cleaner Production**, vol. 92, p. 179–186, 2015.

Rothman, L., Gordon, I., Barber, R., Dothe, H., Gamache, R., Goldman, A., Perevalov, V., Tashkun, S., and Tennyson, J. HITEMP, the high-temperature molecular spectroscopic database, **Journal of Quantitative Spectroscopy and Radiative Transfer**, vol. 111(15), p. 2139–2150, 2010.

Rusinowski, H. Hybrid model of steam boiler, **Energy**, vol. 35(2), p. 1107–1113, 2010.

Sankar, G., Kumar, D. S., and Balasubramanian, K. Computational modeling of pulverized coal fired boilers – A review on the current position, **Fuel**, vol. 236, p. 643–665, 2019.

Scholand, E. and Schenkel, P. **A Solution of Mean Beam Lengths of Radiating Gases in Rectangular Parallelepiped Enclosures**. In 8th Int. Heat Transfer Conf vol. 2, p. 763–768, Washington, DC. Hemisphere, 1986.

Siegel, R. and Howell, J. R. **Thermal Radiation Heat Transfer**. Taylor & Francis, New York, NY, 4 edition, 2002.

Silva, C. V., Indrusiak, M. L. S., and Beskow, A. B. CFD Analysis of the Pulverized Coal Combustion Processes in a 160 MW Tangentially-Fired-Boiler of a Thermal Power Plant., **Journal of the Brazilian Soc. Mechanical Sciences. & Eng**, vol. XXXII, p. 328–336, 2010.

Smith, P. J. and Smoot, L. D. One-Dimensional Model for Pulverized Coal Combustion and Gasification, **Combustion Science and Technology**, vol. 23(1-2), p. 17–31, 1980.

Smith, T. F., Shen, Z. F., and Friedman, J. N. Evaluation of Coefficients for the Weighted Sum of Gray Gases Model, **Journal of Heat Transfer**, vol. 104(4), p. 602, 1982.

Speight, J. G. **Handbook of Coal Analysis**. John Wiley & Sons, Inc., New Jersey, 2005.

Ström, B. A simple heat transfer model for furnaces based on the zoning method, **Wärme- und Stoffübertragung**, vol. 13(1-2), p. 47–52, 1980.

The MathWorks, I. **MATLAB -**, 2012.

Tian, W. and Chiu, W. K. Calculation of Direct Exchange Areas for Nonuniform Zones Using a Reduced Integration, **Journal of Heat Transfer - ASME**, vol. 125(October 2003), p. 839–844, 2003.

Trent, V., Medlin, J., Coleman, S., and Stanton, R. Chemical Analyses and Physical Properties of 12 Coal Samples from the Pocahontas Field, **Geological Survey Bulletin**, vol. 1528, p. 46, 1982.

Tucker, R. Direct Exchange Areas for Calculating Radiation Transfer Transfer in Rectangular Furnaces, **Journal of Heat Transfer**, vol. 108, p. 707–710, 1986.

Turns, S. R. **Introdução à Combustão Conceitos e Aplicações**. McGraw-Hill Book Co, Porto Alegre, RS, 3 edition, 2013.

Üsdiken, B. and Pasadeos, Y. Organizational Analysis in North America and Europe: A Comparison of Co-citation Networks, **Organization Studies**, vol. 16(3), p. 503–526, 1995.

van Eck, N. J. and Waltman, L. Software survey: VOSviewer, a computer program for bibliometric mapping, **Scientometrics**, vol. 84(2), p. 523–538, 2010.

Van Wylen, G., Borgnakke, C., and Sonntag, R. **Fundamentals of Thermodynamics**. vol. 1. John Wiley & Sons, Inc., Hoboken, NJ - USA, 6 edition, 2003.

Vuthaluru, R. and Vuthaluru, H. Modelling of a wall fired furnace for different operating conditions using FLUENT, **Fuel Processing Technology**, vol. 87(7), p. 633–639, 2006.

Wang, F., Ma, S., Wang, H., Li, Y., and Zhang, J. Prediction of NOX emission for coal-fired boilers based on deep belief network, **Control Engineering Practice**, vol. 80, p. 26–35, 2018.

Warnatz, J., Maas, U., and Dibble, R. **Combustion**. Springer-Verlag, New York, 4 edition, 2006.

Wütscher, A., Wedler, C., Seibel, C., Hiltrop, D., Fieback, T., Muhler, M., and Span, R. On the alternating physicochemical characteristics of Colombian coal during pyrolysis, **Journal of Analytical and Applied Pyrolysis**, vol. 123, p. 12–19, 2017.

Xia, J., Chen, G., Tan, P., and Zhang, C. An online case-based reasoning system for coal blends combustion optimization of thermal power plant, **International Journal of Electrical Power & Energy Systems**, vol. 62, p. 299–311, 2014.

Zhang, W.-j., Yi, Z., and Chen, H.-g. A New Simplified Zonal Method for Furnace Thermal Radiation Calculation Based on Imaginary Planes, **Journal of Iron and Steel Research, International**, vol. 21(4), p. 419–426, 2014.

Zhang, X., Yuan, J., Chen, Z., Tian, Z., and Wang, J. A dynamic heat transfer model to estimate the flue gas temperature in the horizontal flue of the coal-fired utility boiler, **Applied Thermal Engineering**, 2018.

Zhao, H., Shen, J., Li, Y., and Bentsman, J. Coal-fired utility boiler modelling for advanced economical low-NOxcombustion controller design, **Control Engineering Practice**, vol. 58(x), p. 127–141, 2017.

Zhou, Q., Huang, G. H., and Chan, C. W. Development of an intelligent decision support system for air pollution control at coal-fired power plants, **Expert Systems with Applications**, vol. 26(3), p. 335–356, 2004.

Zhou, W. and Qiu, T. Zone modeling of radiative heat transfer in industrial furnaces using adjusted Monte-Carlo integral method for direct exchange area calculation, **Applied Thermal Engineering**, vol. 81, p. 161–167, 2015.

Zupic, I. Bibliometric Methods in Management and Organization, **Organizational Research Methods**, vol. 18(3), p. 429–472, 2015.

APPENDIX A – Background Calculation Procedures

This appendix presents some definitions on the radiative heat transfer, based in literature review. Calculation procedures used to fed the models are also detailed.

A.1 Radiative Heat Transfer Fundamentals

Radiation reaching a semitransparent medium behaves as presented in Figure A.1. Fractions of the incident energy can be reflected, absorbed or transmitted. Therefore the

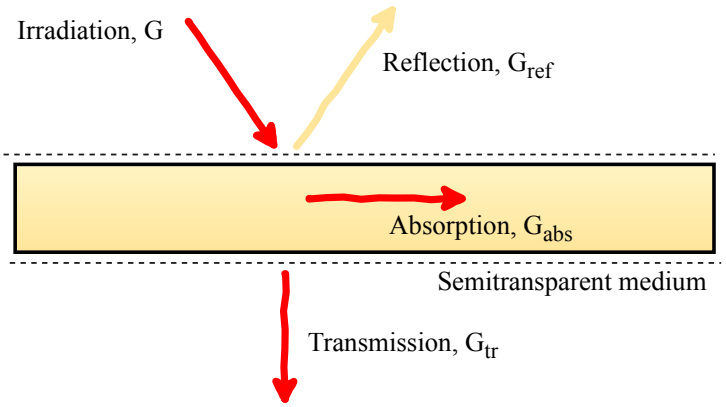

Figure A.1 – Radiation balance in a semitransparent medium.

radiation balance is

$$G = G_{ref} + G_{abs} + G_{tr} \tag{A.1}$$

Three main radiative properties of a surface are stated by Siegel and Howell [2002], namely, Emissivity ϵ, Absorptivity α, Reflectivity ρ and Transmissivity τ. These properties are energy fractions, and their sum equals the unit.

Considering the incident radiation in a opaque surface, overall radiation heat transfer can be characterized by the following relation

$$J = E + G_{ref} \tag{A.2}$$

where G is the incident radiation. Emissive power E for a blackbody is defined as $E_b = \sigma T^4$. The radiation balance is given in watts.

The radiosity of a given surface i can also be expressed by Equation A.3.

$$J_i \equiv E_i + \rho_i G_i \tag{A.3}$$

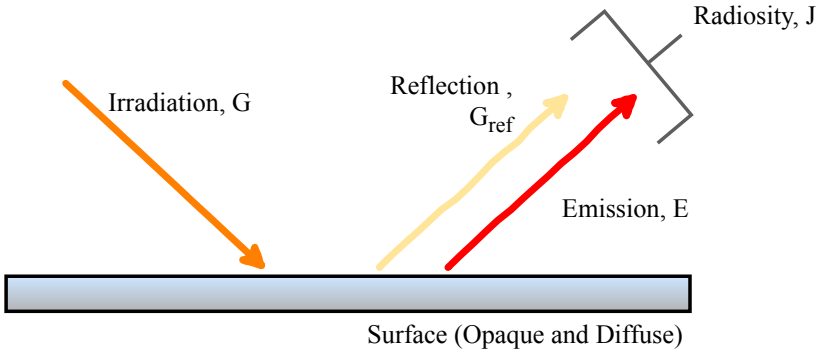

Figure A.2 – Radiation balance in a opaque and diffuse surface.

A.2 Estimation of Flue Gas Temperature

Flue gas temperature is not a current measure in PECÉM boiler furnace. However, devices such as the super heaters are fully instrumented. The energy balance depicted in Figure A.3 report those readings of flow rate, temperature, pressure and enthalpy for several process locations. Performing a energy balance in the super heater 2 (SH2) control

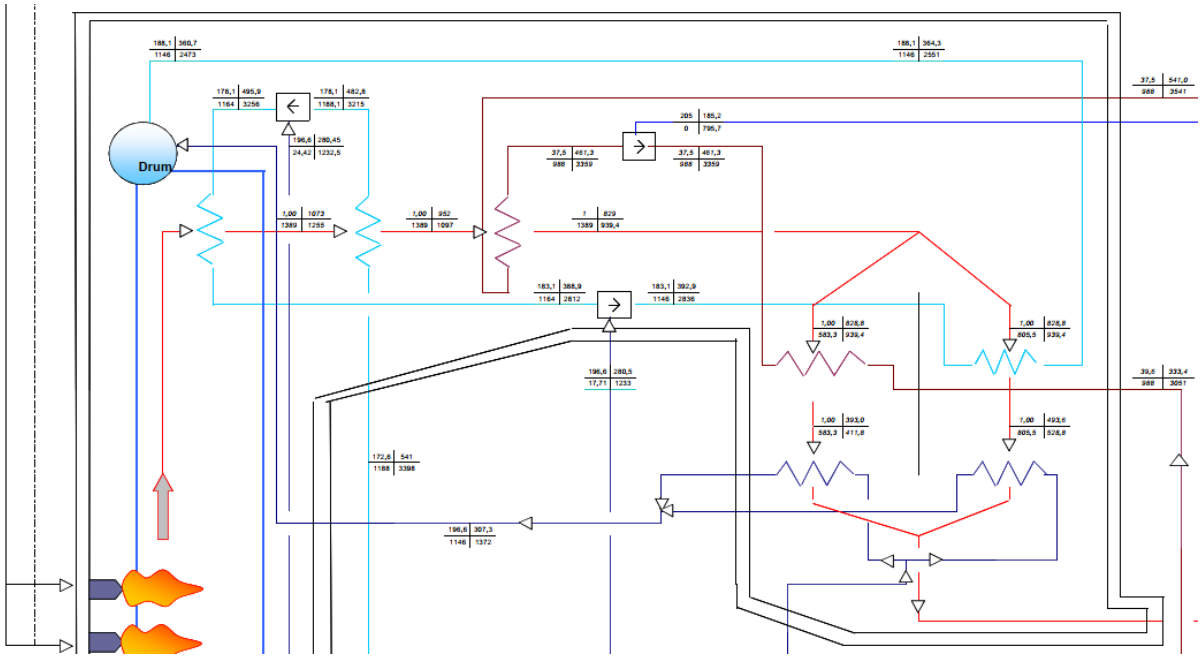

Figure A.3 – Energy Balance of PECÉM 360 MW boiler

volume, displayed in Figure A.4, it is possible to estimate the flue gas temperature from the furnace outlet. The procedure considers the energy balance in the vapor stream

$$Q_{steam} = \dot{m}_{steam}(h_{steam,outlet} - h_{steam,inlet}), \tag{A.4}$$

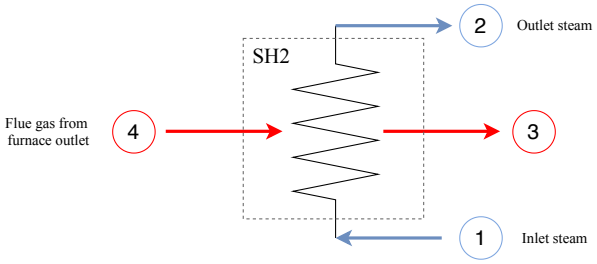

Figure A.4 – Energy Balance in SH2.

and the energy balance in the flue gas stream

$$Q_{gas} = \dot{m}_{gas}(h_{gas,inlet} - h_{gas,outlet}), \tag{A.5}$$

to determine $T_{g,out}$ by assigning a efficiency to SH2. Table A.1 present measured data for process points 1, 2, 3 and 4.

Table A.1 – Process data from PECÉM boiler energy balance.

Location	Temperature (°C)	Pressure (bar a)	Flow rate (kg/s)	Enthalpy (kJ/kg)
1	388.9	183.1	307.2	2815
2	495.9	178.1	307.2	3269
3	-	1	393.1	-
4	1073	1	393.1	1243

Therefore, the flue gas temperature was estimated considering SH2 efficiencies varying from 0.5 to 1. Results are presented in Table A.2.

Table A.2 – Flue gas temperatures as function of SH2 efficiency.

SH2 Efficiency	Flue gas Enthalpy (kJ/kg)	Flue gas temperature (°C)
0.5	1953	1486
0.6	1834	1389
0.7	1750	1320
0.8	1687	1268
0.9	1637	1228
1	1598	1195

ANNEX I – Direct Echange Areas Correlations

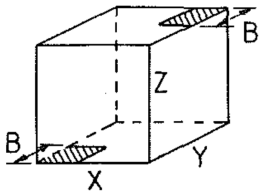

Table I.1 – Correlation coefficients for direct exchange areas between parallel square surfaces; $\overline{ss}/B^2 = C\ exp(-A \times KB)$, [Tucker, 1986].

X/B	Y/B	Z/B	C	A	X/B	Y/B	Z/B	C	A
1	1	1	0.1998	1.1053	1	1	4	0.0191	4.0396
2	1	1	0.0861	1.3014	2	1	4	0.0171	4.1475
3	1	1	0.0153	1.9987	3	1	4	0.0126	4.4615
4	1	1	0.0036	2.9351	4	1	4	0.0082	4.9529
2	2	1	0.0433	1.5172	2	2	4	0.0153	4.2538
3	2	1	0.0105	2.1959	3	2	4	0.0114	4.5627
4	2	1	0.0029	3.088	4	2	4	0.0076	5.0464
3	3	1	0.0045	2.7513	3	3	4	0.0088	4.8569
4	3	1	0.0018	3.5187	4	3	4	0.0061	5.319
4	4	1	0.0009	4.1511	4	4	4	0.0045	5.7494
1	1	2	0.0686	2.071	1	1	5	0.0124	5.0322
2	1	2	0.0481	2.2368	2	1	5	0.0115	5.1224
3	1	2	0.0206	2.7286	3	1	5	0.0093	5.3863
4	1	2	0.008	3.4595	4	1	5	0.0068	5.8053
2	2	2	0.0351	2.4015	2	2	5	0.0107	5.2114
3	2	2	0.0164	2.8812	3	2	5	0.0087	5.472
4	2	2	0.0068	3.5899	4	2	5	0.0065	5.8861
3	3	2	0.0093	3.3165	3	3	5	0.0073	5.7232
4	3	2	0.0046	3.9625	4	3	5	0.0055	6.1231
4	4	2	0.0027	4.5268	4	4	5	0.0043	6.5018
1	1	3	0.033	3.0512	1	1	6	0.0087	6.0271
2	1	3	0.0274	3.1838	2	1	6	0.0082	6.1042
3	1	3	0.0168	3.5683	3	1	6	0.0071	6.331
4	1	3	0.009	4.1582	4	1	6	0.0056	6.6951
2	2	3	0.023	3.314	2	2	6	0.0078	6.1805
3	2	3	0.0146	3.6906	3	2	6	0.0067	6.4052
4	2	3	0.0081	4.268	4	2	6	0.0054	6.7658
3	3	3	0.0101	4.0432	3	3	6	0.0059	6.6235
4	3	3	0.0061	4.5855	4	3	6	0.0048	6.9744
4	4	3	0.004	5.0783	4	4	6	0.0039	7.31

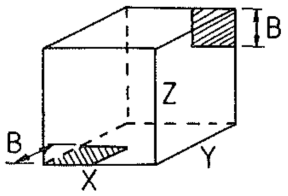

Table I.2 – Correlation coefficients for direct exchange areas between Perpendicular square surfaces; $\overline{ss}/B^2 = C\ exp(-A \times KB)$; $A = a_0 + a_1 * KB ... a_4(KB)^4$, [Tucker, 1986].

X/B	Y/B	Z/B	C	a0	al	a2	a3	a4
1	1	1	0.2	0.539	-6.15E-02	4.29E-03	-1.51E-04	2.06E-06
2	1	1	0.0406	0.9965	-8.78E-02	419E-02	-7.73E-05	0.00E+00
3	1	1	0.0043	1.906				
1	2	1	0.0328	1.571	-3.91E-02	2.08E-03	0.00E+00	0.00E+00
2	2	1	0.0189	1.751				
3	2	1	0.0059	2.384				
1	3	1	0.0089	2.502				
2	3	1	0.0069	2.665				
3	3	1	0.0036	3.129				
1	2	2	0.0329	2.055				
2	2	2	0.023	2.245				
3	2	2	0.0101	2.78				
1	3	2	0.0159	2.86				
2	3	2	0.0129	3.01				
3	3	2	0.0076	3.435				
1	3	3	0.0124	3.481				
2	3	3	0.0107	3.609				
3	3	3	0.0073	3.976				

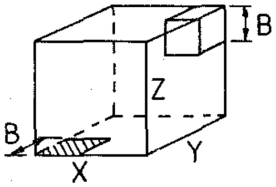

Table I.3 – Correlation coefficients for direct exchange areas between cubic gas zones and square surface zones; $\overline{gs}/(\overline{gs})_b = C\ exp(-A \times KB)$; $A = a_0 + a_1 KB + A_2 * (KB)^2$, [Tucker, 1986].

X/B	Y/B	Z/B	C	a0	al	a2
2	1	1	0.0337	0.4563	-3.11E-02	8.24E-04
3	1	1	0.0048	1.457		
2	2	1	0.0137	0.8332	-4.69E-02	1.03E-03
3	2	1	0.0034	1.674		
3	3	1	0.0017	2.251		
1	1	2	0.0313	1.062		
2	1	2	0.02	1.292		
3	1	2	0.0078	1.933		
2	2	2	0.0135	1.514		
3	2	2	0.0062	2.089		
3	3	2	0.0037	2.602		
1	1	3	0.012	2.033		
2	1	3	0.0098	2.21		
3	1	3	0.006	2.666		
2	2	3	0.0083	2.366		
3	2	3	0.0053	2.806		
3	3	3	0.0037	3.201		

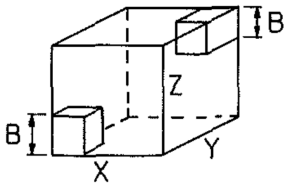

Table I.4 – Correlation coefficients for direct exchange areas between pairs of cubic gas zones; $\overline{gg}/((KB\overline{gs})_b) = C\ exp(-A \times KB)$; $A = a_0 + a_1 KB, ..., A_3(KB)^3$, [Tucker, 1986].

X/B	Y/B	Z/B	C	a0	a1	a2	a3
2	1	1	0.0949	0.3784	-3.31E-02	1.74E-03	-3.60E-05
3	1	1	0.0203	1.43			
2	2	1	0.0445	0.819	-5.99E-02	2.35E-03	-3.47E-05
3	2	1	0.0161	1.657			
3	3	1	0.0099	2.263			
2	2	2	0.0283	1.147	-6.20E-02	1.32E-03	0
3	2	2	0.0132	1.866			
3	3	2	0.009	2.458			